PCCP

ROYAL SOCIETY OF CHEMISTRY

TUTORIAL REVIEW

View Article Online
View Journal | View Issue

Cite this: *Phys. Chem. Chem. Phys.*, 2022, **24**, 19073

Infrared spectroscopic monitoring of solid-state processes

Nikola Biliškov [ab]

Received 28th March 2022,
Accepted 14th June 2022

DOI: 10.1039/d2cp01458k

rsc.li/pccp

Infrared spectroscopy, ubiquitous in contemporary chemical laboratories, is frequently underutilised for just the basic characterisation of products. However, its unique ability to provide rich molecular-level information, its simplicity and flexibility for various applications, and its ability to be combined with a variety of techniques, make it one of the most useful techniques for a deep understanding of the microscopic background of chemical and physical phenomena, especially those of relevance for materials applications. This tutorial review puts a spotlight on IR spectroscopic investigations in materials science by providing a critical insight into the state of the art, covering both fundamental aspects and illustrative examples of its utilisation, as well as current challenges and perspectives focusing on physical and chemical transformations in the solid state.

Introduction

Human curiosity has driven our understanding of the macroscopic manifestations of microscopic structures, the very core of chemistry. From this point of view, structures and transformations of molecules fundamentally determines the function of the materials surrounding us. This is generally true for liquids, gases, crystals, glasses, nanostructures and composites, from the simplest industrial feedstocks to the most complex supramolecules or proteins. In order to gain as detailed an insight as possible into the very fundamental core of these phenomena, numerous analytical techniques have been used, from those found in everyday laboratory work to the most sophisticated experimental facilities.

Infrared (IR) spectroscopy is one of the most ubiquitous methods, and is widely used in chemical laboratories. In most cases, it is routinely used for the characterisation of products. However, its full applicability goes far beyond these routine analyses. It is this gap between the potential of the method and its underutilisation that has led the present author to highlight the possibilities offered by this powerful, yet highly accessible method. Therefore, this review will be focused on mid-infrared spectroscopic monitoring of chemical and physical processes occurring in solid-state systems, relevant to the understanding of materials. Although the various applications of IR spectroscopy to monitor solid-state processes are covered by numerous reviews,[1–10] the author's intention is to bring to focus some specific applications and perspectives, that have so far remained somewhat out of focus. Numerous recent excellent reviews on the specific applications of IR spectroscopy are available, for example on the applications of IR spectroscopy in monitoring liquids[2,11–13] or gaseous systems,[14–16] as well as interfaces.[2,9,17–23]

[a] *Rudjer Bošković Institute, Bijenička c. 54, 10000 Zagreb, Croatia. E-mail: nikola.biliskov@irb.hr*
[b] *Department of Chemistry, McGill University, 801 Sherbrooke St. West, Montreal, QC, H3A 0B8, Canada*

Infrared spectroscopy

An historical overview

The history of IR spectroscopy contains numerous admirable manifestations of scientific passion and ingenuity. The initial period was marked by key discoveries that paved the way for the emergence and development of IR spectroscopy in the full sense of the term (Fig. 1). The understanding of the real meaning of spectra in general is outside the reach of classical physics. However, this did not hinder researchers in their efforts to obtain the highest quality spectra, which led to exciting developments of instrumentation, reaching into the hitherto inaccessible microscopic phenomena.

The very birth of IR spectroscopy can be attributed to experiments performed by Wilhelm Herschel in 1800, which lead to the discovery of infrared radiation.[24] Further developments of the instrumentation include Seeback's discovery of thermoelectricity, Becquerel's application of the thermoelectric effect for precise temperature measurements and Nobili's invention of thermopiles.[25] These discoveries lead to measurement of the Sun's spectrum by J. F. W. Herschel in 1840.[26] The third crucial moment in the early history of IR spectroscopy was Langley's application of Svanberg's bolometer,[27] a highly sensitive thermometer, that enabled an enormous increase in

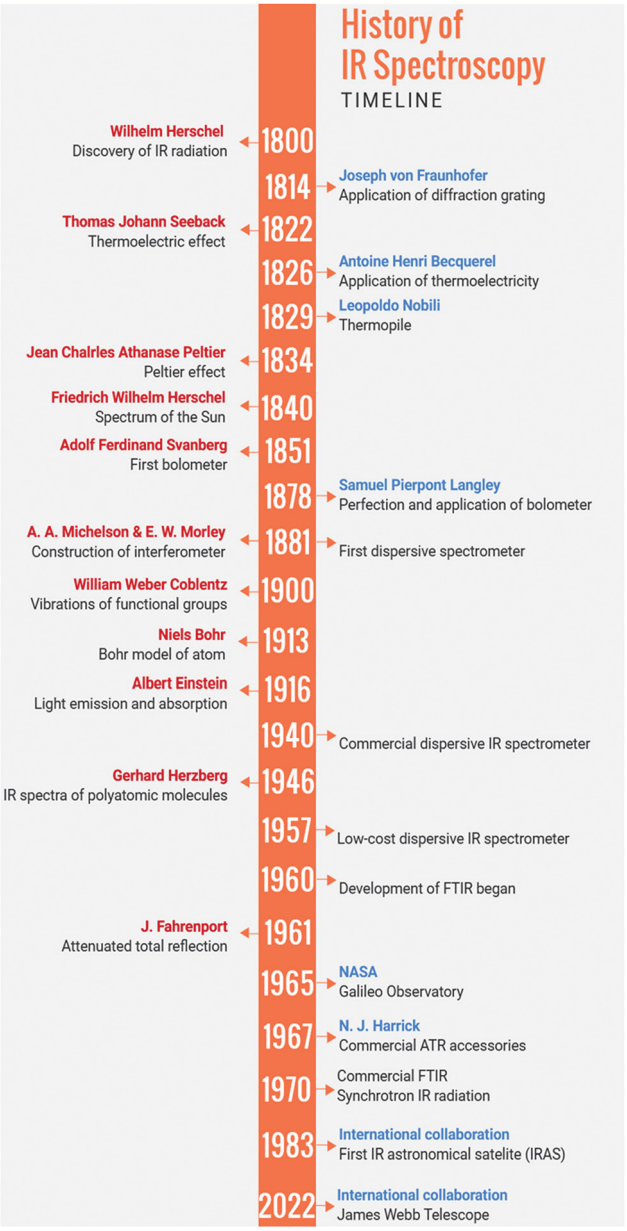

Fig. 1 The timeline of IR spectroscopy. Fundamental discoveries are listed on the left, while breakthrough instrumental developments are shown on the right.

temperature sensitivity, thus allowing measurements of temperature with respect to a particular wavelength. This finally gave rise to the emergence of the first dispersion of instruments in 1881.[28]

In the full sense of the word, the development of IR spectroscopy began in the early 1900s, when William Weber Coblentz demonstrated that chemical functional groups exhibited specific and characteristic absorption features in the mid-IR region of the spectrum. In this early work, Coblentz collected the IR spectra of 135 compounds with high accuracy.[29] This pioneering work paved the way for the use of IR spectroscopy in experimental chemistry in the first few decades of the twentieth century.[30] It was enabled by the rapid development of quantum mechanics[31] and Einstein's theory of the interaction of light and matter,[32,33] which explained the origin and appearance of atomic and molecular spectra, thus enabling their proper interpretation.

The first generation of commercial spectrometers began to appear in the 1940s, and the first low-cost instruments emerged in 1957. These instruments were dispersive IR spectrometers, and they were used exclusively until the emergence of commercial Fourier-transform (FTIR) IR spectrometers. In dispersive spectrometers, the radiation emitted from the source is dispersed by a monochromator (prisms, gratings, or their combination and slits) into its component frequencies, which pass through the sample, and the intensity of transmitted radiation at each frequency is measured. Thus, the acquisition of a typical spectrum required several minutes. This is acceptable in the case of samples not subject to any external change. However, this slow spectral acquisition speed was often a serious drawback, which prevented monitoring dynamic processes.

Thus, a crucial breakthrough in the history of IR spectroscopy was the replacement of the optical dispersion system with a Michelson interferometer, which largely overcame the above mentioned critical drawback of dispersive instruments. In fact, this is an adapted version of the interferometer used by Michelson and Morley in their historical experiment on propagation of light through the hypothetical 'luminiferous aether'. The original interferometer was described in two papers by Albert Abraham Michelson,[34,35] while Lord Rayleigh instantaneously recognised the relation of an interferogram with a spectrum through Fourier transformation.[36]. However, being far ahead of its time, full utilisation of this concept had to wait more than 50 years, when computers enabled the required calculations in an acceptable time. Although the development of FTIR during the 1960s followed three different lines, utilisation of the Michelson interferometer enabled rapid scanning. Its combination with a He–Ne laser fringe referencing system enabled high resolution, thus giving rise to commercial breakthroughs, starting in 1970, giving rise to the widespread presence of FTIR spectrometers in chemical laboratories.[37,38]

Modern low-cost benchtop FTIR spectrometers are extremely easy to use and are able to record high-quality, reproducible and accurate spectra in only a few seconds. Also, the availability of various commercial accessories, and those developed by researchers themselves, make IR spectroscopy one of the most common, practical techniques in contemporary chemistry, physics and materials science. Modern commercial FTIR spectrometers are able to acquire high-resolution (less than 1 cm^{-1}) spectra with Δt up to 4 ns, with a diffraction-limited lateral resolution ($\Delta x \leq 3$ μm).

FTIR spectrometers – basic principles

In order to use FTIR spectrometers to their full capacity, it is important to understand their basic functional principles. For a more elaborate description of applications of Fourier transformation in spectroscopy the reader is directed to other sources.[39]

Most generally, any FTIR spectrometer consists of an IR source, laser, Michelson interferometer, sample compartment

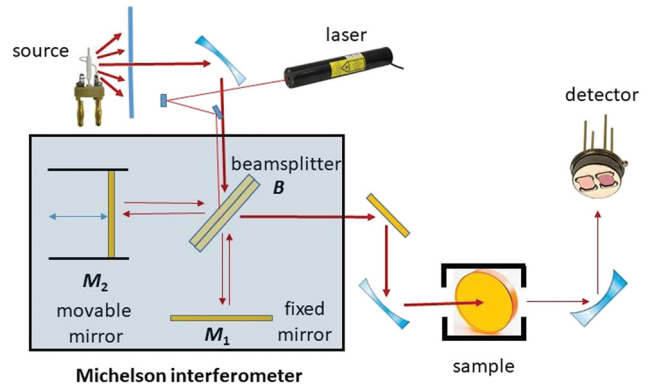

Fig. 2 Scheme of the FTIR spectrometer. IR radiation is shown by red arrows.

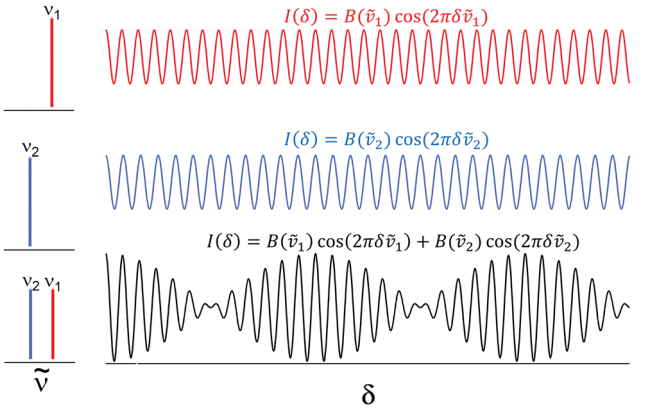

Fig. 3 The interferogram of the monochromatic source is a simple cosine function, and the periodicity is determined by the frequency of the incident light. In the case of a two-frequency (ν_1 and ν_2) source, the resulting interferogram is a linear combination of individual interferograms.

and detector (Fig. 2). As a source of IR radiation, a heated element or glower is used, which is practically considered as a black body radiator, emitting a continual IR spectrum. The emitted light is collimated and the optical system directs it towards the beamsplitter of the Michelson interferometer. The resulting beam then passes through another optical system that focuses it at the position of the sample. The sample partially absorbs the incident light, and the frequency-dependant intensity of the final beam is measured by a detector.

As the central part of the FTIR spectrometer, principal understanding of the Michelson interferometer is crucial for understanding the function of the whole spectrometer. The Michelson interferometer is an optical system consisting of two perpendicular mirrors M_1 and M_2, and semi-transparent beamsplitter B (Fig. 2). Mirror M_1 is fixed, while M_2 is moving. The collimated IR beam comes from the source to the beamsplitter, which for mid-IR, is usually a KBr or CsI supported on a thin film of germanium. It transmits and reflects the incoming IR radiation, sending it simultaneously to M_1 and M_2. Thus, two separate beams are created from the original incident light.

Now, light is reflected from both fixed M_1 and movable mirror M_2 back to the beamsplitter, where the beams combine. The beam which reaches the sample and detector is a sum of these two beams. It is now obvious that the intensity of the resulting beam (I) is directly correlated to the optical path difference δ, which is,

$$\delta = 2(|M_2B| - |M_1B|)$$

(factor 2 comes from the fact that the light travels back and forth from the mirrors); and the wavelength of the light λ.

Consider first the simplest case of monochromatic (single-frequency) light. If $\delta = 0$, the two beams are in phase at the beamsplitter, giving a maximal resulting intensity, $I(\delta)$. However, if M_2 is displaced by $\lambda/4$, it gives the optical path difference of $\delta = \lambda/2$, and the two beams are 180° out of phase and $I(\delta) = 0$. By further movement of the M_2, $I(\delta)$ reaches maxima when δ is an integral multiple of $\lambda(\delta = n\lambda; n = 0, \pm1, \ldots)$ and minima when δ is an odd multiple of $\lambda/2$ $(\delta = (n + 1/2)\lambda)$, giving an interferogram, which follows the cosine function (in terms of wavenumbers $\tilde{\nu} = 1/\lambda$):

$$I(\delta) = B(\tilde{\nu})\cos(2\pi\delta\tilde{\nu}) \quad (1)$$

where $B(\tilde{\nu})$ stands for the intensity of the incident light.

If the light consists of more than one frequency, each frequency can be treated separately, and the resulting interferogram is a sum of individual contributions (Fig. 3), *i.e.* linear combination of contributions given by eqn (1):

$$I(\tilde{\nu}) = \sum_{\tilde{\nu}_1}^{\tilde{\nu}_n} B(\tilde{\nu}_i)\cos(2\pi\delta\tilde{\nu}_i). \quad (2)$$

The spectrum of incident IR light in FTIR spectrometers is a continuum, so summation (2) should be represented as an integral:

$$I(\tilde{\nu}) = \int_0^\infty B(\tilde{\nu})\cos(2\pi\delta\tilde{\nu})\mathrm{d}\tilde{\nu}. \quad (3)$$

The interferogram is shown in Fig. 3. For precise wavelength calibration of the interferogram, a He–Ne laser ($\lambda = 632.8$ nm) is used as an external monochromatic source. At $\delta = 0$, the interferogram of all the present frequencies are in phase, which results in a strong maximum (centerburst). Outward of the center in either direction, the multidinous cosine contributions start to reinforce and cancel each other, so the intensity of the interferogram rapidly decreases into a series of oscillations of lower amplitude. If the source of radiation contains less spectral information, the oscillations decrease more rapidly. Additionally, higher resolution spectral information is contained further out of the center in the interferogram. So, the spectral resolution $\Delta\tilde{\nu}$ increases with δ_{max},

$$\Delta\tilde{\nu} = \frac{1}{\delta_{max}}, \quad (4)$$

however, strictly speaking, this resolution is in practice, compromised by truncation and apodization.

The obtained interferogram represents intensity as a function of time $I(t)$. It is translated into a readable spectrum $B(\tilde{\nu})$ (Fig. 4), expressed by its Fourier pair,

$$B(\tilde{\nu}) = \int_{-\infty}^{\infty} I(\delta)\cos(2\pi\delta\tilde{\nu})\mathrm{d}\delta. \quad (5)$$

Modern algorithms do this translation by fast Fourier transformation (FFT).[39]

To obtain a complete spectrum, as presented by eqn (5), integration must be performed from $-\infty$ to $+\infty$, which is practically impossible. Thus, in practice spectra are obtained by truncating the full interferogram, *i.e.* by limiting it to a finite interval. The original interferogram is convoluted with some function $R(\delta, \delta_{max})$. This process is known as apodization. The simplest apodization function is Boxcar. However, since it significantly distorts the band shape, in practice the most commonly used apodization functions are trianglular and Norton–Beer functions, which minimize the influence of the apodization process on band shape.[39]

In practice, the most usual setup of the Michelson interferometer for FTIR provides continuous-scan interferometry, where the mirror M_2 moves continuously at a constant velocity v, and the optical path difference in time t is given by $\delta = 2vt$. Continuous-scan interferometry is preferred for routine static or relatively slow kinetic measurements that require time resolution no faster than 20 ms. For highly dynamic processes occurring at rates faster than a 20 ms time scale, continuous-scan is no longer applicable, because the temporal Fourier frequencies become convolved with the time-dependence of the processes.

This problem is overcame with step-scan interferometry, which provides advantages for spectroscopic measurements of dynamic processes, where the signal is phase- or time-dependent.[40–42] In a step-scan setup, the mirror M_2 moves incrementally in steps. In this way, the interference of the Fourier modulation encountered in continuous-scan FTIR is overcome, which enables measurements with an explicit function of phase, time, or space.[41] Thus, typical applications of step-scan FTIR are phase-resolved spectroscopy for modulation experiments, such as photoacoustic depth profiling[43,44] and polymer rheo-optical characterization[45] and time-resolved spectroscopy[9,46] for fast kinetic processes down to nanosecond time scales.

Today, depending on the time resolution required, a number of additional advanced interferometric techniques are available. They are based on rapid[9] and ultra-rapid scanning,[47] stroboscopic sampling,[48] or asynchronous sampling.[49] These techniques are capable of covering time domains from seconds to picoseconds.[50–52] IR spectroscopic insight to even faster phenomena, which occur at the femtosecond time scale, are enabled by the recent development of advanced laser pump–probe methodologies.[53–57] The range of mid-IR electromagnetic waves covers the ~10–300 fs region, which defines the limit of time resolution that can be achieved by IR spectroscopy.

Since the FTIR spectrometers are single-beam in their performance, recording of background is required before the acquisition of the spectrum of a sample (Fig. 4). The background spectrum is practically the black-body spectrum of the IR source, partially influenced by the contents of the medium through which the beam is propagated. This means that the

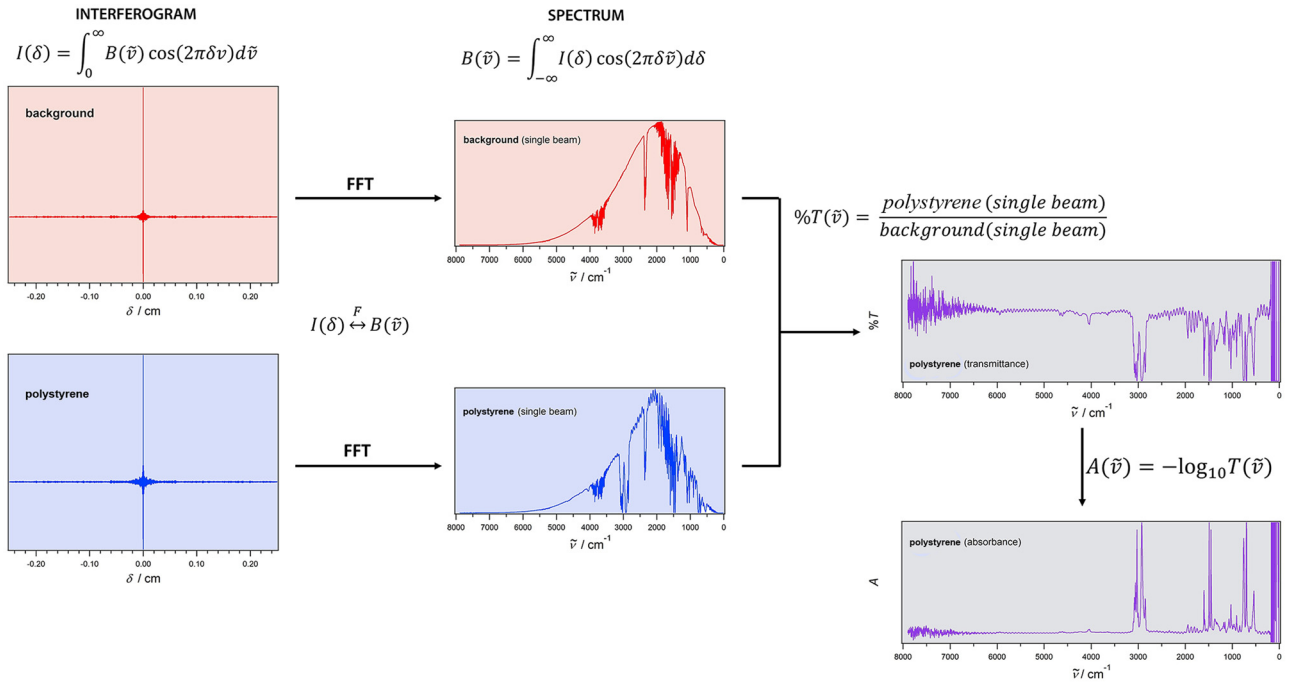

Fig. 4 The generation of IR spectra by FTIR spectroscopy. Two interferograms – the background and sample – were collected and transformed by means of FFT to single beam spectra, which are then combined (divided), giving the transmission (%*T*) spectra. The absorption spectrum, which is linear in Lambert–Beer's law, is then easily obtained. A spectrum of polystyrene is used here for illustration.

background spectrum, if recorded in ambient conditions (normal atmosphere), will contain bands due to H_2O and CO_2, which are IR active components of the air. Single beam spectra, as obtained by passing the IR beam through the sample, will be a superposition of the spectrum of the sample and spectrum of the atmosphere. Division of two of them will give rise to a transmission spectrum:

$$T(\tilde{\nu}) = \frac{B(\tilde{\nu})_{\text{sample}}}{B(\tilde{\nu})_{\text{background}}}. \quad (6)$$

Although $T(\tilde{\nu})$ is the most common form in which IR spectra are presented, one should be aware that Lambert–Beer's law is linear in absorbance $A(\tilde{\nu})$, and not in transmittance:

$$A(\tilde{\nu}) = \varepsilon(\tilde{\nu})cl \quad (7)$$

where $\varepsilon(\tilde{\nu})$ is the molar absorption coefficient, c is concentration, and l the path length of light through the sample. Thus, in some cases it is more convenient to translate the transmittance to absorbance spectra:

$$A(\tilde{\nu}) = -\log T(\tilde{\nu}). \quad (8)$$

At the end of this introduction to basics of FTIR spectroscopy, it should be underlined that in most cases a satisfactorily acceptable approximation of IR spectra, as obtained by a FTIR spectrometer, are practically identical to those obtained by a dispersive IR spectrometer. However, the use of the term "FTIR spectrum" is widespread in the literature, so this requires a brief terminological note. The spectroscopic technique is correctly named FTIR spectroscopy, since in this technique Fourier transform is used to obtain the spectra from interferograms, which are output signals from a FTIR spectrometer (*i.e.* IR spectrometer with Michelson interferometer). However, the resultant spectra are not FTIR, but IR, since the spectrum is information on the interaction of electromagnetic radiation, in this case IR, with a sample. The only difference is in the very delicate details of band shape, which are due to the apodization process. However, this distortion from a natural band shape is important only in strict analyses. In the vast majority of cases, especially in *in situ* process monitoring, a relative change is of central interest, not absolute values of parameters of band shape and intensity.

The basics of *in situ* spectroscopic monitoring

In general terms, spectroscopy is any measurement of the absorption or emission of light and other radiation by matter. Thus, to perform a spectroscopic measurement, one needs a source of light, the optical system that enables separation of individual frequencies of light, a sample and a detector, which measures frequency-dependant intensity of resulting light (Fig. 5(a)). In these terms, the spectrum is simply given by:

$$A(\tilde{\nu}) = \frac{I(\tilde{\nu})}{I_0(\tilde{\nu})} \quad (9)$$

where I_0 and I are frequency-dependant intensities of incident and transmitted light, respectively.

Since the frequencies of the radiation in the IR part of the electromagnetic spectrum correspond to frequencies of intra- and intermolecular vibrations, they mutually resonate.[58–65] Thus, IR spectra result from transitions between quantized

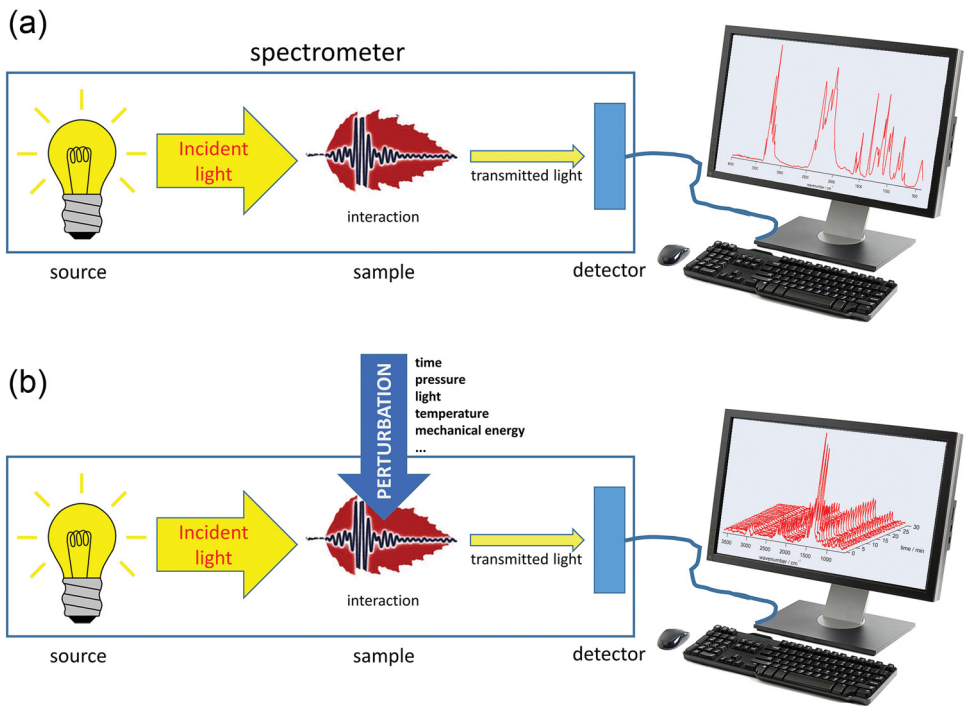

Fig. 5 General scheme of (a) spectroscopy and (b) *in situ* spectroscopy. In *in situ* spectroscopy, the sample is subject to a perturbation, and the resulting spectra reflect changes in the sample as a function of applied perturbation.

vibrational energy states. Basically, if the symmetry of a vibration mode makes it IR active, it will be manifested as an IR spectral band.[31,58,64] Molecular vibrations can range from the simple coupled motion of the two atoms of a diatomic molecule to the much more complex motion of each atom in a large polyfunctional molecule, as well as supramolecular aggregates bound by intermolecular forces. Although information on molecular structure is provided by numerous experimental techniques and the information that can be deduced by IR spectroscopy is complementary to that of other methods, it also provides valuable information on intra- and intermolecular dynamics and interactions, unattainable by other methods. This is especially enabled by the high sensitivity of molecular vibrations to present environmental conditions, which is evidently reflected in parameters of IR spectral features of individual functional groups.

In practice, this means that a change in environmental conditions, such as concentration, temperature, pressure, light, application of mechanical force *etc.* or just a mere passage of time, on the molecular level, will affect the vibrations of particular functional groups (Fig. 5(b)). In IR spectra, this change in vibration will be observed as change of some or all parameters of the spectral band due to this vibration.

Generally, the IR spectral band (Fig. 6) is defined by position $\tilde{\nu}$ at which it reaches maximal absorbance A, intensity I, *i.e.* the area under the band, and full width at half maximum FWHM (Γ). The band lies at the baseline. In the ideal case, the baseline is constant $y = y_0$, and the band shape is described by the Lorentzian:

$$y = y_0 + \frac{\frac{1}{2\pi}\Gamma}{(x - \tilde{\nu}_{\max})^2 + \left(\frac{1}{2}\Gamma\right)^2} \quad (10)$$

or Gaussian function:

$$y = y_0 + A \exp\left[-\left(\frac{x - \tilde{\nu}_{\max}}{\Gamma}\right)^2\right]. \quad (11)$$

It can also be described by their combination, among which the Voigt function has the most direct physical meaning.

In reality, IR spectral bands are associated with higher or lower resolved envelopes on a non-constant and generally nonlinear baseline (Fig. 6b). This prevents the direct extraction of spectral parameters from recorded spectra. In practice, they are derived by fitting the spectral envelope to an appropriate model function (Fig. 7).[66] The accurate parameters, as obtained by fitting, are used in further analysis.

As noted earlier, the purpose of *in situ* IR spectroscopy is not to give information in absolute values of spectral parameters, but to provide accurate quantitative information on their trends, relative to some reference, as a response to applied perturbation. Thus, data analysis of *in situ* measurements comes down to derivation of accurate kinetic parameters from absorbances or intensities or changes in chemical identity of the system from band position or width. Besides curve fitting, data on perturbation-induced evolution of the chemical system can be obtained by other statistical methods, among them factor analysis is the most widely used.[67,68]

In this field, the term '*operando*' is very frequently used to describe the measurement approach. However, a very subtle difference between the terms '*operando*' and '*in situ*' often leads to confusion among readers, due to the frequently incorrectly used terms. For this reason, it is worth making a brief comment on the differences between *operando* and *in situ* techniques at this point. In fact, all *operando* measurements are *in situ*, but not all *in situ* measurements are *operando*. '*In situ*' has always referred to a measurement of the system performed under relevant reaction conditions. On the other hand, '*operando*' refers to measurements of the system under realistic reaction conditions, where the reaction products are measured.[69] For example, the measurement of the behaviors of the catalyst in the conditions relevant to practical catalytic operation is *in situ.* On the other hand, *operando* measurements combine *in situ* characterization of a working catalyst during genuine reaction conditions with simultaneous measurement of catalytic performance, such as monitoring of formation of intermediates and products. There are numerous examples of the misuse of this terminology, and here just a few illustrative examples are mentioned. Although the term '*operando*' mainly refers to what it actually is, *i.e.* monitoring of chemical processes with simultaneous measurement of reaction products,[70] it is very frequent

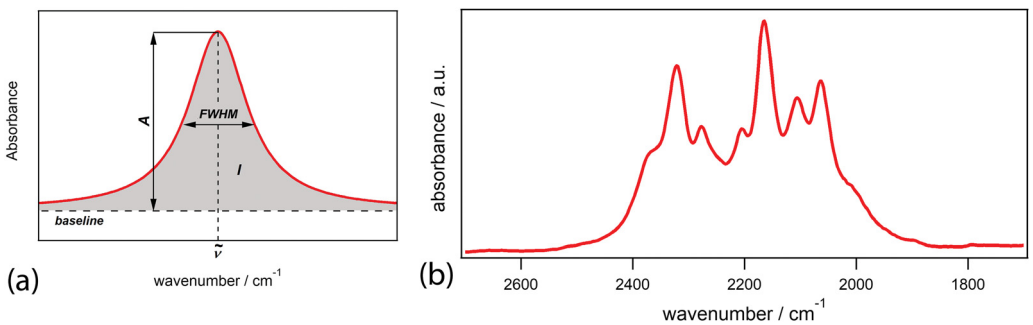

Fig. 6 IR spectral band: (a) ideal Lorentzian band with its parameters. The band lies on a baseline at y_0. Band height A is defined as the difference between the maximal absorption at peak position $\tilde{\nu}_{\max}$ and y_0, intensity I is the area under the band profile and FWHM is full width at half maximum. (b) A real IR spectrum generally consists of envelopes rather than individual bands.

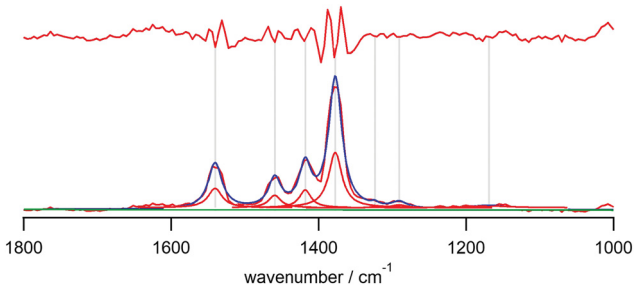

Fig. 7 IR spectral envelopes consist of higher or lower resolved bands, whose parameters are obtained by fitting to Lorentzian or Gaussian functions (red). The sum of the thus obtained contributions model the real spectrum (blue). The difference between the real and modelled spectrum is shown with the red curve above the spectrum (not to scale).

that studies titled '*in situ*' are focused on monitoring the evolution of chemical species during reactions,[71] especially products, which is often evident even from the publication title.[72] For the sake of terminological simplification without losing the essence, exclusively the term '*in situ*' will be used further in this text.

A variety of commercially available spectroscopic accessories are useful for *in situ* measurements. However, specific systems often require adjustments of existing, or the development of, completely novel experimental setups. Due to the universally valid law of conservation of energy, interaction of incident light I_0 with a sample, results in transmission I_T, absorption I_A, reflection I_R and scattering I_S of light (Fig. 8):

$$I_0 = I_A + I_T + I_R + I_S \quad (12)$$

Thus, basic experimental geometries, namely transmission, specular reflection, diffuse reflection (Fig. 8) and attenuated total reflection (ATR), are common to all the techniques.

Transmission. In transmission measurements, the incoming light simply passes through the sample, which results in transmitted light, partially absorbed by the sample, so the transmittance T is given by:

$$T(\tilde{\nu}) = \frac{I_T(\tilde{\nu})}{I_0(\tilde{\nu})}. \quad (13)$$

Normal incidence is required to minimize reflection from the surface of the sample. This geometry is in principle, applicable to samples in all aggregate states.

Transmission IR spectroscopic measurements of powders are usually made by use of KBr pellets, but also some other alkali halide salts can be used for this purpose.[73] These matrices are used due to their high transparency over a wide IR region (Table 1). In order to maximize reproducibility of measurements, the mixture should be finely ground and homogenized. At this point one should be aware that ideal homogeneity of the pellet is never achieved, which is especially the case for *in situ* measurements, where a perturbed sample changes its physical and chemical properties. This causes formation of agglomerates, cracks *etc.* Additionally, particles bigger than 2 μm have a refraction index which significantly differs from KBr result in the Christiansen effect. In this case, the absorption coefficient κ of the complex refraction index, $\hat{n}$:

$$\hat{n}(\tilde{\nu}) = n(\tilde{\nu})[1 - i\kappa(\tilde{\nu})] \quad (14)$$

becomes smaller than the dispersive contribution n due to its increase, which is then manifested in artefacts in the form of spikes that accompany spectral bands.[74] One should also be aware that alkali halides are not necessarily chemically inert with respect to the sample.[75,76]

As an alternative to pellets, mulls, usually in liquid paraffin (Nujol), Fluorolube® (a chlorofluorocarbon polymer) or hexachlorobutadiene can be used. However, all of these matrices have some bands in the mid-IR region, so this technique is reserved for samples that interact with alkali halides.[77,78]

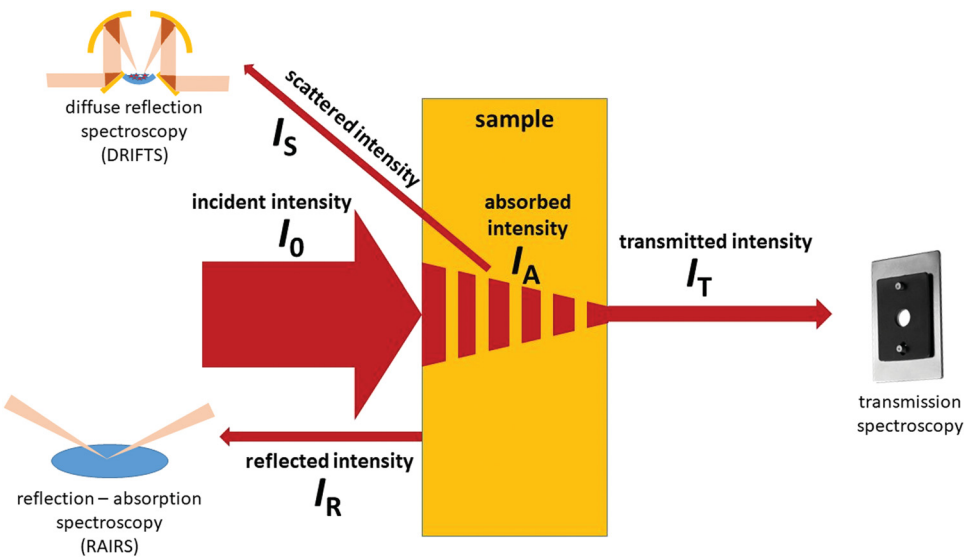

Fig. 8 Balance of radiative energy upon interaction with a sample and corresponding spectroscopic techniques.

Table 1 Materials that are transparent in the mid-IR region that are suitable for transmission and ATR measurements

Material	Transparency range (cm^{-1})	Refraction index (20 °C)	Use	Comments
KBr	40 000–400	1.5	Windows, pellets	Soluble in water and alcohol
NaCl	33 000–625	1.55	Windows, pellets	Soluble in water, slightly soluble in alcohol
CsI	33 000–160	1.74 (1000 cm^{-1})	Windows, pellets	Soluble in water and alcohol
CaF_2	50 000–1000	1.4	Windows	Soluble in solutions of ammonium salts
Si	6700–1000	3.5–3.4	Windows, ATR	Hard
Ge	5000–660	4.1–3.9	ATR	Soluble in HCl + HNO_3 mixtures, and H_2O_2
Diamond	50 000–500	2.4	ATR	Extremely hard and inert
ZnSe (Irtran-4)	16 700–660	2.5–2.3	ATR	Soluble in acid, slightly soluble in water
ZnS (Irtran-2)	20 000–550	2.3–2.0	ATR	Soluble in acid, slightly soluble in water
TlBr + TlI (KRS-5)	33 000–250	2.4	ATR, windows	Toxic, sensitive to organic solvents, slightly soluble in water
TlBr + TlCl (KRS-6)	25 000–250	2.3–2.2	ATR	Toxic, sensitive to organic solvents, slightly soluble in water
$Ge_{33}As_{12}Se_{55}$ (AMTIR-1)	10 000–714	2.5–2.6	ATR	
Al_2O_3 (sapphire)	50 000–2222	1.65 (2500 cm^{-1})	Windows, fibres, ATR	Very hard, highly resistant to acid and alkali up to 1000 °C
As_2S_3	12 500–1000	1.56	Fibres	Sensitive to water
Polyethylene	Down to far-IR	1.5	Windows	Strong absorption around 3000, 1500 and 720 cm^{-1}
Paraffin (Nujol)	50 000–600	1.46	Mulls	Strong absorption around 3000 and 1500 cm^{-1}
Fluorolube®	50 000–500	1.38	Mulls	

Soft or plastic samples are more suitable for the preparation of films. However, by passing light through the films where thickness is comparable to the wavelength of IR radiation, interference fringes of significant intensity are produced.

External reflection. In reflection measurements, the incoming light is reflected and partially absorbed from the optically flat surface of the sample. Similar to transmittance eqn (13), reflectivity R is expressed as:

$$R(\tilde{\nu}) = \left|r^2(\tilde{\nu})\right| = \frac{I_R(\tilde{\nu})}{I_0(\tilde{\nu})} \quad (15)$$

where r is the amplitude coefficient. Transmittance is related to reflectivity by:

$$T(\tilde{\nu}) = 1 - R(\tilde{\nu}),$$

which leads to:

$$I_T(\tilde{\nu}) = (1 - R(\tilde{\nu}))I_0(\tilde{\nu}). \quad (16)$$

Since the measured reflectivity depends on polarisation, the amplitude coefficient for parallel and perpendicular polarisation, respectively, are given by:

$$r_{\parallel}(\tilde{\nu}) = \frac{n_2(\tilde{\nu})\cos\alpha - n_1(\tilde{\nu})\cos\beta}{n_1(\tilde{\nu})\cos\alpha + n_2(\tilde{\nu})\cos\beta} \quad (17)$$

$$r_{\perp}(\tilde{\nu}) = \frac{n_1(\tilde{\nu})\cos\alpha - n_2(\tilde{\nu})\cos\beta}{n_1(\tilde{\nu})\cos\alpha + n_2(\tilde{\nu})\cos\beta}. \quad (18)$$

For absorbing media, the refractive index takes its complex form, eqn (14). Absorption index κ is related to absorption coefficient a and decadic molar absorptivity ε in the Lambert–Beer law (7):

$$\kappa(\tilde{\nu}) = \frac{a(\tilde{\nu})\lambda}{4\pi} = \frac{\varepsilon(\tilde{\nu})c\lambda}{4\pi \ln 10} \quad (19)$$

where c is the molar concentration of the sample, and λ is the wavelength of the light. Due to the complex form of the refraction index for the reflection spectra, they significantly differ from transmission spectra for the same sample. For this reason, the Kramers–Kronig transformation is used to translate reflection to transmittance.[79–81]

In reflection absorption IR spectroscopy (common abbreviations are RAIRS or IRRAS), the sample is placed on a highly reflective substrate, which can be optically flat or diffusively reflective (Fig. 8). In this geometry, the light passes twice through the sample, so effectively a transmission spectrum is obtained. From a very basic geometric consideration it is obvious that the pathlength through the sample increases with angle of incidence. The extreme case is grazing incidence technique, where the angle of incidence is maximized.

The output spectrum is a superposition of the spectrum of the bulk and the sample upon interaction with a substrate. A great advantage of RAIRS over other techniques for surface studies is the fact that it does not require a vacuum environment, making RAIRS one of the most common techniques for characterisation of phenomena at an interface.[82–84] The resulting spectrum, however, very much depends on the thickness of the sample. For thick films, *i.e.* those where pathlength is larger than wavelength ($l > \lambda$), the absorbance of light by the bulk sample dominates, so the measured absorbance values correspond to the pathlength, making the Lambert–Beer law valid. Thus, if one is interested in interactions of the sample with substrate, the sample should be as thin as possible. However, for $l \leq \lambda$, the field amplitude of the standing wave that emerges due to reflection regularly varies, and this effect becomes dominant for very thin films.[83,85–88] The grazing incidence technique is sensitive exclusively to the components of transition dipole moments normal to the reflecting surface. This makes it very important for studies of surface coatings, very thin films and adhesives, as well as studies of near-surface molecular orientation.[89]

It is important to note that the RAIRS spectra of thin films, especially those cast on partially reflective substrate, contain significantly intense fringes, which arise due to the interference of the IR light reflected from the upper and lower layer of the film. These interference fringes can completely shadow spectral features of interest, making the quantification of chemical or

physical changes derived from the spectra, highly inaccurate or impossible. To eliminate this problem, a variety of approaches were employed. This problem was first attacked by calculation of optical constants of the film[90] by applying classical Roessler's application of Kramers–Kronig transformations to analyze the reflection on thin films.[91–93] These initial attempts were enhanced by determination of the effective film thickness[94] and modification of the optical system.[95,96] Later advances brought about the method which in principle combines the two above mentioned approaches: first, the thickness and complex refractive index of the film in regions of little or no IR absorption are determined from interference fringes. This information is then used to calculate the fringe-free optical constant spectra by use of a Kramers–Kronig transformation.[97] This method, with some improvements, is today integrated to IR spectroscopic software and in routine use as a support for RAIRS.

Diffuse reflection. If the surface of the sample is rough at the range of the wavelength, the incident light will partially enter the substrate and will be partially scattered. The former part undergoes absorption within particles, diffraction at grain boundaries, and will re-emerge at the surface and combine with parts just reflected. The measured reflectivity includes all of the mentioned contributions.

The reflectivity of an optically indefinitely thick (I_T) R_∞ sample is:

$$R_\infty(\tilde{\nu}) = \frac{R_\infty(\tilde{\nu})_{\text{sample}}}{R_\infty(\tilde{\nu})_{\text{reference}}}. \quad (20)$$

Using the empirical Kubelka–Munk relation, it can be translated into the parameter $f(R_\infty)$, which is proportional to absorption:

$$f(R_\infty(\tilde{\nu})) = \frac{[1 - R_\infty(\tilde{\nu})]^2}{2R_\infty(\tilde{\nu})} = \frac{k(\tilde{\nu})}{s} \quad (21)$$

where k represents absorption, and s the scattering contribution, and they vary with particle size and packing density. It is assumed that the sample is weakly absorbing, and the scattering contribution s is independent of frequency, which is justified by proper preparation of the sample.

In the mid-IR spectral range, diffuse reflectance is very weak and it became practical only with the breakthroughs of commercial FTIR spectrometers. It is known under the acronym DRIFTS (diffuse reflectance infrared Fourier-transform spectroscopy).[98] Due to the lack of efficient non-absorbing scattering substrates in the mid-IR, relatively large ellipsoidal mirrors are used in order to capture as many scattered photons as possible.[99]

Attenuated total reflection (ATR). In attenuated total reflection, the incoming light passes through the highly refractive crystal, and is totally reflected at the interface between crystal and sample (Fig. 9). The sample partially absorbs (attenuates) the light, and the reflected beam is measured. Since this technique is easy to use and practically does not require any sample preparation, it has become one of the most widespread

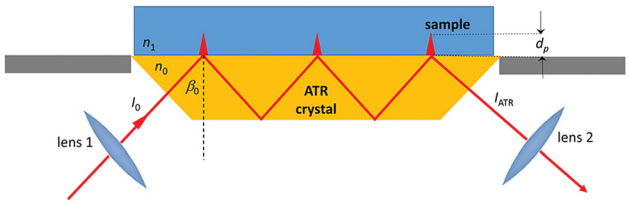

Fig. 9 ATR experiment. In this case, the incident light is triple reflected at the angle β_0 on the boundary between an optically dense crystal n_0 and sample n_1, where $n_0 > n_1$. The evanescent wave, which penetrates the sample by d_p, is shown by red triangles.

techniques in contemporary IR spectroscopy. The popularity of ATR was also boosted by the enormous increase of accessibility of water-containing systems.[100]

The crucial part of ATR is the precisely processed highly refractive crystal (Table 1). The optical system, consisting of plane mirrors and lenses, directs the incident light normally to the crystal. The light is then at least one or more times totally reflected on the interface between optically dense crystals and the sample, which is applied to the exposed face of the crystal. In its design, ATR accessories can allow single- or multiple reflections, as well as fixed or variable angles of incidence (Fig. 10).[101,102]

According to Snell's equation for refraction:

$$n_0 \sin \beta_0 = n_1 \sin \varphi \quad (22)$$

where n_0 and n_1 are the refractive indices of the optically denser and more loosely packed medium, respectively, β_0 is the angle of incidence and reflection, while φ is the angle between the transmitted light and normal of the boundary. Amplitudes of reflected light r are polarisation-dependent and are given by Fresnel equations:

$$r_\parallel(\tilde{\nu}) = \frac{\tan(\varphi(\tilde{\nu}) - \beta_0)}{\tan(\varphi(\tilde{\nu}) + \beta_0)}$$

$$r_\perp(\tilde{\nu}) = -\frac{\sin(\varphi(\tilde{\nu}) - \beta_0)}{\sin(\varphi(\tilde{\nu}) + \beta_0)}$$

Evidently, there is some critical angle of incidence β_c (Brewster angle), for which extinction of the transmitted light is given by:

$$R_T = 0 \quad \forall \quad \beta_0 \geq \beta_c.$$

In this case, the light will be entirely reflected, *i.e.* angle φ becomes imaginary, and this is total reflection. From the condition

$$\sin^2 \beta_0 > {n_{10}}^2$$

of eqn (22), where $n_{10} = n_1/n_0$, imaginary φ is given by:

$$\cos \varphi = \sqrt{1 - \sin^2 \varphi} = i\frac{\sqrt{\sin^2 \beta_0 - {n_{10}}^2}}{n_{10}}$$

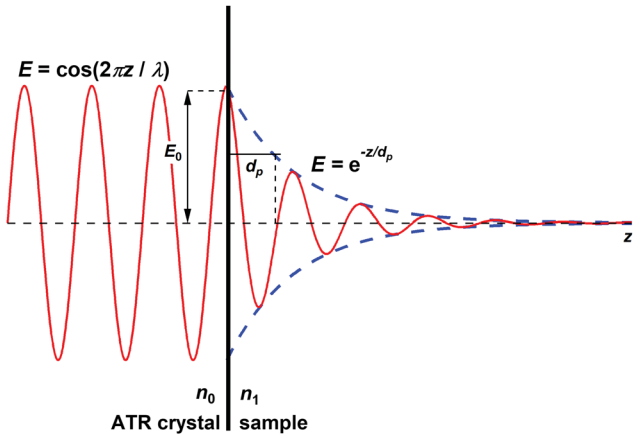

Fig. 10 Behaviour of the E component of incident light at the boundary between the ATR crystal and sample.

and now the Fresnell equations take the following form:

$$r_{\parallel} = \frac{n_{10}^2 \cos\beta_0 - i\sqrt{\sin^2\beta_0 - n_{10}^2}}{n_{10}^2 \cos\beta_0 + i\sqrt{\sin^2\beta_0 - n_{10}^2}}$$
$$r_{\perp} = \frac{\cos\beta_0 - i\sqrt{\sin^2\beta_0 - n_{10}^2}}{\cos\beta_0 + i\sqrt{\sin^2\beta_0 - n_{10}^2}}. \quad (23)$$

However, in his pioneering paper, which introduced ATR, Fahrenport showed that the radiation incident from the optically dense dielectric crystal on its boundary with an optically rare sample at an angle $\beta_0 \geq \beta_c$ will be totally reflected, but only in those frequency regions where the sample does not absorb (where $\kappa = 0$). In regions where $\kappa \neq 0$, reflection will not be total anymore and, accordingly, a spectrum is obtained, which strongly resembles a transmission spectrum. Reflectivity is again given by eqn (23), but refraction index of the sample becomes complex (eqn (14)). The absorbing sample thus causes a perturbation or frequency-dependent attenuation of the totally reflected light. The incident light penetrates the sample, while the frequency is preserved, but the amplitude of electric field E exponentially decreases with distance from the boundary between the ATR crystal and sample:

$$E(\tilde{\nu}) = E_0 e^{-\frac{z}{d_p(\tilde{\nu})}} \quad (24)$$

where z is distance from the boundary, d_p is penetration depth, *i.e.* distance from the boundary at which $E = E_0 e^{-1}$, and is given by:

$$d_p(\tilde{\nu}) = \frac{\lambda_0}{2\pi\sqrt{\sin^2\beta_0 - \left(\frac{n_1(\tilde{\nu})}{n_0(\tilde{\nu})}\right)^2}} \quad (25)$$

where λ_0 is wavelength of the light in the optically denser medium.

The penetrating field E is built on the sinusoid wave on the boundary. It is important to note in eqn (25) that light of bigger λ will penetrate deeper inside the sample, and generally the d_p is not directly transferable to l for transmission geometry. Thus, ATR spectra are not simply related to transmittance, and for this translation the Kramers–Kronig transformation is required, which resolves the real from imaginary part of the complex refraction index, and absorbance is then obtained from κ.[80,100] Further, attenuation by the sample, which is to a higher or lower extent present in the whole spectral region, causes $R(\tilde{\nu}) < 1$, and is given by:

$$R = (1 - a)^{N_R}$$

where a is an absorption parameter and N_R the effective number of reflections, which is obtained from the N, defined by the geometry of ATR element of thickness D:

$$N = \frac{1}{D}\cot\beta_0 \quad (26)$$

which is corrected by taking into account experimental conditions, such as convergence of the beam, diffraction of the parallel polarized component of incident radiation *etc.*[101] However, for the purposes of *in situ* measurements, since only the relative values with respect to the reference spectrum are of importance, these considerations are not required in the majority of cases.

With its ease and flexibility with respect to the nature of sample, ATR is now, together with transmission, the most commonly used technique for the acquisition of IR spectra. Since its applicability encompasses coatings, films, polymers, adhesives *etc.*, it practically pushed out the mull technique. The sample only has to be brought into optical contact with the ATR crystal, which is in practice done with the use of a press. Incident light undergoes single or multiple internal reflections. The bevel edges of the crystal can be flat (for fixed β_0) or rounded (which allows variable β_0). Multireflection crystals could be of trapezoidal, parallelepiped or rod shape. Single-reflection ATR crystals are trigonal prisms in shape. Most commonly used materials are ZnSe, or Ge for multiple-reflection ATR, while for single-reflections, diamond is most commonly used (Table 1).

Physical processes

By definition, physical processes do not influence the chemical identity of the sample. However, they influence the arrangement of the molecules and pattern of intermolecular contacts, thus changing their properties on the macroscopic scale. As it is very sensitive to changes in the molecular environment, IR spectroscopic techniques provide important information on the molecular background of these macroscopic changes.

Mechanics

Needless to say, mechanical properties are crucial for the end-use of numerous materials. Mechanical properties refer to both elastic and plastic deformations as well as fractures which occur under the action of applied load on the molecular crystals. Thus, understanding microscopic manifestations of macroscopic forces, applied to materials from outside, is of

considerable interest. As it is sensitive to the orientation of dipole moments, as well as molecular environments, IR spectroscopy provides a unique means of understanding both the static and dynamic molecular structure of materials. Studies of molecular background of elastic deformation or pressurization, *i.e.* changes in molecular orientation initiated by applied force from outside, are by far the most common in this field.

Elasticity, *i.e.* the ability of a material to return to its original shape after being stretched or compressed, is an important property of polymers. When relaxed, polymeric molecules are disordered. When stretched, they fold in parallel threads. To investigate the elasticity of polymeric materials, Siesler introduced rheo-optical FTIR,[103–105] which enables the recording of IR spectra of elastic materials simultaneous to its stretching and heating or cooling. The theoretical background of the technique has also been well established by the same group.[103] The monitoring of the response of specific vibrational bands to an applied force and temperature recover information on the orientation and orientational relaxation in bimodal blends of PMMA, as well as the strain-induced crystallization of the soft segments during cyclic elongation and recovery of polyurethane elastomers.[104] Conjugated polymers have attracted much attention as semiconductive materials for use in flexible devices, but they are generally more rigid than conventional plastics. Nishino *et al.* applied a combination of X-ray diffraction and polarized IR microspectroscopy to understand the response of crystallites and individual molecules of the amorphous bulk of polythiophene, to stretch and the addition of disiloxane. In this way, the change in orientation of the crystallites by addition of disiloxane, while the polarization-dependent IR absorption bands are more sensitive to stretch, shows that the amorphous bulk of the polymer is responsive to mechanical strain.[106]

Pressure-induced effects on structure and properties of various materials are of considerable interest in materials science. Thus, high-pressure IR (HP-IR) spectroscopic studies are used widely to understand systems, such as strongly correlated electron systems (SCES).[107] Additionally, regular molecular solids under high pressure have also attracted a great deal of attention in this respect. The examples of HP-IR spectroscopic measurements include ice,[108] dense nitrogen,[109] hydrogen,[110] and their mixtures.[111] Another field, highly targeted by HP-IR techniques are the Earth and planetary sciences.[112–114] In this respect, various minerals at high pressures have been studied using IR spectroscopy to understand their properties in the deep interior of Earth and other planets.[115–117] From an application point of view, HP-IR has important implications in industries such as in pharmaceuticals, photonics, *etc.*

Accordingly, HP-IR instrumentation developed by different groups has been reported.[118–126] A diamond anvil cell (DAC)[127,128] is most commonly used as the central part. Ruby particles are used for the precise measurement of the pressure inside a DAC.[129] Due to the quite limited space inside the cell, synchrotron radiation as a brilliant source of IR light is required to obtain accurate spectra.[107] The combination of HP cells with synchrotron sources significantly expanded the scope of these investigations. Such enormous progress in HP science revolutionized the ultrafine characterization of condensed matter.[10] This is particularly true for synchrotron-based IR microspectroscopy (SIRMS) with its extended measurement conditions enabled by the very high signal-to-noise ratio, spatial resolution and sensitivity. In order to get as much data as possible using a single DAC in a synchrotron facility, they are often designed to enable measurements in both reflection and transmission mode.[119,123,124] This is usually accomplished by switching the angle of the corresponding mirrors inside the sample compartment.[123] However, designs that allow reflection exclusively, are also available.[118,121,122]

Generally, the application of force along particular crystal axes causes structural changes, leading to denser crystal packing of the molecules. At high pressures (in the GPa order of magnitude) chemical bonding, molecular configuration and crystal structures are significantly affected. This is especially evident in organic molecular crystals, for example 2,3-dichlorobenzylidine-4-bromoaniline (DBA),[130] 2,6 dichloro-*N*-benzylidene-4-fluoro-3-nitro aniline (DFA) and 2,5-dichloro-*N*-benzylidene-4-chloroaniline (DPA).[131] By application of force, most of the prominent bands – including aromatic and aliphatic CH and CCl bands – showed significant shifts toward higher wavenumbers, which is, together with broadening of the bands, attributed to changes in pattern of intermolecular interactions in the crystals. Structural reversibility upon decompression is evident for all these systems, which reflects essential short-range perturbations. Difference in response to compression and decompression of the two crystals is attributed to difference in their packing configurations. Specifically, results indicate that relative orientation of π stacks plays a pivotal role in overall elasticity of the studied molecular crystals. This evidence leads to precise and detailed models of elasticity for these molecular systems.

Inorganic crystals also respond to applied pressure by structural rearrangements of crystal lattices, which often leads to significant change of their electronic properties. For example, HP-IR spectroscopy in the pressure range from ambient up to 20 GPa, was performed to investigate pressure-induced transitions from the YbS insulator to metal state at room temperature.[132] The original reflectance spectra were translated into optical conductivity, which directly reflects the electronic character of the sample, *i.e.* its transition from an ionic insulator into a metal. In another example, HP-IR was combined with Raman spectroscopy and X-ray diffraction to investigate pressure-induced phase transition in multiferroic h-$Lu_{0.6}Sc_{0.4}FeO_3$. It was observed that symmetry breaking across the transition from the polar to antipolar state takes place *via* changes in the bipyramidal tilting direction and Lu/Sc displacement pattern, which is analogous to the strain-driven distortion in h-$LuFeO_3$ and temperature-induced transitions in rare-earth manganites.[133]

It is especially interesting to explore the behaviour of systems with potential for solid-state hydrogen storage at high pressures. It has been demonstrated that uptake of H_2 drastically increases at the GPa scale of hydrogen pressure. Of particular

interest in this respect, are the various complexes with H_2 and pressure-induced phase transitions of ammonia borane[134–137] and its derivatives,[138] alanates,[139] metal amides[140] and borohydrides.[137,141,142] The majority of these systems were thoroughly explored by means of HP-Raman spectroscopy, but for sure, employment of IR spectroscopy would add very interesting information of high importance for their utilisation. In a recent publication, Marizy *et al.* reported a HP-IR study of polymorphism of $LiBH_4$ and $NaBH_4$.[142] The authors pointed out that it is impossible to determine the details of the phase transition of $NaBH_4$ from tetragonal *Pnma* to α-$LiBH_4$-type monoclinic $P2_1/c$ using Raman spectroscopy,[141] claiming that "it is not possible to confirm the phase transition above 20 GPa from the Raman spectra alone". Thus, they performed HP-IR measurements up to 200 GPa. In this way, the phase diagrams of both $LiBH_4$ and $NaBH_4$ have been experimentally extended to pressure regions above 100 GPa. $LiBH_4$, with at least 5 detected polymorphs, shows richer polymorphism than $NaBH_4$. Important details of these phase transitions were revealed by IR spectroscopy, which shows that the tetragonal phase of $LiBH_4$ undergoes a pressure-induced monoclinic distortion, which is not observed in the case of $NaBH_4$. It is also interesting to note that IR transmission measurements on the tetragonal phase of $LiBH_4$ revealed for the first time the presence of a weak absorption near 4550 cm^{-1}, which is attributed to the stretching vibration of H_2 molecules trapped inside the $LiBH_4$ crystal lattice. Since the calculations of molecular dynamics predicted the formation of a $NaBH_4{\cdot}(H_2)_{0.5}$ complex at pressures above 200 GPa, characteristic IR active absorption due to H–H stretching at $\sim$4400 cm^{-1} would be detected. The preliminary experiments were possible for H_2 pressures up to 88 GPa, and this band was not observed, which is actually in agreement with predictions. This observation raised the question of possible insertion of H_2 to nanosized alkaline borohydrides entrapped in metal–organic frameworks.

Nanodimensional materials

On the nanometer scale, systems generally behave significantly differently to particles of the same substance on the macroscale. This is caused by significant disruption of extended networks of intermolecular contacts, which causes certain properties of molecules to come to the fore, while the bulk properties cease to be expressed. In general, nanomaterials are those systems in which at least one of the dimensions is nanometric (1–100 nm), while other dimensions can be incomparably larger, *i.e.* macroscopic. Thus, two-dimensional (2D) materials are those for which length and width are macroscopic, while their thickness is of nanometer dimensions. So, 2D materials are layered solids, from which individual sheets can be delaminated (exfoliated) from the bulk crystal. One-dimensional (1D) materials are characterised by macroscopic length, while their width and thickness are nanometric: nanotubes, nanowires and nanorods. Zero-dimensional materials are nanoparticles, for which all dimensions are nanometric.

2D materials are obtained by bottom-up or top-bottom approaches. In a bottom-up approach, their preparation starts with the atomic or molecular ingredients and they are assembled together into layers, usually grown on a substrate. The common techniques are chemical vapor deposition (CVD),[143] physical vapor deposition (PVD)[144] or various solution-based chemical synthetic methods.[145,146] Both CVD and PVD require high vacuum conditions, which significantly complicates the instrumentation required for accurate monitoring of film growth. However, due to its flexibility in approaching samples, IR spectroscopy has found its place in this technologically very important area, which includes not only thin films, but also adsorbates on the substrate's surface.[147,148] RAIRS is the IR spectroscopic mode of choice for these phenomena (Fig. 11), especially under ultra-high vacuum (UHV) conditions,[149,150] but transmission[151,152] and ATR[9,152,153] configurations are also employed to solve specific problems. Additionally, a highly sensitive experimental setup for the spectroscopic characterization of submonolayer coverage of hydrocarbon fragments on single crystals under UHV has been developed. In this case, the experiments are performed by focusing the IR beam from a commercial FTIR through a polarizer and a NaCl window onto the sample at grazing incidence, passing the reflected beam through a second NaCl window, and refocusing it onto a detector.[154]

ATR was also employed to provide insight into the processing of silicon wafers in order to facilitate the spatially resolved growth of thin solid films on their surfaces. Specifically, Guo and Zaera tested a combination of silylation and UV/ozonolysis as a way to control the concentration of the surface OH groups required for subsequent atomic layer deposition (ALD) of metals or oxides.[153] In this regard, ATR-IR spectroscopy enabled *in situ* monitoring of the evolution of the surface of Si(100) wafers after

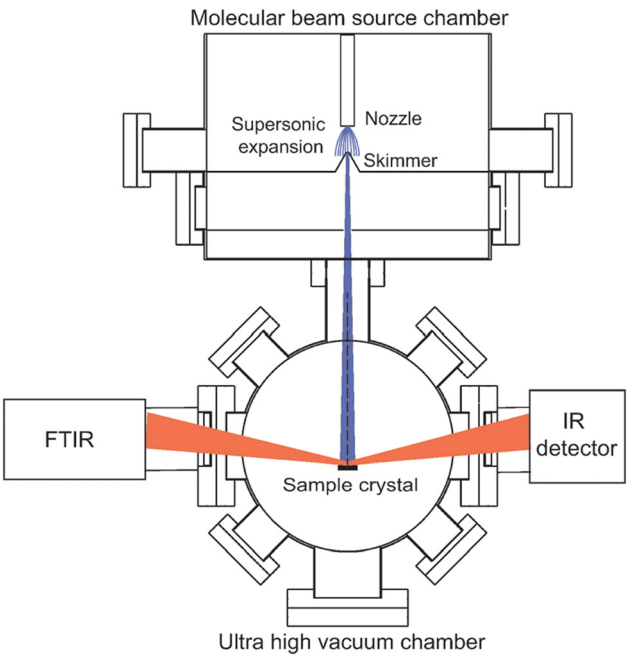

Fig. 11 General scheme of a chamber for ultrahigh vacuum RAIRS experiments. Reprinted with permission from ref. 150, Copyright 2016, the Royal Society of Chemistry.

silylation and O_3/UV-ozonolysis steps. After the treatment of the Si surface with hexamethylenedisilazane (HMDS), the growth of the band at 1257 cm^{-1} due to symmetric deformation of the CH_3 in the newly formed $SiCH_3$, indicates silylation. Additionally, the reaction of the HMDS with the Si surface is indicated by the disappearance of the peaks at 945 and 1184 cm^{-1} due to the symmetric SiNSi stretching and NH deformation modes, respectively, with the simultaneous rise of a broad peak at 1120 cm^{-1} associated with the Si–O–CH_3 moiety. The monitoring of the further step shows that the spectra for the sample exposed to O_3, but not to UV radiation, is similar to that recorded for the surface before treatment; the feature at 1120 cm^{-1} from the $SiOCH_3$ moiety and the double 1251 + 1257 cm^{-1} envelope due to the SiO_2 and CH_3 deformation modes, respectively, remain the same. From this observation, it is evident that methyl groups of the adsorbed HMDS survive intact upon exposure to O_3. On the other hand, the spectra from the sample treated with both O_3 and UV only retains the sharp absorption from the SiO_2 substrate at 1251 cm^{-1}, while the features at 1257 and 1120 cm^{-1}, associated with the surface CH_3 groups are no longer visible, which indicate removal of the organic matter from the surface.

However, in the case of small-sized mono- or few-layered samples, the ratio $\Delta R(\tilde{\nu})/R(\tilde{\nu})$ or $\Delta T(\tilde{\nu})/T(\tilde{\nu})$ are of the 10^{-5} order of magnitude, and the traditional RAIRS and ATR methods cannot obtain a satisfactory signal-to-noise ratio, which makes the resultant spectra useless for further analysis. In these cases, a step-scan FTIR spectroscopic photoreflectance (PR) or photoluminescence (PL) approach, modulated by a lock-in amplifier, is used (Fig. 12).[155] The setup enables measurements under vacuum, which eliminates the influence of atmospheric CO_2 and water. For modulated PR and PT measurements, a halogen or globar can be used as the source of the probe beam. In using switchable mirrors, different experiment modes and detectors can be selected within the same setup configuration and by sample mounting. The pump laser beam is mechanically chopped. A lock-in amplifier enables phase sensitive detection, and thus a high optical response was obtained, which significantly increases the signal-to-noise ratio, thus making accurate IR spectroscopy of nanomaterials possible.

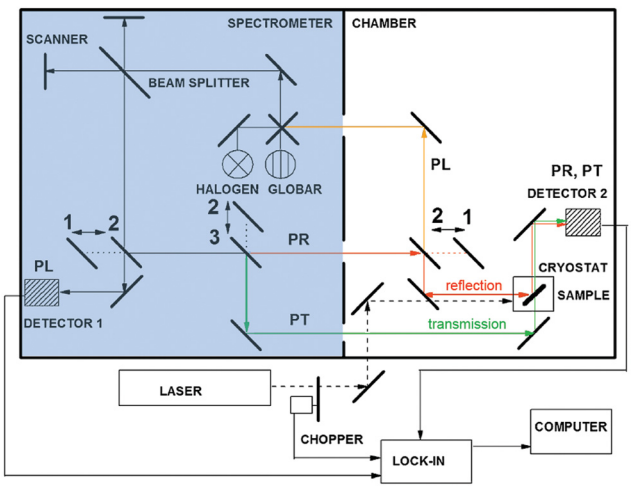

Fig. 12 Scheme of the FTIR photoluminescence (PL), photoreflection (PR) and phototransmission (PT) setup. The module is a FTIR spectrometer together with a vacuum chamber. Mirror positions 1, 2, 3, and detector positions 1, 2 show the setup versatility with possible configurations for PL, PR, and PT measurements. The laser pumping beam is chopped by a mechanical chopper and phase sensitive lock-in amplifier detection is employed. Adapted with permission from ref. 155, Copyright 2009, the Japan Society of Applied Physics.

Due to the fundamental experimental limitations associated with diffraction limit, conventional IR spectroscopy cannot be directly applied to directly characterize individual particles of nanoscale materials. However, in the past decade, significant progress in this respect was made with the development of FTIR nanospectroscopy (nano-FTIR), which combines scanning near-field optical microscopy with FTIR spectroscopy. It provides a powerful tool to study polymers, 2D-materials, semiconductor devices, and biomaterials on the nanoscale.[156] The probe of a typical nano-FTIR setup is generally made of metal or metal-coated (*e.g.* Au, Ag, Pt) dielectric materials. Because of the probe's mirror dipole effect, and lightning-rod effect, the tip-sample region will form a strong electric field enhancement, *i.e.* a "hot-spot". The interaction between the tip, sample and light induces an elastic scattering signal that contains the sample fingerprint information. Then, this scattered light is collected by an off-axis parabolic mirror and forms an interference spectrum with the reference beam. Finally, the IR spectra of this tip-sample region, including the amplitude and phase spectra, is obtained. Among the other applications, this technique is used for characterization of 2D materials, especially to distinguish monolayer and few-layer 2D materials,[157] which is only indirectly reachable by conventional IR spectroscopy. Nano-FTIR was also employed to study the surface phonon polarons (SPhP) on the surface of hexagonal BN.[158,159] It is found that the SPhP dispersion characteristics of hexagonal BN systematically change with the sample-edge distance, which can be applied in the design of sensors and in modulating nanophotons. An additional important application of nano-FTIR is a study of perovskite materials,[160] which are currently among the most popular materials for photovoltaic cells. They became especially attractive since they reach a power conversion efficiency of over 20%. However, under the influence of different external factors such as light, temperature, and humidity, they are prone to organic depletion and structural changes, resulting in the degradation of material properties. Szostak *et al.* employed nano-FTIR to study single nanoparticles in the organic–inorganic hybrid perovskite (OIHP) film, revealing the process of material property depletion,[160] while Wang *et al.* applied it to detect the formation of intersubband polariton states for the first time in a single nanoantenna (Fig. 13).[161]

A continuous and ever growing interest in porous materials has led to the development of the rational design of these materials. Equally important for their utilisation is understanding the mechanism of their interactions with guest molecules, that govern sorption, confinement and desorption. Being inherently highly sensitive to intermolecular interactions and molecular arrangements and the microenvironment, IR spectroscopy provides a unique insight into these processes, especially when combined with other available techniques. Thus, a huge body of

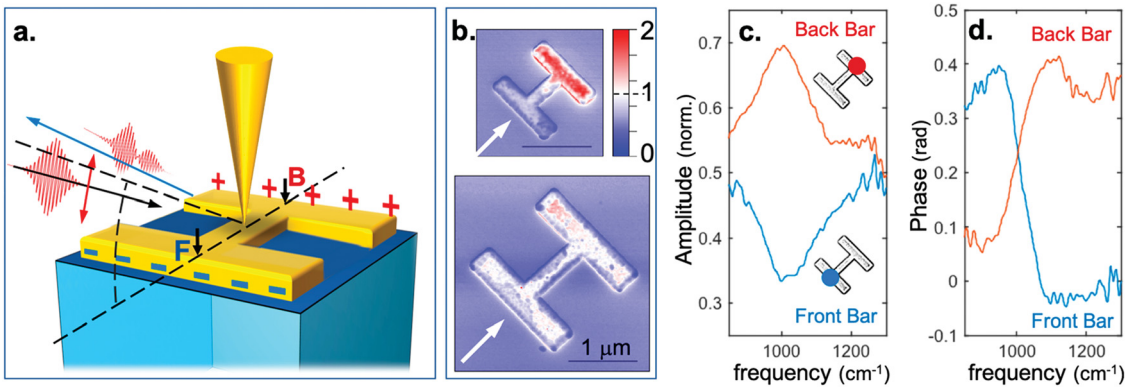

Fig. 13 Near-field imaging and nano-FTIR spectroscopy of dogbone nanoantennae. (a) Schematic diagram of the experimental setup with black arrows marking the position of the scattering-type scanning near-field optical microscope probe on the front (F) and back (B) bars. (b) Near-field amplitude images for two nanoantennae illuminated at 1000 cm^{-1}: (top) nanoantenna in resonance with excitation (λ = 950 nm) and (bottom) nanoantenna with the resonance below 1000 cm^{-1} (λ = 1600 nm). In both images, the scale bars are 1 μm, and the scattered field amplitude is normalized to the average amplitude on the gold surface of the nonresonant (bottom) antenna. The white arrows indicate the propagation direction of the excitation beam. Nano-FTIR amplitude (c) and relative phase (d) for the λ = 950 nm nanoantenna at the front/back (blue/red) bars; positions on the antenna surface where the spectra were taken are marked in the insets in part c. Reprinted with permission from ref. 161, Copyright, 2019, the American Chemical Society.

literature about the applications of IR spectroscopy in investigations of processes relevant for understanding the action of porous materials is available and extensively reviewed.[162–166] Here, only a few representative examples will be presented.

IR spectroscopy is often employed to monitor the occupation of the pores in porous materials, such as metal–organic frameworks (MOF),[167–170] zeolites,[171–174] porous carbons[166,175–177] *etc.*[178] IR spectroscopy can confirm the successful and controllable preparation of C_{60} encapsulated inside the pores of zeolitic-imidazolate framework 8 (ZIF-8) by solvent-free mechanochemical processes.[170] Having large cages and narrow cage-apertures, this MOF cannot accept rigid C_{60} molecules, so the author's approach was to build the cage around the guest molecule. The occupancy of ZIF-8 cavities by C_{60} was quantitatively determined by IR spectroscopy (Fig. 14). Additionally, a combination of measured IR spectra with molecular dynamics simulations show that the fullerene is accommodated in the cage centers and that the cage-to-cage transport is a unfeasible and energetically unfavored process.[170]

On the other hand, small H_2O molecules, confined in the cavities of MOF, can interact with each other and migrate between neighbouring voids. However, nanoconfined water shows distinct properties that are markedly different from those of the bulk. These unique properties stem not only from the $H_2O\cdots H_2O$ interaction, but also from the interactions between water and the surrounding confining environment. The authors have employed a combination of vibrational spectroscopy (Raman, FTIR, and IR electroabsorption) and a multivariate curve resolution to study the interactions of water within a prototype of pillared layer-type MOFs.[168] Multivariate curve resolution analysis of IR spectra, obtained by monitoring water desorption from MOF allowed accurate distinction of the MOF's carboxylate vibrational modes of the water-filled and empty nanopores, respectively, and a quantification of these pores. Furthermore, IR electroabsorption measurements showed that the hydrogen-bonding interaction with confined water has little impact on the response to electric fields of the MOF's vibrational modes.

In another example, scattering-type scanning near-field optical microscopy (sSNOM) combined with nano-FTIR spectroscopy was employed to reveal the vibrational characteristics of systems where large molecules are encapsulated in MOFs.[169] Probing individual MOF single crystals, the authors pinpoint the local molecular vibrations, thus shedding new light on host–guest interactions at the nanoscale (Fig. 15). Their strategy not only confirms the successful encapsulation of luminescent guest molecules in ZIF-8, but further provides new methodology for nanoscale-resolved physical and chemical identification of materials with widely varying frameworks and porous systems for highly sophisticated applications.

Phase transitions

Although phase transitions are already addressed in the previous section, the importance of these processes and understanding of their underlying mechanisms requires special consideration. During a phase transition of a given system, certain properties change, often discontinuously, as a result of the change of external conditions, such as temperature, pressure *etc.* These macroscopically observed changes are caused by microscopic, molecular-level processes. Thus, understanding the microscopic background of phase transitions is an important objective, addressed by numerous methods, including, of course, IR spectroscopy in all of its incarnations. All applications of IR spectroscopy to monitor phase transitions would be too wide a topic to be considered here, and specific aspects of this enormously broad topic are discussed in other available reviews.[179–183] On the other hand, phase transitions are occasionally discussed thorough this text. Thus, this section will be focused exclusively on a few, readily accessible and easy-to-perform approaches.

It has been shown that simple analysis of variations in the IR baseline of absorption spectra obtained in transmission mode

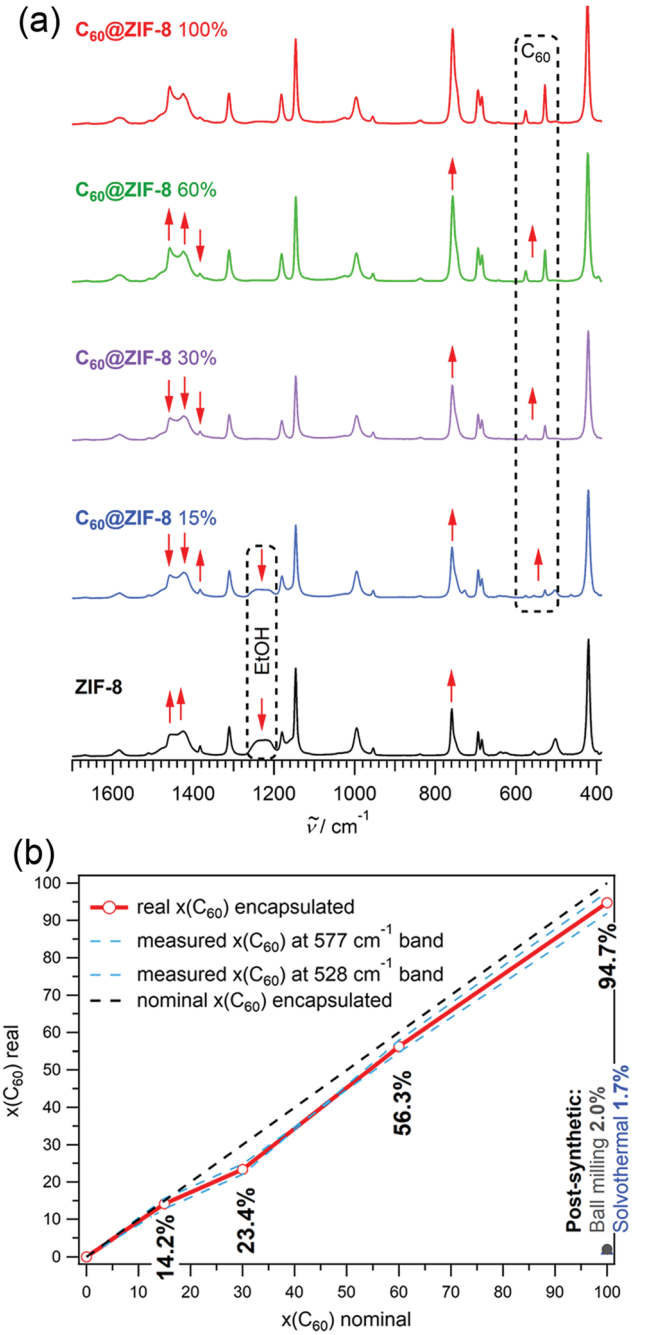

Fig. 14 (a) Changes in the experimental IR spectra of ZIF-8 occurring due to encapsulation of C_{60}. Features due to the dynamic relation of C_{60} and EtOH are framed by the dashed rectangles. (b) Efficiency of mechanochemical C_{60} encapsulation by ZIF-8. The postsynthetic loading attempts were done in excess fullerene but resulted in low loading of ZIF-8 (black and blue text in the lower right corner). Reprinted with permission from ref. 170, Copyright 2020, American Chemical Society.

with respect to perturbation applied to an observed sample, bear information on perturbation-induced phase transitions. It is well known that the baseline of perturbation-dependant transmission IR spectra varies with application of the perturbation. However, the obtained raw spectra are usually corrected before further analysis, *i.e.* the baseline is usually subtracted from them. The rationale of the developed method lies in the fact that the IR baseline appearance is a direct result of optical properties of the sample and therefore cannot be automatically excluded without taking care of the sample nature. The concept was confirmed for variable temperature transmission IR spectroscopy, but it is generally applicable for perturbations other than temperature. In the first study dealing with this problem, phase transition temperatures were determined by 2D correlation analysis,[184] using the whole IR spectrum –including the temperature-induced baseline variations.[185] However, the primary cause of noticeable spectral changes remained unclear. This problem was resolved by Zimmermann and Baranović, who performed a simple analysis of temperature-induced variation of the baseline, and compared this approach with results obtained by 2D correlation analysis, showing that IR spectroscopy can be applied for the rapid determination of conditions at which phase transitions occur.[186,187] In practice, baseline absorption was taken from raw (as-recorded) spectra as absorbance at an arbitrary chosen wavenumber, assumed to be free of sample absorption, most often in the 2800–1800 cm^{-1} region. Then, a simple plot of baseline absorbance *vs.* temperature (or more generally perturbation) indicates temperatures at which phase transitions occur (Fig. 16). In the paper which introduces the method, the concept was applied to several systems, namely phenanthrene, *trans*-4-haptylcyclohexanecarboxylic acid, benzo[*a*]pyrene and a series of phenylacetylenes.[186] This simple measurement of baseline absorbance was compared with 2D correlation analysis,[185] which proves the comparability of the obtained results.

The methodological ease and accuracy of the important data provided by the simple measurement of baseline absorbance makes this method highly applicable in the determination of conditions that induce phase transitions. For this reason, it is somewhat surprising that this method has not come into wider use, and the literature in which it has been applied is limited to a very narrow circle of authors.[187–195] Beyond its original use to detect temperature-induced solid–solid phase transitions, the method found use in monitoring isothermal crystallization of the cocrystalline phase from the melt.[194] Additionally, the temperature-dependant baseline measurements, together with changes in spectral features of a series of picrate surfactants indicate a phase transition, not evident from differential scanning calorimetry (DSC) or differential thermal analysis (DTA) measurements, thus indicating an adiabatic phase transition, which causes change in the optical but not thermal properties of the sample. This finding is important in light of the ability of IR spectroscopy to detect phase transitions invisible for thermal methods (Fig. 16).[192]

Gas sorption and desorption

In general, the rationale for using spectroscopy for investigating the sorption behavior of materials, lies in the wealth of information available at the molecular level, which is unavailable when relying on purely gravimetric data. In practice, IR

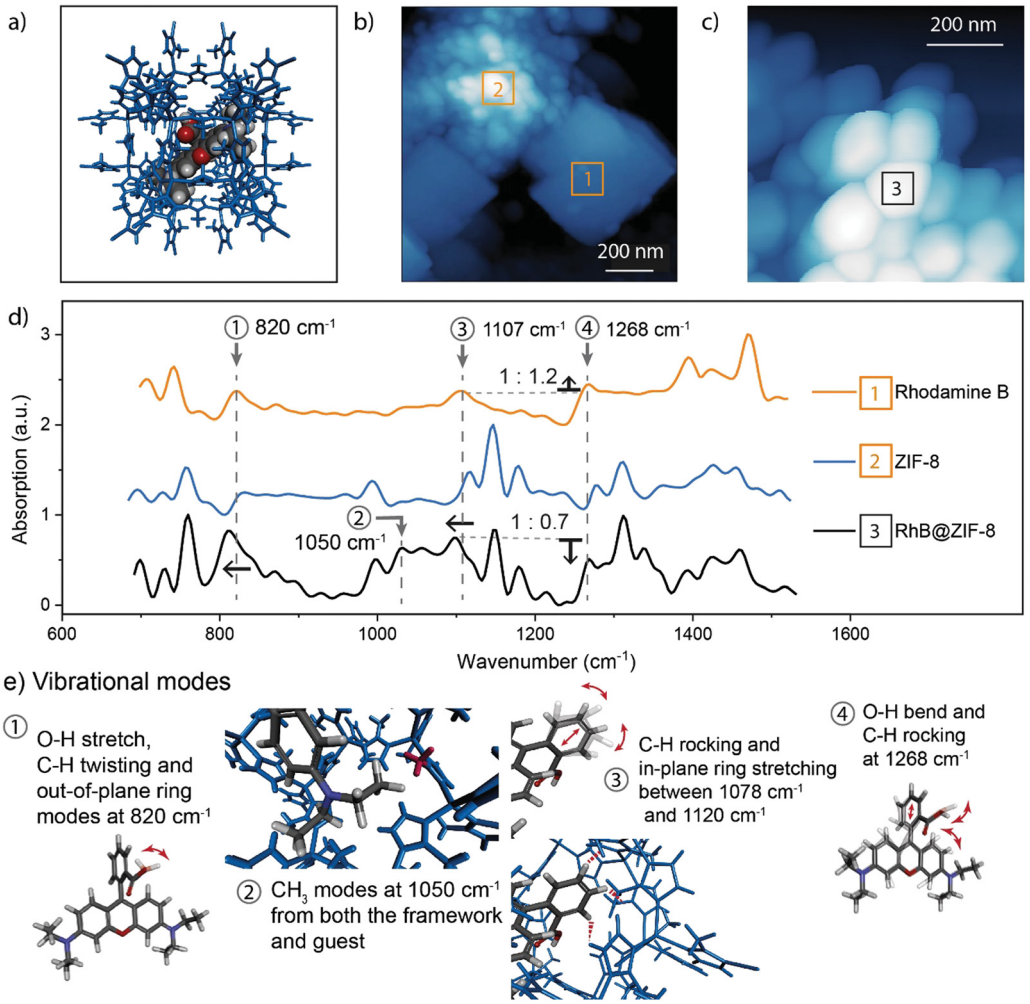

Fig. 15 Vibrational analysis of rhodamine B (RhB) and ZIF-8 *via* nano-FTIR and DFT calculations. (a) Schematic representation of the Rh@ZIF-8 composite, depicting an RhB guest molecule being encapsulated in the pore of the ZIF-8 host framework (in blue). (b) AFM image of the as-synthesised sample containing two distinctive phases: (1) RhB and (2) ZIF-8 showing the positions where IR spectra were recorded. (c) AFM image of a single-phase sample of ZIF-8 nanocrystals adsorbing RhB. (d) Nano-FTIR spectra determined at the designated locations on the AFM image. (e) Vibrational modes of the RhB@ZIF-8 composite illustrating the interactions between the ZIF-8 host framework and the RhB guest. Reprinted with permission from ref. 169, Copyright 2020, the American Chemical Society.

spectroscopy is applicable for monitoring the evolution of both gaseous and solid products, including parameters of diffusion, which will be discussed in a separate section.

It should be pointed out that qualitative and quantitative changes of both gaseous and solid phases involved in gas sorption and desorption processes, can be monitored by IR spectroscopy. Experimental setups for IR spectroscopy of solid samples are discussed thoroughout the text. Although they are in general applicable for monitoring changes in solid materials by gas sorption or desorption, there are numerous examples of advanced dedicated setups tailored for specific problems.[152]

A variety of cells for IR spectroscopic analysis of gases are commercially available. Effective pathlengths of IR light through gaseous sample varies from a few centimeters to several meters. The longer pathlengths are usually obtained in compact cells by providing reflective internal surfaces, so that the beam effectively passes many times through the sample before exiting the cell. Very often, FTIR spectrometers are coupled with a thermogravimetric balance. Such a setup enables accurate chemical identification of the gaseous products of thermal decomposition. Besides these commonly used pieces of equipment, there are numerous examples of more specific setups that meet particular, more complex requirements. For example, online monitoring of gases in industrial processes is an ambitious task due to adverse conditions such as mechanical vibrations and temperature fluctuations. To meet these conditions, Köhler *et al.* designed a compact gas measurement system, that combines the advantages of conventional FTIR spectrometers with a static single-mirror. The setup works in the range 650 to 1250 cm^{-1} at measurement rates of up to 200 Hz. Additionally, with the use of a gas cell that allows an optical pathlength of up to 120 Hz, gases in the low ppm range can be accurately quantified.[196]

The experimental protocol for quantitative IR measurements of gas sorption by solid materials is described in detail by

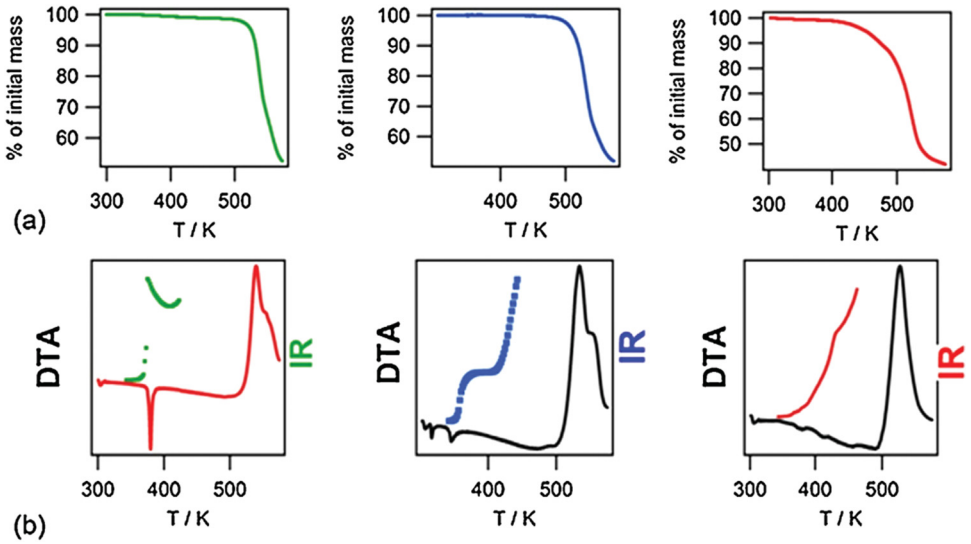

Fig. 16 Thermogravimetry, TG (a), and (b) differential thermal analysis, DTA (black lines) with temperature-dependent IR baseline variation (coloured dots) of oligomeric picrates, as measured at 2000 cm^{-1}. Reprinted with permission from ref. 192, Copyright 2013, Elsevier.

Drenchev *et al.*[16] The procedure and the power of the technique is demonstrated by the water-enhanced CO_2 adsorption on a metal–organic framework, UiO-66. For this purpose, a custom-made system, consisting of a combination of high- and low-temperature sample cells, was designed. For high-temperature measurements, the KBr pellet with the sample is placed in a mobile holder that enables transition of the sample from the heating zone (furnace) to the IR beam. The cell also provides the possibility of fixing the pellet in an intermediate position, allowing easy acquisition of the background spectrum while cooling the sample down to room temperature. Low-temperature measurements were enabled by fixing the sample, surrounded by a Dewar filled with liquid nitrogen, in a position on the path of the IR beam. In order to prevent the condensation of water vapor on the outside walls of the system, a water circulating system was built between the Dewar and cell windows (Fig. 17). The adsorption efficiency was measured by monitoring the absorbance of a band due to adsorbed CO_2 *vs.* the total amount of introduced CO_2. On the other hand, monitoring of the ν(OH) envelope enabled a response of the UiO-66 to adsorption of the CO_2. Additionally, the results of IR spectroscopy indicated the enhancement of the CO_2 adsorption by water.[16]

Due to the importance of the process, publications focused on IR monitoring of the sorption of CO_2 [197–207] or methane[208–211] by solids are numerous. In principle, qualitative or semi-quantitative monitoring of the changes in solid samples due to gas sorption does not require any additional accessories. For example, it is well known that the products of decomposition of ammonia borane, as obtained by its heating at 150 °C, show an increase of mass when exposed to air. Biliškov *et al.* have observed this system by time-dependent IR spectroscopy.[75] They used a simple transmission to monitor the changes due to air exposure of the thermal decomposition products of ammonia borane, obtained by its heating to 125, 150 and 200 °C. While the low-temperature product did not show any changes, the products

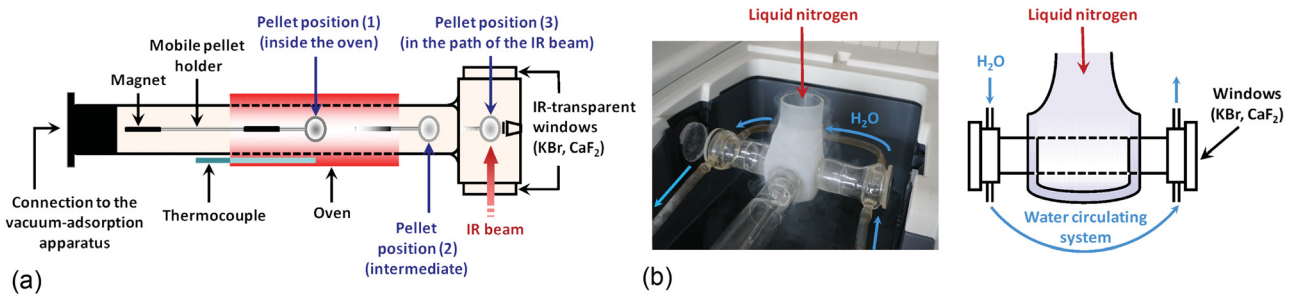

Fig. 17 Simple horizontal glass IR cell for adsorption studies. (a) Scheme of the cell. The sample pellet is put into the holder which can be moved along the cell with a ferrite block magnet. Position (1) is in the sample oven and allows thermal treatment. Position (2) is the intermediate and allows tempering of the sample and registering the background immediately before registering the sample spectrum. In position (3), the sample is fixed perpendicularly to the IR beam to take the spectrum. To ensure transmission of the IR beam, the cell is equipped with IR transparent windows. The cell can be connected to a vacuum/adsorption device. (b) When the sample is fixed in a position on the path of the IR beam, it is surrounded by a Dewar which can be filled with liquid nitrogen. Between the Dewar and the cell windows there is a water circulating system aimed at keeping the temperature of the window high enough to prevent condensation of water vapor. Reprinted with permission from ref. 16, Copyright 2020, JoVE.

obtained at 150 and 200 °C show significant changes, reflected in an increase of the mass, as well as absorption of both ν(NH) and ν(BH) envelope. However, the authors did not further investigate the system, leaving the results as just an interesting observation.

IR spectroscopy is also frequently employed to investigate materials for chemical solid-state hydrogen storage. In this regard, only physisorptive processes will be addressed here. However, only a weak interaction of H_2 with metal–organic frameworks and other porous or low-dimensional solids is responsible for its physisorption. Thus, IR spectroscopy is here only of limited use, mainly oriented to second-order effects of hydrogen sorption. Actually, there is only one example where IR spectroscopy was employed for the direct measurement of changes due to the H_2 physisorption, namely monitoring of hydrogen and deuterium sorption by lithium-intercalated fulleride $Li_{12}C_{60}$. In this case, IR spectra indicate that physisorption is only apparent, and chemisorption is actually responsible for the successful storage of H_2 in this system. Namely, only a minor part of absorbed hydrogen is present in ionic hydride LiH, while the major part is covalently bound to C_{60}.[212] The other types of material for solid-state hydrogen storage, where hydrogen is chemically bound through covalent interactions, will be addressed together with other thermal decompositions.

Beyond the common materials, the use of IR spectroscopic monitoring can expand to complex materials such as gas-processing metalloenzymes.[213] In a perspective publication, the author introduces ATR-FTIR for the analysis of gas-processing metalloenzymes, such as cytochrome *c* oxidase, nitrogenase, and hydrogenase. In this respect, IR spectroscopy provides information about the geometry and redox state of the catalytic cofactors, the protonation state of amino acid residues, the hydrogen-bonding network, and protein structural changes. For this purpose, the gas exchange and deuteration experiments exploring the reactivity of these enzymes with their natural reactants were monitored. This approach allows recording sensitive steady-state difference ATR-IR spectra with time resolution in a seconds timescale. The author also noted that IR spectroscopy allows investigation of the protein samples under biologically relevant conditions, that is, at ambient temperature, ambient pressure, and in the presence of liquid water.

Besides gas sorption processes, IR spectroscopy is frequently employed for investigations of sorption of various liquids and solids. Among the sorption of liquids, probably the most important process is confinement of water in porous matrices.[214–224] Sorption of solids by encapsulation is also frequently investigated by IR spectroscopy.[170,225–229]

Surface processes

A surface can be generally defined as a thin layer of a substance at the boundary of contiguous bodies, media, or phases. Surface phenomena arise from excess free energy and the particular features of the surface's structure and composition. They may be purely physical, or they may be accompanied by chemical transformations. The molecular nature and properties of a surface may be radically altered as a result of the formation of surface monomolecular layers or polymolecular films. These changes usually result from adsorption, surface diffusion, spreading of liquids, or from the chemical interaction of components of the contiguous phases. Evidently, any modification of the surface layer causes a change of molecular interaction between contacting phases. From a chemical point of view, physical or chemical transformation of the surface layer strongly affects the nature and rate of various highly important heterogeneous phenomena: such as adsorptions, as well as corrosive, electrochemical, catalytic, and membrane processes. For these reasons, interest in the detailed understanding of the microscopic background of surface and interface phenomena is rising, and various experimental techniques are employed in this field.

Structure and properties of the surface, including the presence of the exposed functional groups responsible for intermolecular contacts with adsorbed species, is crucial for understanding surface phenomena. For this reason, it is of high importance to characterize surfaces at the molecular level. IR spectroscopy is one of the first techniques employed for the characterization of surface phenomena, especially heterogeneous catalysis, and still its popularity does not fade. Actually, among all the available optical spectroscopies applied in this respect, IR spectroscopy is by far the most used. Thus, it sounds paradoxical that IR spectroscopy in general is not surface sensitive, but it may be made so by applying a proper experimental geometry. In particular, due to its high sensitivity to intermolecular interactions, it is able to differentiate between free molecules in gas or liquid phases and adsorbates bound to a solid surface. Raman spectroscopy is also frequently utilised to investigate surfaces,[230] especially in the case of phenomena out of the reach of IR spectroscopy.[231]

Regarding techniques used for acquisition of spectral information, ATR is frequently thought to be applicable for spectroscopic characterisation of surfaces. However, strictly speaking, this technique does not specifically address the very surface, since the evanescent wave penetrates a few micrometers inside the sample.[100,102] Thus, ATR spectra consist of unresolved information about the surface and near-surface layer of the sample. Although in principle all external reflection techniques are useful for the investigation of surfaces, RAIRS and a variety of its derivatives are better suited. However, regardless of this critical review, the variety of surface phenomena allows the use of all available and combined techniques to obtain high-quality spectroscopic information – of course depending on the nature of the sample to be probed and what the researcher is interested in.

The set-up of a RAIRS experiment is conceptually simple, and it relies on collection of the IR light reflected by an optically flat, mirror-like surface, thus making RAIRS a highly specialized technique. The samples, which are typically monolayers adsorbed on a small area, yield weak IR signals, thus requiring effort to improve the intensity, for example using multiple-reflection arrangements. Despite these difficulties, RAIRS is

particularly useful for the characterization of systems with low surface area, as well as to investigate adsorption of gas/solid and liquid/solid interfaces,[232,233] by providing accurate information on intermolecular interactions and additionally the bonding geometry of adsorbates.[234–243] Actually, the pioneering application of RAIRS was to investigate the adsorption of carbon monoxide on metal films.[244,245] The application of polarization modulation is also frequently used to improve the signal-to-noise ratio and to discriminate between adsorbed and free surrounding molecules.[246,247]

Heterogeneous catalysis on metal surfaces

Understanding the adsorption of small molecules to the surface of transition metals is an important prerequisite for the rational design of new materials with improved catalytic properties. Since the adsorption geometry might critically affect the ability of the surface to activate the selected chemical bonds, it is important to investigate sorption to a particular crystal plane. It is clear that in dealing with such problems, the full power of the RAIRS technique comes to the fore. The dependence of the intramolecular vibrational frequency of adsorbates on the site of their adsorption on the surface of the metal is well documented.[248–251] This reflects the weakening or strengthening of a particular bond with respect to the surface interaction, which is in turn of crucial importance for understanding the catalytic action of the metal. Recent examples of studies focused on this issue include adsorption of acetophenone or carbon monoxide on Pt(111),[238,239] methane on Pt(211) (Fig. 18a),[252] acetic acid on Ni(110)[240] or titanyl phthalocyanine on Au(111) surfaces.[243]

A very illustrative example of the reactive specificity of a particular surface site to the dissociation of adsorbed species is the RAIRS monitoring of adsorption of CO and the dissociation of CH_4 on various Pt surfaces, cut along different Miller indices. CO has been widely used to detect and identify the presence of different absorption sites on single crystal metal surfaces due to its large dynamic dipole moment, which leads to highly sensitive surface-site-resolved detection of adsorbed CO by RAIRS (Fig. 18b).[250,253] In fact, the frequency of adsorbed CO is almost a linear function of the coordination number of the atom of the substrate which binds the CO molecule.[254]

Dissociation of CH_4 was also extensively studied by RAIRS.[255–260] It is shown that the adsorbed CO forms terraces on the surface of Pt, which are site-dependent. Fig. 18(a) shows the three different types of surface atom on Pt(211), referred to as steps (orange), terraces (blue) and corners (white) with coordination numbers 7, 9, and 10, respectively.[252] It is observed that dissociation of CH_4 on Pt(531) and Pt(210) requires a lower energy with respect to CH_4 molecules on Pt(211) and Pt(110). The broad RAIRS feature, observed on

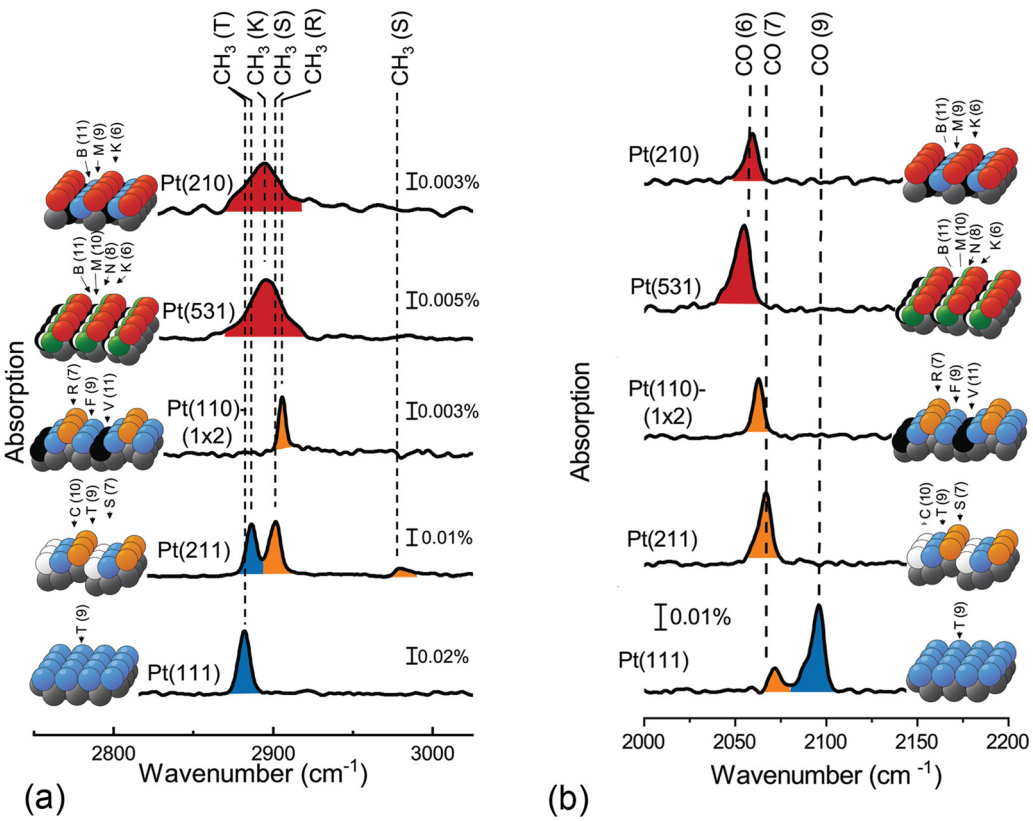

Fig. 18 RAIRS detection of (a) methane and (b) CO dissociation products on specific Pt planes at T_s = 120–150 K with incident kinetic energies, E_{KIN} = 62–65 kJ mol^{-1}. The vibration of products adsorbed on terrace (T), step (S), ridge (R), corner (C), and kink (K) sites of Pt are indicated by color coding. The coordination numbers of the different surface sites are given in parentheses. Adapted with permission from ref. 252, Copyright 2020, the Royal Society of Chemistry.

Pt(210) and Pt(531), is due to methane dissociation products adsorbed on the kink sites. Currently, there is no satisfactory explanation as to why CH_4 dissociation on the kink sites leads to a broader $\tilde{\nu}$(CH) band than for terrace and step sites.

An important advantage of RAIRS is its non-invasive character. Contrary to high-energy electrons or X-rays, IR radiation does not perturb chemisorption, which allows real time, *in situ* monitoring of the product uptake as the sorption proceeds. For example, RAIRS spectra clearly show the dose-dependent evolution of the adsorbed CH_4 layer on the surface of Pt(211).[252] The RAIRS time sequence can be converted into site-specific uptake curves for adsorbed CH_3 as a function of the incident dose of CH_4. Thus, RAIRS enables a highly controlled approach for surface-site-resolved studies of dissociation of small molecules on metal surfaces, by providing highly accurate and precise experimental evidence for quantum state-specific reactant preparation and detection of surface-site-specific products. In this way, RAIRS measurements provide simultaneous information on reaction probability and mechanism, energy barrier heights and transition state geometry for dissociation on the different surface sites of a given surface. Thus, these measurements provide valuable information to test first principles theoretical models that aim to describe and predict gas/surface reactivity at the microscopic level, including the role of different atoms of the surface of the catalyst, which is of crucial importance for understanding the catalytic action of metals.

Heterogeneous catalysis on non-metallic surfaces

The interest in surface phenomena is not limited to metals; investigating surface interactions of semiconductive or insulating materials with various molecules is also of high interest. Beyond catalysis, they is also interest in the various applications in energy storage and conversion, molecular electronics, gas sensing *etc.*

For example, hydration processes at ZnO surfaces are relevant for numerous catalytic reactions, such as the production of CH_3OH from syngas and the water–gas shift reaction, which produces H_2.[261–266] The structural evolution of water on the anisotropic mixed-terminated ZnO(10$\bar{1}$0) surface was investigated by polarization-, azimuth-, and temperature-dependent RAIRS over a large range of coverages.[261] The combined results demonstrate that the hydration process is rather complex in nature and is initiated by the formation of intact water monomers. The thermally induced diffusion of isolated water molecules leads to the formation of dimer species in which autocatalytic dissociation occurs *via* proton transfer to the substrate (Fig. 19). Increase of the coverage by water causes the building of an extensive hydrogen-bonded network, including the well-ordered 2D OD/D_2O monolayer, anisotropic water bilayer, and isotropic 3D multilayers. The comprehensive results provide detailed insight into the orientation and strength of hydrogen bonds within the 2D and 3D water networks.

CO_2 adsorption on the surface of various oxides is another highly interesting surface adsorption reaction: first, CO_2 is an abundant chemical feedstock with wide applications in industry; second, capture and sequestration of CO_2 has recently received enormous attention. In this respect, alkaline-earth oxides such as CaO were found to be promising materials: they are abundant in nature, low-cost, and exhibit high CO_2 uptake and good thermal stability.[137,267,268] Although the formation of $CaCO_3$ from CaO and CO_2 is elementary school-level chemistry, there is still great interest in understanding the initial stages of CO_2 adsorption by CaO.[269–271] The RAIRS study of the adsorption of CO_2 to well-ordered CaO(001) films grown on Pt(001) and Mo(001) single crystals was recently conducted.[242] The results show that CO_2 first adsorbs as monodentate carbonate, CO_3^{2-}. Its adsorption energy decreases with increased coverage due to agglomeration of carbonates in pairs and chains. However, at high exposures, CO_2 desorbs at considerably higher temperatures corresponding to increased adsorption energy. Temperature-programmed desorption and RAIRS spectra

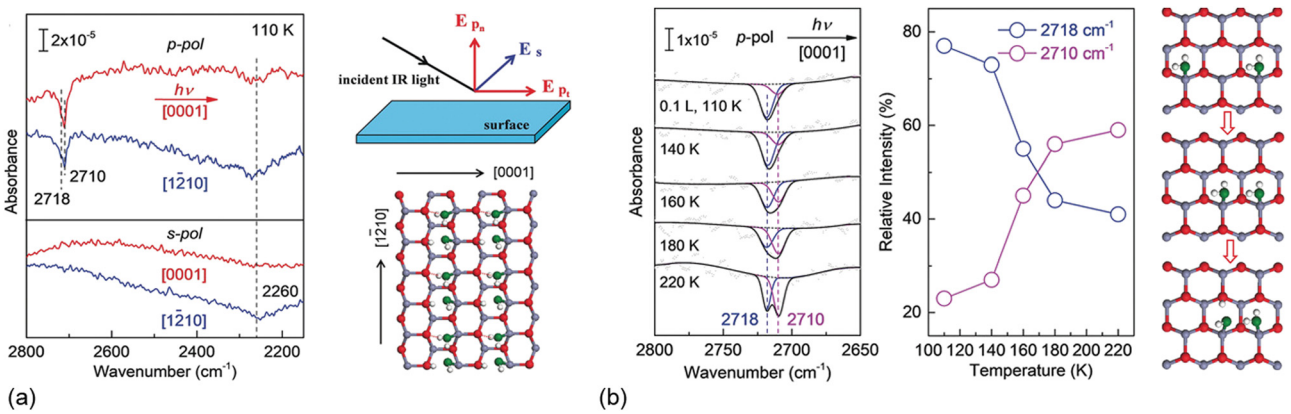

Fig. 19 RAIRS spectra of the adsorption of D_2O on the surface of ZnO(10$\bar{1}$0) at 110 K with a DFT structurally optimized water monolayer formed with non-polar hydrogen bonds (Zn grey, O_s red, O_w green, H white). All spectra were measured with p-polarized light incident along the [0001] azimuth. (a) Polarization- and azimuth-resolved RAIRS spectra obtained after saturation adsorption. Orientation of the s- and p-polarized components for the incident light are depicted in the scheme. (b) Polarization-resolved RAIRS spectra obtained after exposing the clean surface to D_2O under gradual heating to the indicated temperatures. The averaged data were deconvoluted by fitting individual components with Gaussian curves. The blue and magenta lines illustrate $D_f{}^{16}OD$ and $^{16}O_wD$ species, respectively. The graph shows the relative intensity of OD groups as a function of temperature. Adapted from ref. 261, 2019, published open access under a CC-BY license.

revealed the critical role of residual water in CO_2 interactions with CaO under ultra-high vacuum conditions. H_2O molecules readily dissociate within the carbonate ad-layer formed at room temperature. Comparative RAIRS measurements show that surface hydroxyl coexists with carbonate species, thus affecting their adsorption geometry rather than forming bicarbonate. Therefore, surface hydroxyls show the stabilizing effect of the carbonate layer.

Assembly of adsorbed molecules

An interesting aspect of the adsorption of molecules to surfaces is their orientation with respect to the surface plane. Namely, according to the surface selection rule, only vibrational modes with dynamic dipoles with a non-zero component perpendicular to the surface can be detected by RAIRS. As a consequence, the relative intensities of different vibrational bands of a given adsorbate can be used to determine its adsorption geometry:[272–274] for example, the RAIRS study of temperature-induced assembly of methanol molecules on the Cu(100), Cu(111) and Cu(110) surface, show significant spectral changes, most importantly in the ν(OH) band, associated with the structural transformation of hydrogen bonded CH_3OH clusters. Annealing of the CH_3OH layer on Cu(111) converts the hydrogen bonded chains to cyclic hexamers, whereas this transformation is not fully complete on Cu(100) and Cu(110).[275]

Self assembly of the long-chain molecules is of particular interest, since this can be of crucial importance for tuning their reactivity and rearrangements when adsorbed to a surface. For example, the formation and structure of supported bilayer membranes of 11-mercapto-undecanoic acid on a Au surface, has been investigated using sum frequency generation (SFG) vibrational spectroscopy, supplemented by RAIRS.[276] It was found that tethering the proximal lipid leaflet resulted in an increase in the conformational order of the self-assembled lipid monolayers. Furthermore, careful spectroscopic analysis has shown that a better ordered and more biologically relevant lipid bilayer was formed when the distal leaflet was added using Langmuir–Blodgett deposition. In another study, self assembly of the monolayers of peptide nucleic acids on gold surfaces was investigated.[277] A combination of RAIRS with X-ray photoelectron spectroscopy (XPS) allowed the authors to affirm that the structure of the self-assembled monolayers is stabilized by intermolecular interactions through non-complementary adjacent nucleic bases. The results indicate a tilted rather than normal orientation of the molecular chains, which facilitates hydrogen bonding between neighbouring molecules of nucleic acids, thus stabilizing the structure.

Other examples of IR studies of surface adsorption include larger molecules, like porphyrins,[241] which are essential for their functionality at hybrid interfaces. RAIRS spectroscopy reveals the numerous mechanistic details of this adsorption. RAIRS was also used to study the interaction and complex chemistry of relevant molecules on model astrophysical surfaces, like acetonitrile on astrophysical dust grains and ices.[278] Additionally, IR spectroscopy provides important information on environmentally relevant processes, like the adsorption of water on nylon, as one of the initial steps of nylon decompsition.[279]

Surface-affected chemical transformations

From a conceptual IR spectroscopy point of view, heterogeneous catalytic reactions are just an upgrade of the above discussed surface adsorptions. *In situ* spectroscopy of heterogeneous catalysis by definition requires simultaneous measurement of catalytic performance to identify the structure and composition of species relevant to the catalytic process, as well as evolution of adsorbed species. In other words, while the above text describes processes that generally do not involve significant chemical reactions, in the case of heterogeneous catalysis, the focus shifts precisely to surface-affected chemical transformations. For this reason, the RAIRS configuration does not meet all the requirements of the experiment, and it is practically impossible to cover all the ingenious experimental setups in the framework of this review, and here only a few of them are presented as an illustration. Interested readers are invited to consult more detailed reviews focused on this issue.[3,7,20,280–286]

From a fundamental point of view, the *in situ* approach enables the identification of changes and interplay of cluster and nanoparticle structures and compositions during ongoing catalytic reactions, thus revealing how molecules interact with surfaces and interfaces.[20] Case studies cover the full scale from clusters *via* nanoparticles to mesoscale aggregates, and demonstrate the benefits of specific *in situ* methods. Restructuring, mobility of ligands and atoms, as well as evolution of surface composition during the reaction have pronounced effects on activity and selectivity. The nanoscale metal oxide interface steers catalytic performance *via* a long range effect. Combining *in situ* spectroscopic methods with techniques that enable a controlled modulation of concentration provide further mechanistic insight. The obtained fundamental understanding is a prerequisite for improving catalytic performance and for the rational design of catalysts. Examples include the CO oxidation reaction, accompanied by dynamic structure changes of $Au_{38}(SR)_{24}$ clusters on CeO_2 (Fig. 20)[287] or Co_3O_4,[288] reformation of methane on Ni/ZrO_2,[289] as well as oxidation of CH_3OH by steam reforming on Pd_2Ga/Ga_2O_3 (Fig. 21).[290]

IR spectroscopy is extensively applied in practically all steps of preparation, treatment and utilization of heterogeneous catalysts.[291] For sure, one of the most interesting and important applications of IR spectroscopy in heterogeneous catalysis is monitoring of the catalytic reactions, in order to detect and characterize the intermediates and their evolution across the reaction coordinate, thus enabling a reconstruction of mechanistic details at molecular level.[164,283,292–304] Although the majority of work is focused on simple compounds, catalytic conversion of complex species are also traced. Examples include catalytic hydroformylation of ethylene on the Rh/Al_2O_3 surface.[305] In this study, the authors applied a rapid-scan technique,[306] which enabled a millisecond-range time resolution, thus resolving high intermediates, together with kinetic data for individual species (Fig. 22).

The DRIFTS technique is also frequently used for monitoring solid–gas catalytic reactions.[9] One of the chronologically oldest

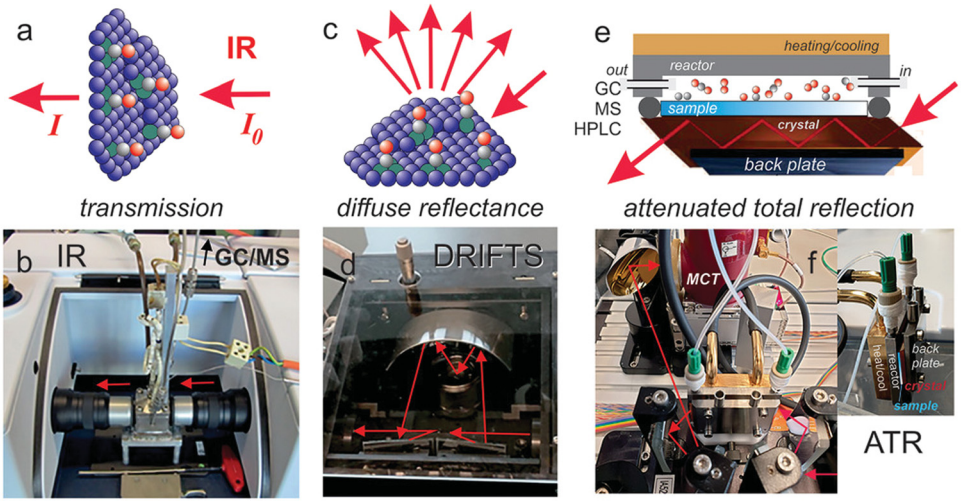

Fig. 20 IR cells with different geometries for monitoring catalytic reactions (a) and (b) transmission, (c) and (d) DRIFTS, (e) and (f) ATR mode. Cell design and IR beam paths are shown in the lower row (b, d and f). For transmission and diffuse reflectance, catalyst powders are pressed to pellets or into small crucibles, respectively, for ATR the crystals are coated with thin catalyst films. Reprinted from ref. 20, 2021, published open access under a CC-BY license.

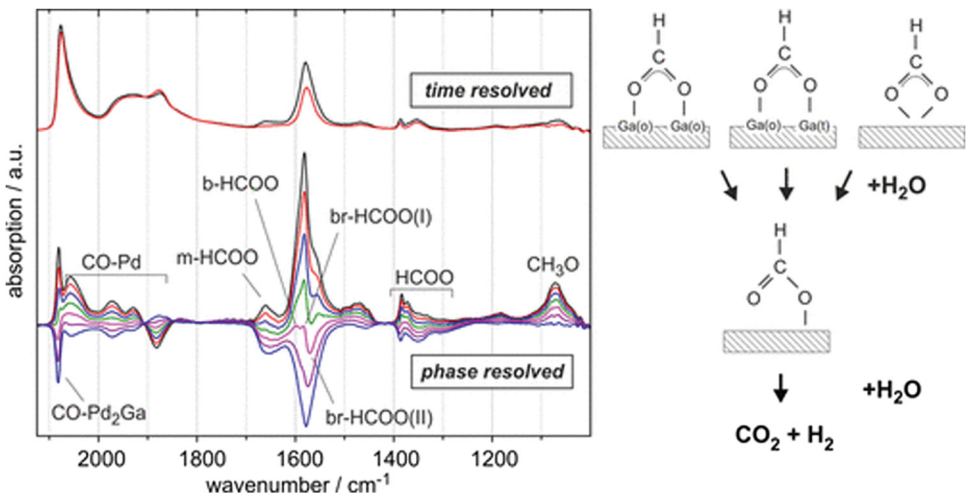

Fig. 21 Average time-resolved DRIFTS spectra recorded at the end of each half-period of $CH_3OH/CH_3OH^+H_2O$ modulation on the Pd_2Ga/Ga_2O_3 surface (top) and corresponding phase-resolved spectra in a phase angle range of 060° calculated using phase-sensitive detection. Schematic representation of mechanistic findings from *in situ* concentration modulation FTIR are depicted. Reprinted with permission from ref. 290, Copyright 2012, the American Chemical Society.

examples is its application to study the oxidation of CO on a Rh/Al_2O_3 catalyst.[309] In this study, the catalytic activity was correlated with surface coverage, which led the authors to the conclusion that CO occupies the oxidized Rh sites, which is the predominant intermediate. Further, DRIFTS was combined with gas chromatography and mass spectrometry to understand the selectivity of H_2 in the preferential oxidation process on a Au/Fe_2O_3 catalyst.[310] Another interesting example includes an innovative design of DRIFTS cell, which minimizes dead volume, thus providing a faster and more reliable response to changes in gas composition (Fig. 23).[311] It is utilised to investigate CO oxidation on the Pt/CeO_2 catalyst by time-resolved spectroscopy using steady-state isotope transient kinetic analysis. DRIFTS, in combination with a multiple-reflection IR gas cell, was applied to investigate photocatalytic oxidation of ethanol to acetone on nanocrystalline TiO_2. This study has shown the formation of both formate and acetate intermediates on the TiO_2 surface, while acetaldehyde is formed in the gas phase.[312]

A more challenging issue is to apply IR spectroscopy for monitoring heterogeneous catalytic reactions in liquid medium.[313] In this field it is crucial to minimize the path of the IR radiation through the solvent, and here the strengths of the ATR technique come to the fore.[314–316] The illustrative example is the so-called Orito reaction, where enantioselectivity of hydrogenation of α-keto esters is promoted by Pt. *In situ* IR monitoring of this reaction has shown that the adsorption geometry changes with surface coverage,

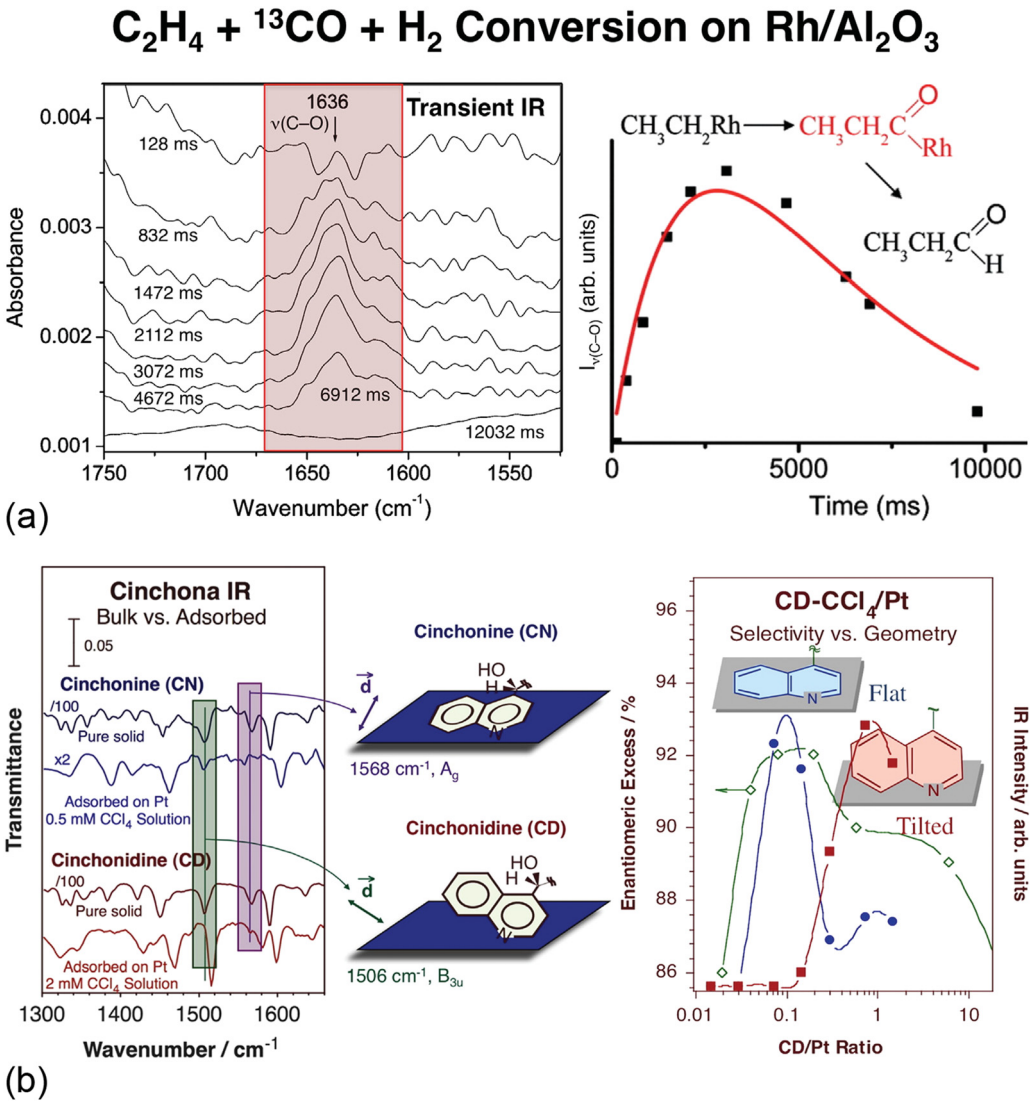

Fig. 22 (a) Example of the use of *in situ* IR to follow the formation and consumption of surface intermediates during catalysis.[305] IR spectra acquired at different times after the start of an ethylene hydroformylation reaction promoted by a Rh/alumina catalyst, and plot of the peak signal intensity of that feature as a function of time to show its transient nature and to calculate the kinetic parameters of the reaction. (b) *In situ* IR characterization of the adsorption geometry of chiral modifiers from solution onto platinum surfaces, and correlation with their catalytic modification efficiency. Left: low and high coverage spectra for cinchonine (CN, top) and cinchonidine (CD, bottom).[291,307] Center: orientation of the aromatic ring of the adsorbed molecules relative to the surface plane, estimated from the relative intensities of the different peaks in the IR spectra.[39] Right: Correlation between ring orientation and the enantioselectivity excess obtained during the hydrogenation of ethyl pyruvate.[291,308] Optimum performance is seen at the intermediate CD concentrations that favor adsorption with the aromatic ring flat on the surface. Adapted from ref. 291, 2021, published open access under a CC-BY license.

which is related to concentration in solution. The optimal configuration of the adsorbed cinchona is when the aromatic rings are oriented parallel to the surface, which is enabled at low concentrations. The tilted orientation, obtained at higher concentrations, is detrimental to enantioselectivity of the catalytic process (Fig. 22b).[308,317]

Electrochemical processes

A very interesting application of ATR IR spectroscopy is its utilisation to investigate the processes relevant to water splitting.[2] Since the catalytically active layer can be grown on the top surface of the ATR crystal, this technique provides a robust and stable platform for *in situ* monitoring of the relevant catalytic processes (Fig. 24). The rationale of the method lies in the fact that the incident radiation, totally reflected on the interface between ATR crystal and sample, partially penetrates into the sample by the evanescent wave, and the typical depth of penetration is $\sim$2 μm. This is deep enough for acquisition of the spectroscopic information on the layer of the solution in contact with the catalytically active layer. Thus, the acquired spectrum contains information on both the thin film of catalyser and on the solution in contact with it (Fig. 24c). The simplicity of the setup provides potential for its development as a routine method for the characterization of liquid–solid

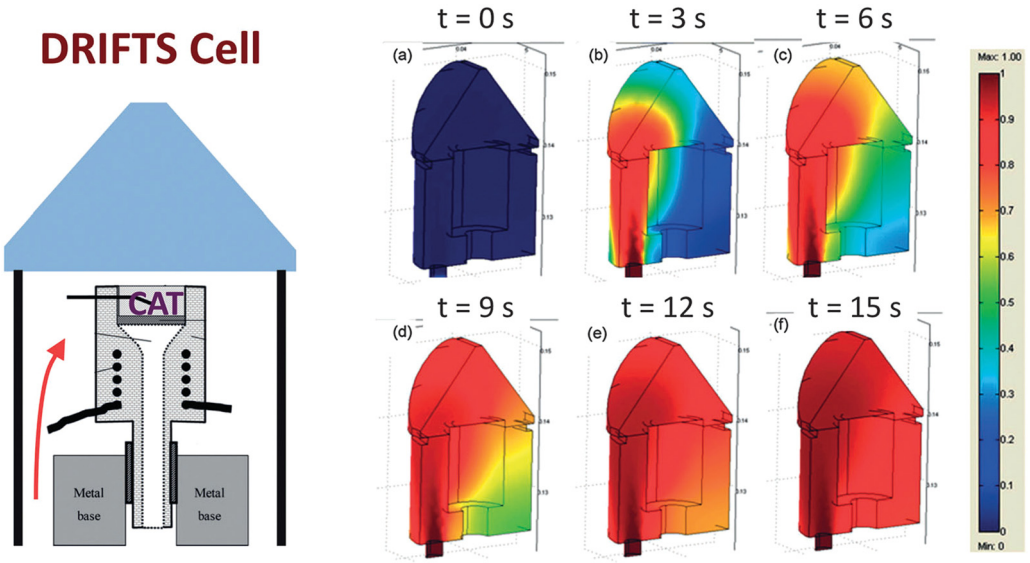

Fig. 23 Schematic representation of high temperature/high pressure DRIFTS cell design for homogeneous flow through a catalyst in short time periods[311] and flow dynamics images acquired for the distribution of gas within the DRIFTS cell volume as a function of time. Reprinted with permission from ref. 9, Copyright 2014, the Royal Society of Chemistry.

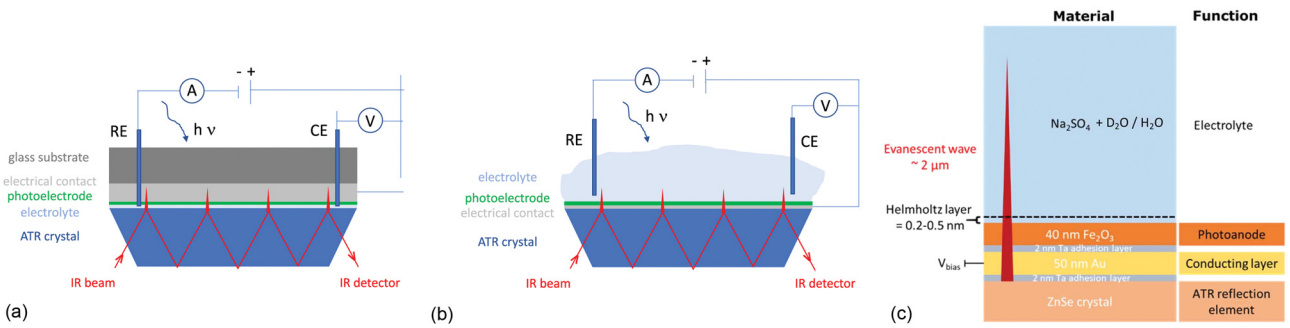

Fig. 24 (a) Separated and (b) integrated for setup for *in situ* ATR-FTIR water splitting measurements. (WE – working electrode, CE – counter electrode, RE – reference electrode, A – ammeter, V – voltmeter.) (c) Sample design and penetration of the evanescent wave in an integrated measurement setup. Adapted from ref. 2, 2021, published open access under a CC-BY license.

interfaces in water splitting. Two types of setup have been developed. The separated setup consists of the sample surface, pressed with the active surface onto the ATR crystal. It was used to study photoelectrochemical cells.[318,319] In another design, the surface to be measured is deposited on top of the ATR crystal, so this is an integrated setup.[2] These setups have been tested using the example of hematite-catalysed water splitting reaction.

Surface processes play a crucial role in a number of other important chemical processes, such as electrochemical reactions,[166,282,320] processes on membranes[320–322] and corrosion.[323–325]

Corrosion is the natural deterioration of a material, which it undergoes as a result of interaction with the environment, most commonly the atmosphere or water. It is a chemical or electrochemical process that converts a material into chemically more stable species such as oxide, hydroxide, carbonate, sulfide *etc.* Corrosion commonly occurs locally, especially at weak parts, for instance where grain boundaries and defects are situated, and the nanoscale of initial and localized corrosion makes it difficult to understand and predict,[326] so sensitive techniques with a high spatial resolution are required to investigate the fundamental mechanisms behind corrosion. Among them, IR spectroscopy is especially interesting, since it provides chemical and structural information on the molecular level of corroded surfaces, as well as a chemical factor that catalyses or inhibits the corrosion process.[323,327] However, a drawback of classical IR microspectroscopy is limited by spatial resolution, which is nowadays resolved by combining IR spectroscopy with AFM, that overcomes the diffraction limit, hence improving the spatial resolution down to 10 nm.[328] Using this approach, it is possible to simultaneously obtain valuable information on nanoscale topography and present chemical species and their evolution. Typical experimental designs involve RAIRS or ATR, and they are presented in Fig. 25. For example, steel corrosion inhibition by polyphosphonates, which is marketed, although

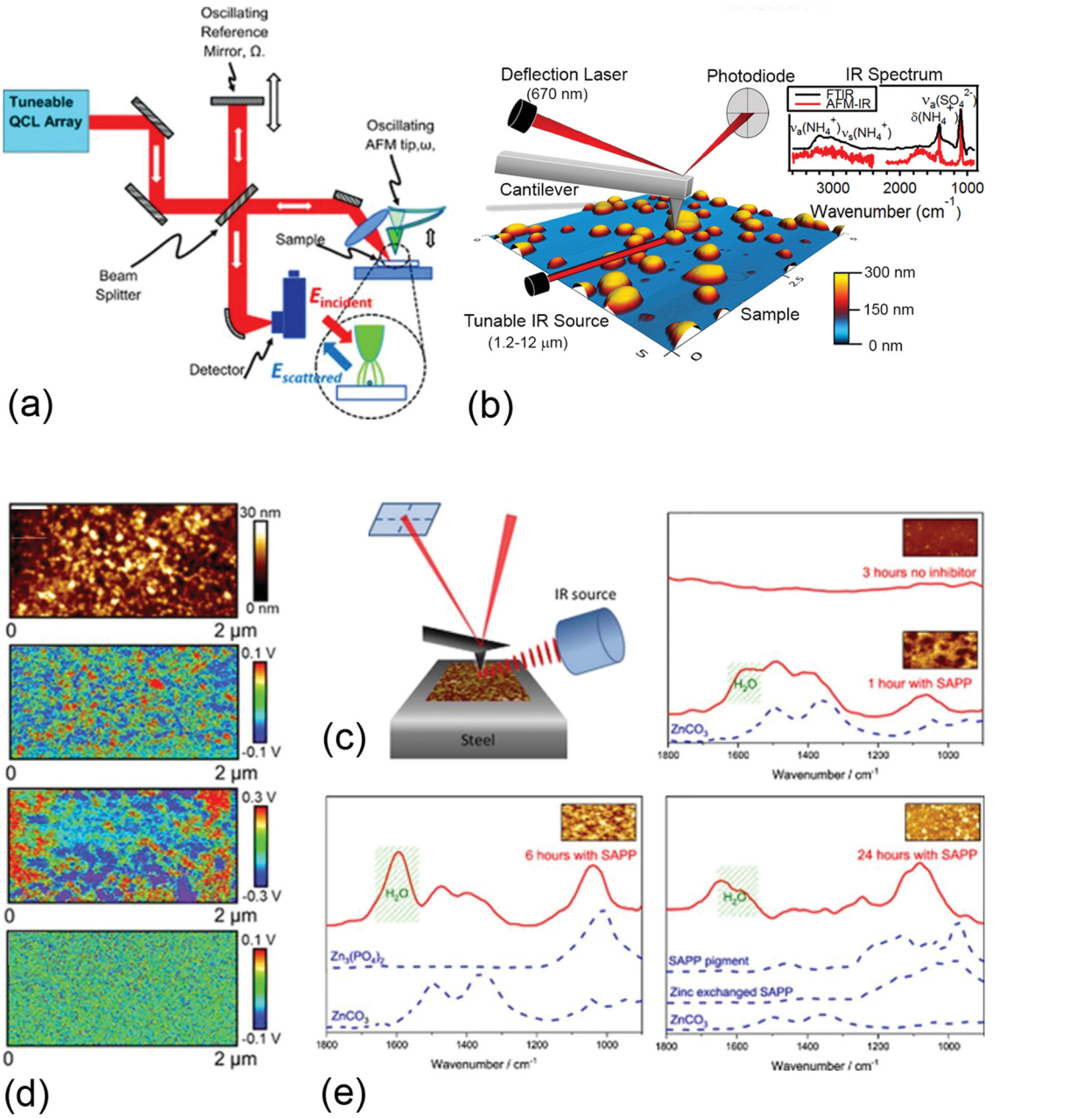

Fig. 25 Schematic diagram of (a) scanning near-field optical microscopy (s-SNOM); (b) general scheme of AFM-FTIR. Reprinted with permission from ref. 411, Copyright 2017, the American Chemical Society; (c) the AFM-FTIR setup; (d) height image of a 100 nm thick microtomed section of epoxy phenolic resin cured with a catalyst at 150 °C for 10 min, and the corresponding maps of peak-to-peak IR-induced deflection following irradiation at 1116 cm^{-1}; (e) AFM-IR spectra, gathered from the steel cathode after immersion in NaCl with or without the addition of saturated concentrations of an inhibitor (red solid lines). Bulk ATR-IR spectra (blue dashed lines) are shown for comparison. Adapted from ref. 325, 2019, published open access under a CC-BY license.

not fully understood, was investigated by combination of RAIRS-AFM and bulk ATR IR spectroscopy.[329] It has been shown that cathodic inhibition dominates at the galvanised steel cut edge in the presence of a dissolved strontium aluminium polyphosphate inhibitor, which is caused by the rapid precipitation of the thick film to cathodic regions. EDX elemental analysis and the AFM-IR technique shown that the rapid formation of a cathodic film is in fact due to the presence of highly soluble strontium carbonate impurities in the commercially available pigment, which leads to the capture of zinc ions in the form of a zinc carbonate layer (Fig. 25d and e).

Electrochemical processes are of crucial importance for energy storage, conversion, electrocatalysis, photoelectrocatalysis, sensorics and a variety of other applications. Thus, their detailed understanding continuously attracts wide research interest. Classical electrochemical methods provide important information about the thermodynamics and kinetics of electron transfer across interfaces, and in many cases enables the identification of

chemical species *via* the measurement of redox potentials. However, the molecular information is limited by this classical approach, so additional characterisation tools are needed for a complete picture of physical and chemical processes at interfaces that govern the electrochemical processes. Obviously, there is a room in this respect for a variety of applications of IR spectroscopy. It enables not only detection and identification of unknown molecular species but, particularly in the case of solid–liquid interfaces, reveals important, information-rich insights into the nature of surface adsorbates, such as the binding mode, bond strength and molecular orientation.[330]

Various cells for *in situ* IR spectroscopy, usually based on ATR, have been designed to investigate the various processes responsible for the action of batteries. Examples include cells that enable monitoring of the decomposition of lithium sulfide battery electrolytes, compatible with various cathodes and anodes,[331,332] A very important utilisation of IR spectroscopy in the field of lithium sulfide batteries includes chemical identification of polysulfide species.[332,333] For instance, an *in situ* ATR-IR study indicated the evolution of polysulfide species and triflate anion coordination states during cycling.[333] The transport kinetics and the degree of polysulfide dissolution in either polymer or ionic liquid electrolytes is clearly demonstrated. Moreover, the authors further pointed out that this *in situ* IR monitoring has high potential to be applied in assisting the design of novel functional electrolytes, additives, and new systems for lithium sulfide batteries, such as polymeric and all-solid-state electrolytes. Further, a combination of *in situ* IR and Raman spectroscopy gives real-time information of adsorbed species on the interface of the electrode of the lithium oxide battery system, and reveals the in-depth reaction mechanism on the electrode–electrolyte interface.[320]

The power of surface-enhanced Raman spectroscopy (SERS) has encouraged the development of analogous IR technique, SEIRS.[330,334] This is especially interesting due to the limitations of Raman spectroscopy. Although the two techniques share a great deal in common, they are significantly different in their practical implementation, which makes IR spectroscopy the method of choice in a variety of electrochemically-relevant applications. The SEIRS effect is based on amplification of the electromagnetic field due to localised surface plasmons and chemical effects in operation.[334–336] SEIRS allows submonolayer detection of molecules adsorbed at surfaces and, as demonstrated by the pioneering work of Osawa's group, can provide a valuable tool for investigating electrochemical interfaces *in situ*.[335] Although SEIRS is far less powerful than SERS, and for this reason it is not widely applied, recent developments in surface Raman scattering techniques could in principle be extended to SEIRS, so there is scope for further innovation.[330] The most common configuration of the electrochemical SEIRS experiment is to use ATR: with the working electrode deposited as a thin film on the surface of a bevelled prism and the IR beam reflected off the interior wall of this prism (Fig. 26). In this way, the incident IR beam does not pass directly through the electrolyte solution, but instead the evanescent wave penetrates into the solution, thus minimising losses.[337]

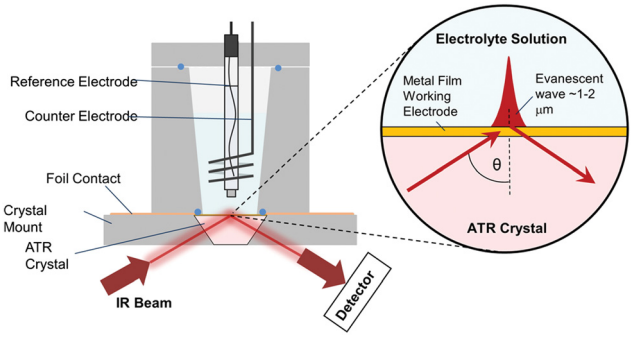

Fig. 26 Schematic depiction of the ATR configuration commonly employed for electrochemical surface-enhanced IR absorption spectroscopy (EC-SEIRAS). Adapted from ref. 330, 2017, published open access under a CC-BY license.

Despite its limitations, that have not yet been satisfactorily overcome, *in situ* IR spectroscopy, especially in its ATR-SEIRS incarnation, where the IR beam targets the working electrode,[338–340] is relatively frequently employed to investigate electrochemical capacitors.[166] Its first use in this respect was the measurement of ion dynamics of an ionic liquid, 1-ethyl-3-methylimidazolium triflate, in a functioning capacitor with RuO_2 as a pseudocapacitor.[338] Since then, it has revealed new insights into the charging mechanism of electrochemical capacitors, and clearly demonstrates the role of surface chemistry of carbon electrodes in the charge storage mechanism.[341–343] A very interesting and important application of IR spectroscopy to follow the degradation of battery electrodes includes the monitoring of the generation of solid electrolyte interfaces on the surface of anodes of lithium batteries, which suppresses cycling thus causing passivation of the battery.[344–349]

Other examples

2D materials find a wide range of applications in the field of electrochemical devices, since they have a large active surface area, they are often semiconductors with tunable band gaps.[350] IR spectroscopy is especially interesting as a tool for the characterisation of phase transformations of electrodes made of 2D materials, as well as identification and chemical reactions of active sites, and characterisation of the role of intercalated species.

Development of efficient procedures for CO_2 capture is initiated by aspirations to reduce its concentration in the atmosphere by chemical or electrochemical methods, and thus to contribute to the mitigation of climate change by realizing various versions of so called net-zero energetic scenarios. IR spectroscopy is an especially interesting technique in this regard, since it enables the elucidation of very accurate information on binding and chemical transformations of CO_2 molecules on the surface of the electrode or catalyser.[17,351,352] For this purpose, ATR mode is ideally suited.[23,353,354] Metal electrodes made of silver, gold or platinum can further amplify the signal, practically enabling SEIRS (Fig. 27),[355,356] which

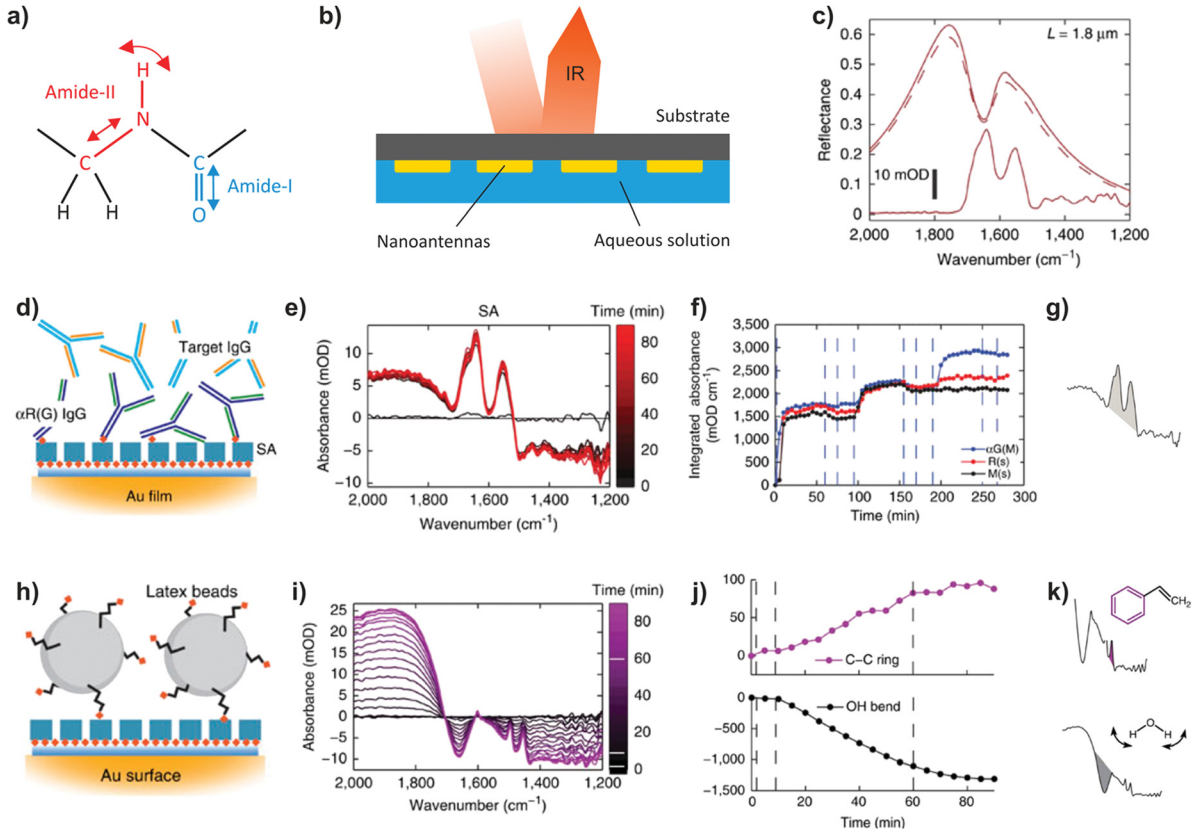

Fig. 27 (a) Molecular structure of the amide group and vibrational modes as indicated by arrows. (b) Schematic illustration of the plasmon internal reflection (PIR) (not to scale). (c) Reflectance spectra before (dashed) and after (solid) streptavidin (SA) binding for the L = 2.2 μm antenna array sampled in aqueous media. The absorbance is displayed at the bottom of the panel (solid line) with units indicated by the scale bar. (d) Schematic of protein-binding interactions measured. The gold antennas (Au film) are covered with a self-assembled monolayer of a biotin-labeled alkanethiol (blue and red dots), to which SA binds. They are further functionalized with G(M) IgG, which allows for the selective adsorption of the respective target IgG (see text). (e) Time series of spectra taken during SA. (f) Peak integral (integrated absorbance) evolution over time during the protein-binding measurements for the three samples. Abbreviations are as follows: G(M), antigoat (mouse host) IgG; R(s), rabbit IgG; M(s), mouse IgG. Vertical lines indicate the rinsing process. In all experiments, for each step the protein solution is allowed to flow for 60 min (first horizontal line). Each step is followed by a 15 min rinse with a detergent (second vertical line), then pure buffer (third vertical line). (g) Amide band peak integral used to assess protein binding. (h) Schematic of the biotin-labeled latex bead (LBSA binding (labeling as in (d)). (i) Time-series absorbance spectra during the LB-binding steps. The vibrational features at 1450 and 1490 cm^{-1} are associated with the benzene ring; the vibrational feature at 1650 cm^{-1} originates from the OH vibration in H_2O (see also (k)). (j) Evolution of the peak integrals (integrated absorbance, units of mOD (optical density) cm^{-1}) over time during LB-binding steps. Vertical dashed lines indicate the rinsing process. (k) Specific chemical structures and their corresponding IR fingerprints (peak integrals) used to monitor their presence during the flow experiments. Reprinted with permission from ref. 355, Copyright 2017, the American Chemical Society.

enables detailed insight into the mechanism of CO_2 transformations to usable products, through the identification and quantification of intermediates.[357–359] Beyond studies of the dependence of electrocatalytic transformation of CO_2 on metal type, it is shown that the activity and selectivity strongly depend on the exposed surface of the metal.[360–362] Recent advances of ATR-SEIRS have led to studies involving real catalytic systems, different from model electrode surfaces. In one of the experiments, a Au film was chemically deposited on the basal plane of a hemicylindrical Si ATR element, covered by a layer of Zn.[363] This setup enabled monitoring of the Li-tuned electrochemically Zn-catalysed CO_2 reduction reaction with a time resolution of 2 s. Such a high time resolution enabled accurate detection and quantification of reaction intermediates, thus revealing the mechanism of interfacial reduction of CO_2 to CO at the molecular level.

Diffusion

Recent breakthroughs in the field of solid-state chemistry, especially mechanochemistry and ageing reactions, undoubtedly show that solids are much more dynamic systems, more susceptible to mutual chemical changes, in contrast to recently held opinions.

Although examples of such reactions have only recently increased, for example the unexpectedly fast and furious reaction of NaH with NH_3BH_3[195] (still unexplored by IR spectroscopy), the classical cocrystallization of diphenylamine and benzophenone was only recently thoroughly studied by IR spectroscopy.[194] In this example, the eutectic liquid intermediate is responsible for promoting the reaction by transporting the reactants. To investigate the mechanistic details of this reaction, an extremely simple experimental setup, consisting of

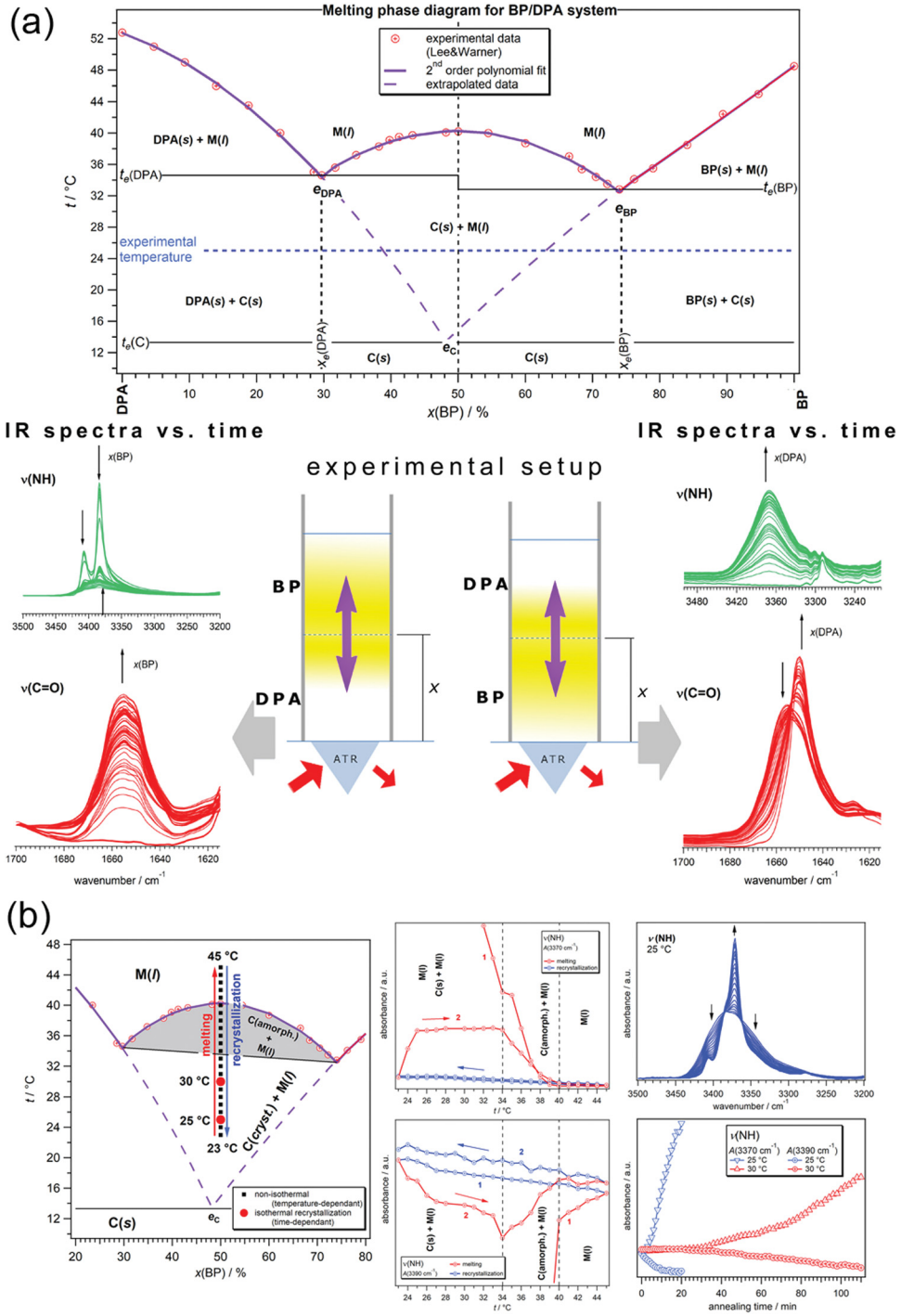

Fig. 28 (a) Scheme of the isothermal experiment; melting phase diagram for a benzophenone–diphenylamine (BP/DPA) system. The experimental setup, consisting of a glass tube vertically placed on the ATR element of an IR spectrometer, practically enables the spectroscopic consideration of two separated two-component phase diagrams, which reflect the experimentally observed events along the reaction coordinate. Upon contact, the reactants melt and the front of the liquid intermediate phase travels along the column in both directions with respect to the original contact surface, as indicated with the violet arrows. As a result, IR spectra, here represented by ν(NH) (green) and ν(CO) regions (red) of the corresponding systems, are obtained. (b) Non-isothermal transmission IR spectroscopic monitoring of the melting and recrystallization of the BP/DPA cocrystal. A nonisothermal experiment at 2345 °C is denoted by black dots in the phase diagram, while red dots indicate temperatures at which recrystallization was followed over time. The gray region arbitrarily indicates the amorphous phase that precedes cocrystal melting. Two cycles of nonisothermal melting recrystallization are indicated by the hysteretic temperature dependence of the IR absorbance of individual contributions of ν(NH). The same spectral features are followed to monitor the isothermal recrystallization over time. Reprinted with permission from ref. 194, Copyright 2021, the American Chemical Society.

a glass tube vertically placed on the single-reflection ATR element was constructed, which enabled the effective separation of the two sides of the benzophenone–diphenylamine melting phase diagram. IR spectroscopic monitoring enabled the detailed observation of all stages of the cocrystallization process. It consists of a series of mechanisms including molecular diffusion, formation of eutectic phase, and cocrystallization through an amorphous phase. The cocrystallization itself is enabled by continuous feeding of the eutectic phase by solvation of the starting phases, which then flow through and combine together in a liquid phase. The overall process is evidently driven by hydrogen-bonding interactions of NH···O=C type, while the melting of individual starting phases and their efficient transport through the liquid is improved by the difference in conformational flexibility. Isothermal and non-isothermal monitoring shows that the melting of the cocrystal and its recrystallization are not single-step processes. Upon heating, the system passes through an amorphous phase. Upon cooling, the liquid phase recrystallizes to the cocrystal, but this process requires some time, which can be very long. In this respect, similar IR spectroscopic studies are needed to resolve generalities in solid-state transformations that involve the formation of eutectic liquid intermediates (Fig. 28).

Additionally, IR spectroscopy was employed to monitor the diffusion and transport low molecular weight compounds and to provide the predictive thermodynamic description of sorption processes in polymers.[18] Examples include exploration of structure and dynamics of H_2O molecules in polymeric matrices,[364] as well as diffusion of acetone, methyl ethyl ketone and benzene polyethylene,[365] which aims to demonstrate the feasibility and accuracy of the ATR measurement of diffusion coefficients.

Other chemical processes

Monitoring thermal decomposition processes is one of the classic fields of utilisation of *in situ* IR spectroscopy. The accessories that satisfy the needs of these experiments are now widely commercially available from various providers. Basically, chemical identity of the sample is completely changed upon decomposition, which generally causes dramatic changes in the IR spectra with respect to applied perturbation, most commonly temperature. Another perturbation causing decomposition could be the presence of reactive chemicals, radiation or time. More generally, decomposition can be defined as a chemical alteration caused by exposure of the sample to environmental conditions over time.

Since the products of decomposition frequently involve the gas phase, IR spectroscopy can be used to follow the evolution of both solid and gaseous products. The approach is thus similar to those described for monitoring of gas sorption and desorption processes. Although decomposition can be caused by different chemical and physical agents, thermal decomposition is most widely investigated. Commercially available accessories include variable-temperature ATR plates, heating jackets for transmission measurements, variable-temperature DRIFTS chambers, high-pressure high-temperature cells, TG instruments coupled to IR spectrometers equipped with gas cells *etc.* The variety of available equipment, together with high flexibility of IR spectroscopy enable accurate IR spectroscopic insight into practically all chemical processes that involve changes in covalent bonds, hydrogen bonding network and intra- and intermolecular rearrangements governed by various intermolecular interactions. In this respect, a highly helpful review with a thorough discussion of the design and characteristics of numerous cells for *in situ* vibrational spectroscopic reaction monitoring is available.[366] The opportunities are diverse, limited only by the creativity of the researcher.

In line with this comment, it is clear that it is impossible to cover all the applications of IR spectroscopy to monitor decomposition processes. This paper will highlight only a few illustrative examples, without trying to cover all possible concepts. Actually, surprisingly few reviews on methodology itself are available,[367–369] so the interested reader should screen the specialized reviews and primary publications in accordance with his/her field of interest.

The use of IR spectroscopy to monitor non-thermal decomposition and chemical alterations of materials involve the study of UV aging of asphalt involving carbon nanotubes/polystyrene composite,[370] as well as alterations of microplastics,[371] discharge-initiated decomposition of SF6,[372] and environmental degradation of various real-world materials.[373,374]

The experiments in transmission mode usually require the use of alkaline halogenide matrix materials, most commonly KBr. However, in some cases such a matrix can influence the sample, thus one should always take into account this possibility and critically consider the obtained results. One of the relatively recent examples is an investigation of thermal decomposition of ammonia borane, NH_3BH_3.[75] In this study, decomposition of NH_3BH_3 was monitored in both transmission and ATR mode, and comparison of the obtained results undoubtedly shows that interaction with KBr significantly affects the mechanistic pathway of technologically relevant thermal decomposition of this material, considered for solid-state hydrogen storage. As usual, KBr pellets were used for transmission measurements, while ATR measurements were done for both neat NH_3BH_3 and NH_3BH_3 : KBr = 1 : 1 mixtures. While neat NH_3BH_3 shows two-step decomposition, its mixing with KBr is a one-step process in the same temperature range (Fig. 29). Although KBr does not affect the chemical identity of NH_3BH_3, it dramatically affects the thermal decomposition, which is especially pronounced by partial solvation of KBr in molten highly polar NH_3BH_3. Additionally, thermally induced dimerization of NH_3BH_3, a crucial step in its decomposition, is evidently promoted by ionic species such as KBr.

In another study, the thermal decomposition of a series of derivatives of NH_3BH_3, namely $Li_2Ca(NH_2BH_3)_4$ and $Na_2Ca(NH_2BH_3)_4$, was monitored by transmission IR spectroscopy, supported by mass spectrometry for evolved gas analysis.[195] From Fig. 30, it is evident that $Na_2Ca(NH_2BH_3)$ decomposes through a two-step mechanism, while $Li_2Ca(NH_2BH_3)$ goes straight to the end product. Although both species are similar,

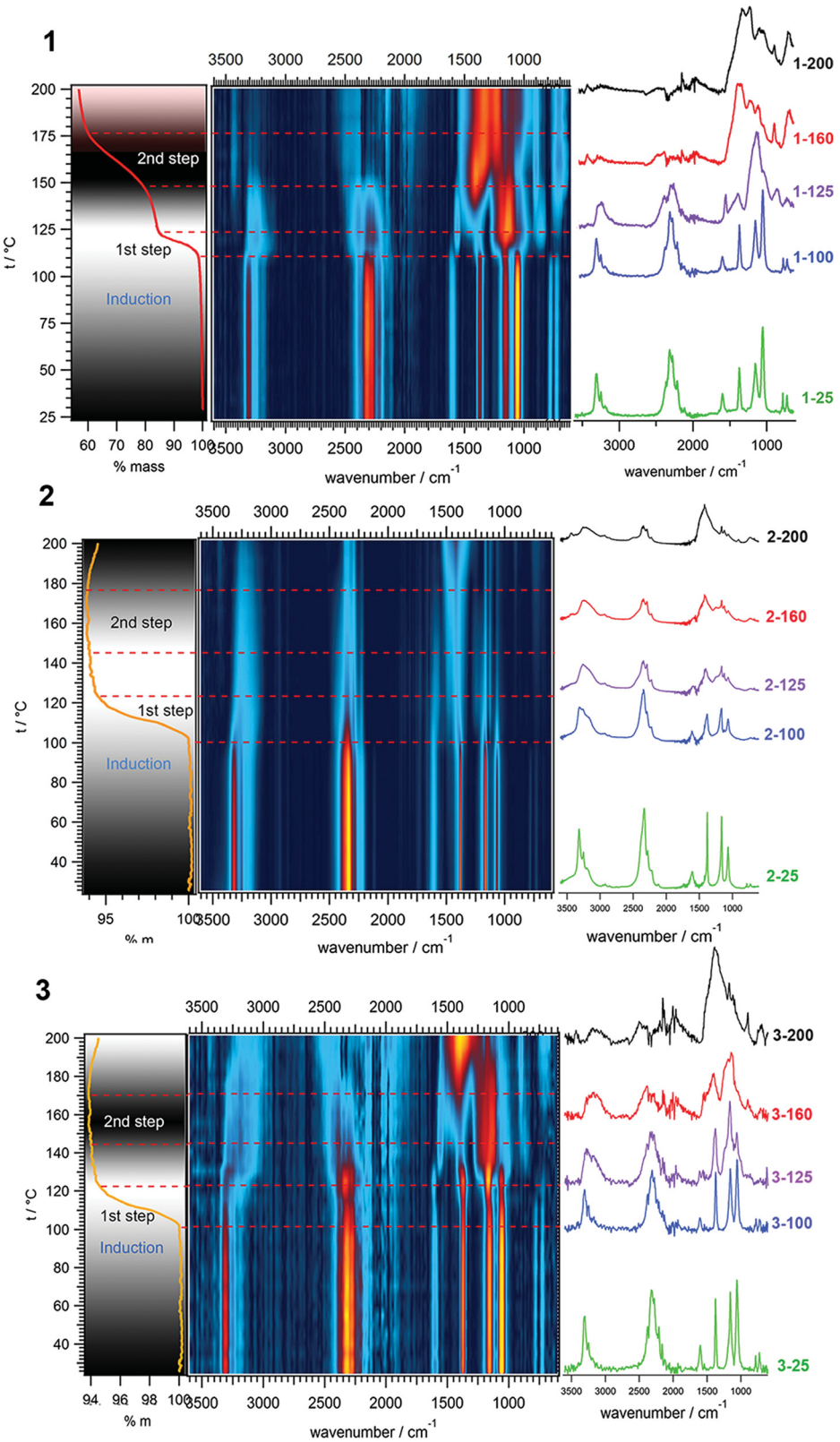

Fig. 29 Comparison of variable-temperature IR spectra with TG/DTA for ATR spectra of neat NH_3BH_3 (**1**), transmission spectra of KBr pellets of NH_3BH_3 (**2**) and ATR spectra of 1 : 1 mixtures of KBr and NH_3BH_3 (**3**). These measurements clearly indicate the pronounced influence of KBr on the thermal decomposition of NH_3BH_3. Reprinted with permission from ref. 75, Copyright 2016, the American Chemical Society.

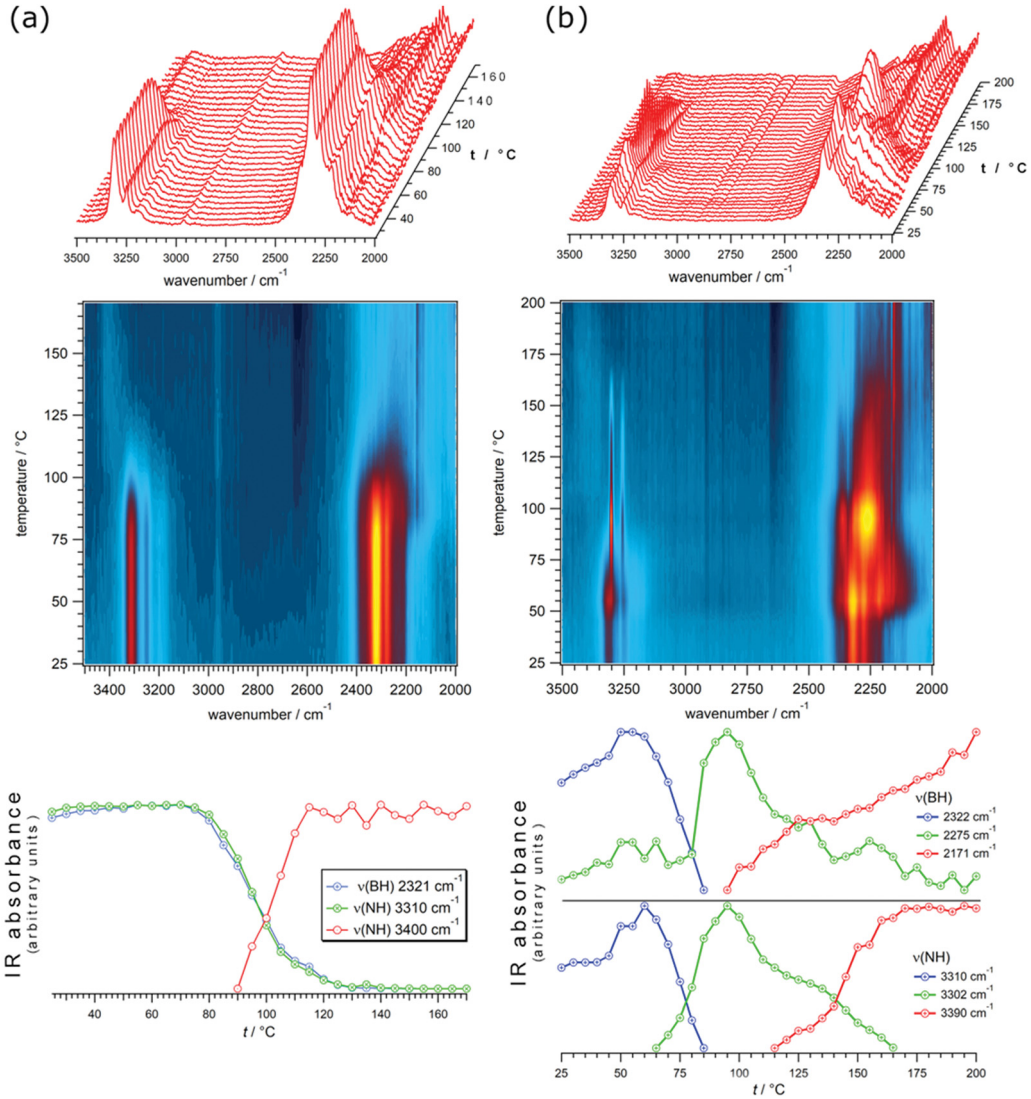

Fig. 30 Temperature-dependent IR spectra of (a) $Li_2Ca(NH_2BH_3)_4$ and (b) $Na_2Ca(NH_2BH_3)_4$ in the 3500–2000 cm^{-1} spectral range, and room temperature up to 200 °C at a 2 °C min^{-1} heating rate. Reaction profiles for different ν(NH) and ν(BH) bands are shown on the bottom row. The profiles show absorbance normalized with respect to maximal values, and are obtained by fitting the envelopes to Lorentzian profile functions. Reprinted with permission from ref. 195, Copyright 2021, the American Chemical Society.

their crystal structures are significantly different. These findings and their comparison with familiar systems indicate that generally all sodium-containing amidoboranes follow two competitive thermal dehydrogenation pathways.

In this domain, the advantages provided by 2D correlation analysis have come to the fore.[105,375–390] Although in principle this is just another method of visualisation of measured data, it also provides good insight into perturbation-induced evolution of the chemical system, by emphasizing changes in the background, and indicating the ranges of perturbation where the changes occur, which facilitates further analysis.

Challenges, perspectives and horizons

Although very simple and flexible in its performance and simultaneously very sophisticated in the wealth of information it can provide, IR spectroscopy is still most frequently used only as a routine technique for the characterisation of chemical products. In this light, it is a pity that researchers often overlook the benefits of this widespread and widely available technique. Examples of its utilisation in the text so far clearly illustrates its high flexibility and usability over a huge range of chemical and physical problems. Today, the availability of highly sophisticated instrumentation, together with advances in dedicated on-line accessible software,[61] enables really unique opportunities, which are limited only by researcher creativity. I hope these examples will be inspiring enough for at least some further research. Finally, I would like to give an overview of the problems and challenges for the further development and applications of the method. This discussion is by no means exhaustive, and should be considered as the author's perspective.

Development of new accessories

Needless to say, many arising problems are solvable by IR spectroscopy which inspires new techniques and approaches, enabled by the design and development of new accessories and instrumentation. In some cases just a very simple setup can do the required job well.[194] This is especially true with the recent development and dramatic drop in price of 3D printing, which in turn enables making devices in accordance with the researcher's own needs and ideas, quick and simple.[391,392]

However, the vast majority of new challenges require very sophisticated, often multi-instrumental approaches. The use of synchrotron radiation enabled until recently, unattainable spatial and temporal resolutions, which in turn enable accurate real time monitoring of various solid-state systems through detailed mapping.[393] This is especially true for surface and interface phenomena, where there is plenty of room for further development.[57,394–398] The development in the field of femtosecond IR spectroscopy also promises deep insight into ultrafast dynamics of solid-state systems, and significant breakthroughs are also to be expected here.[399–401]

Microspectroscopy. The brilliance of synchrotron radiation now enables analysis of hitherto elusive processes over a wide spectral range of electromagnetic radiation, including IR.[10,124,393,402–405] High intensities enable very accurate microspectroscopy. In this respect, especially interesting is synchrotron-based infrared microspectroscopy (SIRMS) with its very high signal-to-noise ratio, high spatial resolution, extended measurement conditions and high sensitivity. Altogether, this provides a platform for the investigation of very small amounts of material that need to be used in various investigations performed using IR spectroscopy. In a recent review, Kong and Liu presented well organised parameters of available IR beamlines, together with other useful information.[10] However, the greatest challenge of using IR microspectroscopy to analyse and monitor the changes of submicrometer particles has been the diffraction limited resolution of IR light (Abbe limit), which is typically 2–20 μm.[406] Recent development of commercial infrared focal plane array (FPA) detectors[407,408] has enabled rapid acquisition of chemical images with fields of view greater than 100×100 μm^2. Although the imaged pixel size of FPA detectors can be less than 1×1 μm^2, the spatial resolution remains limited by diffraction, and can only be marginally improved beyond the Abbe limit through oversampling and point spread function deconvolution techniques. By combining simultaneous single-particle measurements of physical properties by atomic force microscopy (AFM) with chemical composition as obtained by IR spectroscopy, AFM-IR overcomes size limitations with imaging capabilities on the scale of ~50 nm chemical resolution (Fig. 25).[409–414]

The current AFM-IR technique is relatively simple and it uses an IR tunable pulsed laser to induce a photothermal effect in the sample, and an AFM to detect the resulting mechanical expansion *via* the cantilever tip that is in contact with the sample. To relax the excess of stress induced by the local increase of temperature of the sample, the absorbing region expands and pushes the cantilever tip in contact with the sample surface. So, the idea of AFM-IR is not to detect the induced photothermal heat but to detect the thermal expansion with an AFM tip, using the high sensitivity of the AFM system to vertical height changes of the sample (tens of picometers) and its excellent lateral resolution (10–20 nm). For sure, this principle enables the best spatial resolution currently achievable by IR spectroscopy. However, the local radiation-induced heating of the sample could be seen as a potential drawback of the technique, since it can modify the sample, which in turn can cause a deviation from its real chemical nature. It could be expected that further development of IR spectroscopic techniques will in some way overcome this drawback.

Still unexplored chemical processes

The importance of solid-state chemical reactions is growing, since they often result in the targeted products, without the presence of by-products in significant amounts. Usually diffusion and interpenetrations of reactants are crucial for these processes, which can be in some cases, unexpectedly fast.[194,195,415] These phenomena are still unsatisfactorily understood. In combination with molecular dynamics, IR spectroscopy can provide a deep and detailed insight into the mechanisms of these important processes, that open up new perspectives in solid state dynamics.

A very interesting and important, still unexplored field of potential utilisation of IR spectroscopy for *in situ* monitoring of chemical reactions, comprises mechanochemistry, especially ball milling as the most commonly used mechanochemical method. Even though its origin is very old, literally prehistoric, mechanochemistry has only relatively recently attracted significant interest of chemists and the chemical industry. In practice, ball milling reactions are carried out by adding one or more steel balls to a reaction mixture closed in a reaction vessel. The mill shakes the vessel, which causes rapid moving of the balls inside the vessel, and the mechanical energy of the balls is transferred to the reaction mixture and converted to chemical energy. Very recently, a series of publications on resonant acoustic mixing has started to appear, which does not require balls to convert mechanical energy to the chemical system, which is very promising with respect to energy efficiency and greenness of the chemical process.[416] One of the most important benefits of mechanochemistry is its inherently solvent-free means of chemical and materials transformations, which sets it on the frontline for developing green chemistry concepts aimed towards an environmentally friendlier chemical and pharmaceutical industry.[417–419] The range of chemical transformations achieved by mechanochemistry has been rapidly expanding in the last two decades, and it is now present across preparative chemistry processes, with high potential for wide industrial implementation.[382,420–430]

Regardless of their ever-growing importance and prevalence, mechanochemical reactions remain as some kind of black box. Only recent implementation of various techniques for *in situ* monitoring of ball milling reactions has enabled insight under the hood of rapidly moving mechanochemical

milling vessels.[195,431–440] Monitoring of ball milling reactions enables significant progress in understanding of their mechanistic pathways and kinetics, influence of additives and environmental conditions. However, due to serious technical problems facing the design of appropriate equipment, IR spectroscopy has not entered this playground yet. Its introduction would enable deeper insight into the intra- and intermolecular background of mechanochemical processes, since it is more sensitive to intermolecular interactions and changes in the local microenvironment, than any other method. The use of IR spectroscopy in the field of mechanochemistry is still limited to *ex situ* routine spectroscopy. To the best of our knowledge, the first example of the use of IR spectroscopy to monitor ball milling reactions was described very recently by Rathmann *et al.*[441] Actually, they connected an FTIR spectrometer to the milling jar by gas capillary, and combine IR spectroscopy with EGA-MS to analyse the composition of the gas phase inside the milling jar. However, solid phase transformations, essential for full mechanistic understanding of the mechanochemical reactions, still remains unattainable to IR spectroscopy, but development in this direction is to be expected.

Concluding remarks

Although a ubiquitous technique, available in many chemical laboratories, and capable of providing rich information on intra- and intermolecular arrangement of matter on the molecular scale, IR spectroscopy is frequently underutilized and used merely as a routine method for the quick characterisation of products. All the possibilities offered by this technique that is simple and flexible in its application, and rich in information on chemical systems, are often neglected by researchers. Thus, this tutorial review serves as a reminder or introduction to the fundamental and practical aspects of this technique, which could provide crucial information on not only solids, but also liquids and gases. Specifically, the review is focused on solids, with an emphasis on those of relevance in contemporary materials science. Although many examples were beyond the scope of this review, we provide a variety of unique illustrative and, the author hopes, inspiring examples in the field, along with the various techniques involved in data acquisition and their analysis.

Today, IR spectroscopy is successfully coupled with various techniques and integrated in most sophisticated facilities, enabling deep and detailed insight into the molecular processes underlying the chemical and physical phenomena, which are fundamental for understanding the action of materials. Whilst the authors do not suggest in any way that IR spectroscopy alone will ever replace other available methods that enable investigation of matter at the molecular level, they underline its power in providing unique insight into intra- and intermolecular forces and the molecular environment, through direct measurement of vibrations of functional groups.

In the short term, the authors anticipate the implementation of *in situ* IR spectroscopy to address various chemical and physical problems. However, in the longer term, the development of new technologies, such as 3D printing, automation, robotics, machine learning and artificial intelligence, and their implementation to IR spectroscopy will revolutionise its applications and enable its penetration even deeper under the hood of matter. This, in the author's humble opinion, is the next frontier of IR spectroscopy and its utilisation.

Conflicts of interest

The author declares no conflicts of interest.

Acknowledgements

This review was written under the financial support in the framework of H2020-MSCA-IF-894705 (GrindCore) action. Additionally, the author wishes to thank COST action CA18112, and the reviewers for valuable comments.

References

1 E. Kraka, W. Zou and Y. Tao, Decoding chemical information from vibrational spectroscopy data: Local vibrational mode theory, *Wiley Interdiscip. Rev.: Comput. Mol. Sci.*, 2020, **10**, e1480.
2 A. Bieberle-Hütter, A. Bronneberg, K. George and M. Van De Sanden, Operando attenuatedtotal reflection Fourier-transform infrared (ATR-FTIR) spectroscopy for water-splitting, *J. Phys. D: Appl. Phys.*, 2021, **54**, 133001.
3 K. Feng, Y. Wang, M. Guo, J. Zhang, Z. Li, T. Deng, Z. Zhang and B. Yan, Insitu/operando techniques to identify active sites for thermochemical conversion of CO_2 over heterogeneous catalysts, *J. Eng. Chem.*, 2021, **62**, 153–171.
4 D. Murgida, *In situ* spectroelectrochemical investigations of electrode-confinedelectron-transferring proteins and redox enzymes, *ACS Omega*, 2021, **6**, 3435–3446.
5 C. Nunes, I. Reva and R. Fausto, Chapter 1: Direct observation of tunnelling reactions by matrix isolation spectroscopy, *RSC Theor. Comput. Chem. Ser.*, 2021, 1–60.
6 B. Chen, Exploring nanomechanics with high-pressure techniques, *Matter Radiat. Extremes*, 2020, **5**, 115981.
7 C. Wöll, Structure and chemical properties of oxide nanoparticles determined by surface-ligand IR spectroscopy, *ACS Catal.*, 2020, **10**, 168–176.
8 A. Alodhayb, F. Khan, H. Etayash and T. Thundat, Review – Nanomechanical calorimetric infrared spectroscopy using bi-material microuidic cantilevers, *J. Electrochem. Soc.*, 2020, **167**, 037504.
9 F. Zaera, New advances in the use of infrared absorption spectroscopy for the characterization of heterogeneous catalytic reactions, *Chem. Soc. Rev.*, 2014, **43**, 7624–7663.
10 L. Kong and G. Liu, Synchrotron-based infrared microspectroscopy under high pressure: An introduction, *Matter Radiat. Extremes*, 2021, **6**, 068202.

11 C. Kratz, A. Furchner, G. Sun, J. Rappich and K. Hinrichs, Sensing and structure analysis by *in situ* IR spectroscopy: From mL ow cells to microfluidic applications, *J. Phys.: Condens. Matter*, 2020, **32**, 393002.
12 K. Grabow and U. Bentrup, Homogeneous catalytic processes monitored by combined *in situ* ATR-IR, UV-VIS, and Raman spectroscopy, *ACS Catal.*, 2014, **4**, 2153–2164.
13 V. Mittal, G. Mashanovich and J. Wilkinson, Perspective on thin film waveguides for on-chip mid-infrared spectroscopy of liquid biochemical analytes, *Anal. Chem.*, 2020, **92**, 10891–10901.
14 B. Napier, *et al.*, Ultra-broadband infrared gas sensor for pollution detection: The TRIAGE project, *J. Phys. Photonics*, 2021, **3**, 031003.
15 B. Giechaskiel and M. Clairotte, Fourier transform infrared (FTIR) spectroscopy for measurements of vehicle exhaust emissions: A review, *Appl. Sci.*, 2021, **11**, 7416.
16 N. Drenchev, K. Chakarova, O. Lagunov, M. Mihaylov, E. Ivanova, I. Strauss and K. Hadjiivanov, *In situ* FTIR spectroscopy as a tool for investigation of gas/solidinteraction: Water-enhanced CO_2 adsorption in UiO-66 metal-organic framework, *J. Visualized Exp.*, 2020, e60285.
17 R. Kas, O. Ayemoba, N. J. Firet, J. Middelkoop, W. A. Smith and A. Cuesta, *In situ* infrared spectroscopy applied to the study of the electrocatalytic reduction of CO_2: Theory, practice and challenges, *ChemPhysChem*, 2019, **20**, 2904–2925.
18 G. Mensitieri, G. Scherillo, C. Panayiotou and P. Musto, Towards a predictive thermodynamic description of sorption processes in polymers: The synergy between theoretical EoS models and vibrational spectroscopy, *Mater. Sci. Eng., R*, 2020, **140**, 100525.
19 I. Mudunkotuwa, A. Minshid and V. Grassian, ATR-FTIR spectroscopy as a tool to probe surface adsorption on nanoparticles at the liquid-solid interface in environmentally and biologically relevant media, *Analyst*, 2014, **139**, 870–881.
20 G. Rupprechter, Operando surface spectroscopy and microscopy during catalytic reactions: From clusters *via* nanoparticles to meso-scale aggregates, *Small*, 2021, **17**, 2004289.
21 X. Li, S. Wang, L. Li, Y. Sun and Y. Xie, Progress and perspective for *in situ* studies of CO_2 reduction, *J. Am. Chem. Soc.*, 2020, **142**, 9567–9581.
22 L. Jin and A. Seifitokaldani, *In situ* spectroscopic methods for electrocatalytic CO_2 reduction, *Catalysts*, 2020, **10**, 481.
23 Y. Zhang, S.-X. Guo, X. Zhang, A. Bond and J. Zhang, Mechanistic understanding of the electrocatalytic CO_2 reduction reaction – New developments based on advanced instrumental techniques, *Nano Today*, 2020, **31**, 100835.
24 E. F. J. Ring, The discovery of infrared radiation in 1800, *Imaging Sci. J.*, 2000, **48**, 1–8.
25 A. Rogalski, History of infrared detectors, *Opto-Electron. Rev.*, 2012, **20**, 279–308.
26 J. F. W. I. Herschel, On the chemical action of the rays of the solar spectrum on preparations of silver and other substances, both metallic and non-metallic, and on some photographic processes, *Philos. Trans. R. Soc. London*, 1840, **130**, 1–59.
27 S. P. Langley, The bolometer and radiant energy, *Proc. Am. Acad. Arts Sci.*, 1880, **16**, 342–358.
28 E. Barr, The infrared pioneers III. Samuel Pierpont Langley, *Infrared Phys.*, 1963, **3**, 195–206.
29 W. W. Coblentz, Reminiscences of early investigations of infrared absorption spectra, *Appl. Spectrosc.*, 1953, **7**, 109–111.
30 R. B. Barnes and L. G. Bonner, The early history and the methods of infrared spectroscopy, *Am. J. Phys.*, 1936, **4**, 181–189.
31 E. B. Wilson, J. C. Decius and P. C. Cross, *Molecular Vibrations: The Theory of Infrared and Raman Vibrational Spectra*, Dover Publications, London, 1980.
32 A. Einstein, On the theory of light production and light absorption, *Ann. Phys.*, 1906, **325**, 199–206.
33 A. Einstein, Strahlungs-emission und absorption nach der quantentheorie, *Deutsch. Phys. Gesellsch.*, 1916, **18**, 318–323.
34 A. A. Michelson, XXX. On the application of interference methods to spectroscopic measurements. II, *Philos. Mag., Ser. 5*, 1892, **34**, 280–299.
35 A. A. Michelson, XXVIII. Visibility of interference-fringes in the focus of a telescope, *Philos. Mag., Ser. 5*, 1891, **31**, 256–259.
36 L. Rayleigh 2nd, XLVII. On the interference bands of approximately homogeneous light; in a letter to Prof. A. Michelson, *Philos. Mag., Ser. 5*, 1892, **34**, 407–411.
37 P. R. Griffiths, The early days of commercial FT-IR spectrometry: A personal perspective, *Appl. Spectrosc.*, 2017, **71**, 329–340.
38 P. Connes, Early history of Fourier transform spectroscopy, *Infrared Phys.*, 1984, **24**, 69–93.
39 P. R. Griffiths and J. A. de Haseth, *Fourier Transform Infrared Spectrometry*, John Wiley & Sons, Inc., Hoboken, New Jersey, 2nd edn, 2006.
40 E. Y. Jiang, *Advanced FT-IR Spectroscopy – Principles, Experiments and Applications Based on Research-Grade Nicolet FT-IR Spectrometers*, Thermo Electron Corporation, 2008.
41 E. Y. Jiang, Phase-, time-, and space-resolved step-scan FT-IR spectroscopy: Principles and applications to dynamic and heterogenous systems, *Spectroscopy*, 2002, **17**, 22–34.
42 A. Mezzetti, J. Schnee, A. Lapini and M. Di Donato, Time-resolved infrared absorption spectroscopy applied to photoinduced reactions: how and why, *Photochem. Photobiol. Sci.*, 2022, **21**, 557–584.
43 R. M. Dittmar, J. L. Chao and R. A. Palmer, Photoacoustic depth profiling of polymer laminates by step-scan fourier transform infrared spectroscopy, *Appl. Spectrosc.*, 1991, **45**, 1104–1110.
44 E. Jiang and A. Grenov, Extension of two-dimensional global phase difference correlation analysis to step-scan FT-IR photoacoustic spectral depth profiling of layered systems, *J. Mol. Struct.*, 2006, **799**, 188–195.

45 H. Wang, R. A. Palmer and C. J. Manning, Study of impulse polymer rheo-optics by step-scan FT-IR time-resolved spectroscopy, *Appl. Spectrosc.*, 1997, **51**, 1245–1250.
46 W. Uhmann, A. Becker, C. Taran and F. Siebert, Time-resolved FT-IR absorption spectroscopy using a step-scan interferometer, *Appl. Spectrosc.*, 1991, **45**, 390–397.
47 I. Offenbach, S. Gupta, T. Chung, R. Weiss and M. Cakmak, Real-time infrared-mechano-optical behavior and structural evolution of polypropylene and hydroxyl- functionalized polypropylene during uniaxial deformation, *Macromolecules*, 2015, **48**, 6294–6305.
48 V. G. Gregoriou, M. Daun, M. W. Schauer, J. L. Chao and R. A. Palmer, Modification of a research-grade FT-IR spectrometer for optional step-scan operation, *Appl. Spectrosc.*, 1993, **47**, 1311–1316.
49 R. A. Palmer, G. D. Smith and P. Chen, Breaking the nanosecond barrier in FTIR time-resolved spectroscopy, *Vib. Spectrosc.*, 1999, **19**, 131–141.
50 G. D. Smith and R. A. Palmer, *Handbook of Vibrational Spectroscopy*, John Wiley Sons, Ltd, 2006, pp. 121–144.
51 Z. Ganim, S. Hoi, A. Smith, L. Deores, K. Jones and A. Tokmakoff, Amide I two dimensional infrared spectroscopy of proteins, *Acc. Chem. Res.*, 2008, **41**, 432–441.
52 J. Hetmańczyk, L. Hetmańczyk and K. Gassowska, Phase transition, structure and reorientational dynamics of H_2O ligands and ReO_4^- anions in $[Ba(H_2O)_3](ReO_4)_2{\cdot}H_2O$, *J. Mol. Struct.*, 2019, **1188**, 173–184.
53 S. Nihonyanagi, S. Yamaguchi and T. Tahara, Ultrafast dynamics at water interfaces studied by vibrational sum frequency generation spectroscopy, *Chem. Rev.*, 2017, **117**, 10665–10693.
54 Z. Hong, S. Rezvani, Q. Zhang and P. Lu, Ultrafast mid-IR laser pulses generation *via* chirp manipulated optical parametric amplification, *Appl. Sci.*, 2018, **8**, 744.
55 C. Fang, L. Tang and C. Chen, Unveiling coupled electronic and vibrational motions of chromophores in condensed phases, *J. Chem. Phys.*, 2019, **151**, 200901.
56 R. Liao, H. Tian, W. Liu, R. Li, Y. Song and M. Hu, Dual-comb generation from a single laser source: Principles and spectroscopic applications towards mid-IR – A review, *J. Phys. Photonics*, 2020, **2**, 042006.
57 J. Wang, K. Wang, Y. Shen, Z. Han, F. Li, Z. He, D.-W. Wang, A. V. Sokolov and M. O. Scully, Femtosecond time-resolved infrared-resonant third-order sum- frequency spectroscopy, *ACS Photon.*, 2021, **8**, 1137–1142.
58 G. Herzberg and B. L. Crawford, Infrared and Raman spectra of polyatomic molecules, *J. Phys. Chem.*, 1946, **50**, 288.
59 C. Cannon, The nature of hydrogen bonding: A review of published work and discussion, *Spectrochim. Acta*, 1958, **10**, 341–368.
60 S. Bratos, Profiles of hydrogen stretching ir bands of molecules with hydrogen bonds: A stochastic theory. I. Weak and medium strength hydrogen bonds, *J. Chem. Phys.*, 1975, **63**, 3499–3509.
61 K. M. Jablonka, L. Patiny and B. Smit, Making molecules vibrate: Interactive web environment for the teaching of infrared spectroscopy, *J. Chem. Educ.*, 2022, **99**, 561–569.
62 G. Socrates, *Infrared and Raman Characteristic Group Frequencies: Tables and Charts*, 3rd edn, 2004.
63 R. M. Silverstein, F. X. Webster, D. J. Kiemle and D. L. Bryce, *Spectrometric Identification of Organic Compounds*, 8th edn, 2014.
64 K. Nakamoto, *Infrared and Raman Spectra of Inorganic and Coordination Compounds: Part A: Theory and Applications in Inorganic Chemistry*, 6th edn, 2008.
65 K. Nakamoto, *Infrared and Raman Spectra of Inorganic and Coordination Compounds: Part B: Applications in Coordination, Organometallic, and Bioinorganic Chemistry*, 6th edn, 2008.
66 W. F. Maddams, The scope and limitations of curve fitting, *Appl. Spectrosc.*, 1980, **34**, 245–267.
67 M. K. Antoon, L. D'Esposito and J. L. Koenig, Factor analysis applied to fourier transform infrared spectra, *Appl. Spectrosc.*, 1979, **33**, 351–357.
68 E. R. Malinowski, *Factor Analysis in Chemistry*, Wiley, New York, 3rd edn, 2002.
69 C. W. Jones, F. F. Tao and M. V. Garland, Introduction to special issue on operando and *in situ* studies of catalysis, *ACS Catal.*, 2012, **2**, 2444–2445.
70 B. M. Koo, D. A. D. Corte, J. Chazalviel, F. Maroun, M. Rosso and F. Ozanam, Lithiation mechanism of methylated amorphous silicon unveiled by operando ATR-FTIR spectroscopy, *Adv. Energy Mater.*, 2018, **8**, 1702568.
71 J. A. Lercher, V. Veefkind and K. Fajerwerg, *In situ* IR spectroscopy for developing catalysts and catalytic processes, *Vib. Spectrosc.*, 1999, **19**, 107–121.
72 J. King, C. Liu and S. Chuang, *In situ* infrared approach to unravel reaction intermediates and pathways on catalyst surfaces, *Res. Chem. Intermed.*, 2019, **45**, 5831–5847.
73 G. Gauglitz and T. Vo-Dinh, *Handbook of Spectroscopy*, Wiley-VCH, Weinheim, Germany, 2003, vol. 1.
74 X. Liu, L. Hou and H. Wang, Investigations into the mid-infrared Christiansen effect of the dispersive materials, *Infrared Phys. Technol.*, 2002, **43**, 401–405.
75 N. Biliškov, D. Vojta, L. Kótai, I. M. Szilágyi, D. Hunyadi, T. Pasinszki, S. Flinčec Grgac, A. Borgschulte and A. Züttel, High influence of potassium bromide on thermal decomposition of ammonia borane†, *J. Phys. Chem. C*, 2016, **120**, 25276–25288.
76 A. Delgado, R. Paroli and J. Beaudoin, Comparison of IR techniques for the characterization of construction cement minerals and hydrated products, *Appl. Spectrosc.*, 1996, **50**, 970–976.
77 D. Ritter and K. Weiser, Suppression of interference fringes in absorption measurements on thin Films, *Opt. Commun.*, 1986, **57**, 336–338.
78 D. Poelman and P. F. Smet, Methods for the determination of the optical constants of thin Films from single transmission measurements: a critical review, *J. Phys. D: Appl. Phys.*, 2003, **36**, 1850–1857.
79 N. H. A. Raof, S. S. Ng, H. A. Hassan and Z. Hassan, Kramers–Kronig Analysis of Infrared Reflectance Spectra for Quaternary $In_xAl_yGa_{1-x-y}N$ Alloy, *AIP Conf. Proc.*, 2010, **1250**, 337–340.

80 N. Biliškov, Infrared optical constants, molar absorption coefficients, dielectric constants, molar polarisabilities, transition moments and dipole moment derivatives of liquid *N*,*N*-dimethylformamide-carbon tetrachloride mixtures, *Spectrochim. Acta, Part A*, 2011, **79**, 302–307.
81 H. Okamura, in *Optical Techniques for Solid-State Materials Characterization*, ed. R. Prasankumar and A. J. Taylor, CRC Press, Boca Raton, FL, 2011, pp. 111–150.
82 R. Mendelsohn and C. R. Flach, *Peptide-Lipid Interactions; Curr. Topics in Membranes*, Academic Press, 2002, vol. 52, pp. 57–88.
83 R. Mendelsohn, G. Mao and C. R. Flach, Infrared reflection-absorption spectroscopy: Principles and applications to lipid-protein interaction in Langmuir Films, *Biochim. Biophys. Acta, Biomembr.*, 2010, **1798**, 788–800.
84 I. Brand, Application of Polarization Modulation Infrared Reflection Absorption Spectrosocpy Under Electrochemical Control for Structural Studies of Biomimetic Assemblies, *Z. Phys. Chem.*, 2016, **230**, 133–183.
85 A. Blume and A. Kerth, Peptide and protein binding to lipid monolayers studied by FTIRRA spectroscopy, *Biochim. Biophys. Acta, Biomembr.*, 2013, **1828**, 2294–2305.
86 Y. Wang and C. Wöll, IR spectroscopic investigations of chemical and photochemical reactions on metal oxides: bridging the materials gap, *Chem. Soc. Rev.*, 2017, **46**, 1875–1932.
87 M. Ito, Structures of water at electrified interfaces: Microscopic understanding of electrode potential in electric double layers on electrode surfaces, *Surf. Sci. Rep.*, 2008, **63**, 329–389.
88 R. Dluhy, S. Shanmukh and S. Morita, The application of two-dimensional correlation spectroscopy to surface and interfacial analysis, *Surf. Interface Anal.*, 2006, **38**, 1481–1496.
89 C. Stefaniu, G. Brezesinski and H. Möhwald, Langmuir monolayers as models to study processes at membrane surfaces, *Adv. Colloid Interface Sci.*, 2014, **208**, 197–213.
90 J. A. Bardwell and M. J. Dignam, Routine determination of the absorption and dispersion spectra of solids with a Fourier-transform infrared spectrometer, *Anal. Chim. Acta*, 1985, **172**, 101–110.
91 D. M. Roessler, Kramers-Krönig analysis of reflection data, *Br. J. Appl. Phys.*, 1965, **16**, 1119–1123.
92 D. M. Roessler, Kramers - Krönig analysis of non-normal incidence reflection, *Br. J. Appl. Phys.*, 1965, **16**, 1359–1366.
93 D. M. Roessler, Kramers - Krönig analysis of reflectance data: III. Approximations, with reference to sodium iodide, *Br. J. Appl. Phys.*, 1966, **17**, 1313–1317.
94 R. Brendel, The concept of effective film thickness for the determination of bond concentrations from IR spectra of weakly absorbing thin Films on silicon, *J. Appl. Phys.*, 1991, **69**, 7395–7399.
95 R. F. Edgar and B. J. Stay, Techniques For Suppressing Optical Interference Errors In Infrared Film Thickness Gauging, *Infrared Technology and Applications*, 1986, pp. 316–321.
96 P. J. Farrington, D. J. T. Hill, J. H. O'Donnell and P. J. Pomery, Suppression of Interference Fringes in the Infrared Spectra of Thin Polymer Films, *Appl. Spectrosc.*, 1990, **44**, 901–903.
97 C. Gamsky, G. Howes and J. Taylor, Infrared Reflection Absorption Spectroscopy of Photoresist Films on Silicon Wafers: Measuring Film Thickness and Removing Interference Fringes, *Anal. Chem.*, 1994, **66**, 1015–1020.
98 D. J. Dahm, *Interpreting Diffuse Reflectance and Transmittance: A Theoretical Introduction to Absorption Spectroscopy of Scattering Materials*, IM Publications LLP, 2007.
99 S. Sun and F. Zhang in *Semiconductor photocatalysis: Materials, mechanisms and applications*, ed. W. Cao, Chapter Insights into the Mechanism of Photocatalytic Degradation of Volatile Organic Compounds on TiO_2 by Using *In situ* DRIFTS, Intechopen, London, UK, 2016, pp. 185–206.
100 J. Fahrenfort, Attenuated total reflection: A new principle for the production of useful infra-red reflection spectra of organic compounds, *Spectrochim. Acta*, 1961, **17**, 698–709.
101 N. J. Harrick, *Internal Reflection Spectroscopy*, Interscience, New York, 1st edn, 1967.
102 N. J. Harrick and K. H. Beckmann in *Characterization of Solid Surfaces*, ed. P. F. Kane, G. B. Larrabee, Springer US, Boston, MA, 1974, pp. 215–245.
103 H. W. Siesler, in *Oriented Polymer Materials*, ed. S. Fakirov, John Wiley & Sons, 1996, pp. 138–166.
104 H. W. Siesler, G. G. Hoffmann, O. Kolomiets, F. Pfeifer and M. Zahedi, in *Vibrational Spectroscopy of Polymers: Principles and Practice*, ed. N. J. Everall, J. M. Chalmers and P. R. Griffiths, John Wiley & Sons, Ltd, 2007.
105 M. Unger and H. W. Siesler, *In Situ* Orientation Studies of a Poly(3-hydroxybutyrate)/Poly(\epsilon-caprolactone) Blend by Rheo-Optical Fourier Transform Infrared Spectroscopy and Two-Dimensional Correlation Spectroscopic Analysis, *Appl. Spectrosc.*, 2009, **63**, 1351–1355.
106 J. Shen, M. Kashimoto, T. Matsumoto, A. Mori and T. Nishino, Structural deformation of elastic polythiophene with disiloxane moieties under stretching, *Polym. J.*, 2020, **52**, 1273–1278.
107 S.-i Kimura and H. Okamura, Infrared and Terahertz Spectroscopy of Strongly Correlated Electron Systems under Extreme Conditions, *J. Phys. Soc. Jpn.*, 2013, **82**, 021004.
108 K. Aoki, H. Yamawaki, M. Sakashita and H. Fujihisa, Infrared absorption study of the hydrogen-bond symmetrization in ice to 110 GPa, *Phys. Rev. B: Condens. Matter*, 1996, **54**, 15673–15677.
109 A. F. Goncharov, E. Gregoryanz, H.-K. Mao, Z. Liu and R. J. Hemley, Optical Evidence for a Nonmolecular Phase of Nitrogen above 150 GPa, *Phys. Rev. Lett.*, 2000, **85**, 1262–1265.
110 C.-s Zha, Z. Liu, M. Ahart, R. Boehler and R. J. Hemley, High-Pressure Measurements of Hydrogen Phase IV Using Synchrotron Infrared Spectroscopy, *Phys. Rev. Lett.*, 2013, **110**, 217402.

111 D. K. Spaulding, G. Weck, P. Loubeyre, F. Datchi, P. Dumas and M. Hanfland, Pressure-induced chemistry in a nitrogen–hydrogen host–guest structure, *Nat. Commun.*, 2014, **5**, 5739.
112 H. K. Mao and R. J. Hemley, The high-pressure dimension in earth and planetary science, *Proc. Natl. Acad. Sci. U. S. A.*, 2007, **104**, 9114–9115.
113 E. C. Thompson, A. H. Davis, N. M. Brauser, Z. Liu, V. B. Prakapenka and A. J. Campbell, Phase transitions in -FeOOH at high pressure and ambient temperature, *Amer. Mineral.*, 2020, **105**, 1769–1777.
114 W. Montgomery, J. Tuff, S. Kohn and R. Jones, Reactions between organic acids and montmorillonite clay under Earth-forming conditions, *Chem. Geol.*, 2011, **283**, 171–176.
115 M. Koch-Müller, S. Jahn, N. Birkholz, E. Ritter and U. Schade, Phase transitions in the system $CaCO_3$ at high P and T determined by *in situ* vibrational spectroscopy in diamond anvil cells and first-principles simulations, *Phys. Chem. Miner.*, 2016, **43**, 545–561.
116 N. L. Ross, T. A. Detrie and Z. Liu, High-Pressure Raman and Infrared Spectroscopic Study of Prehnite, *Minerals*, 2020, **10**, 312–318.
117 S. R. Shieh, T. S. Duffy, Z. Liu and E. Ohtani, High-pressure infrared spectroscopyof the dense hydrous magnesium silicates phase D and phase E, *Phys. Earth Planet. Inter.*, 2009, **175**, 106–114.
118 K. Syassen and R. Sonnenschein, Microoptic double beam system for reflectance and absorption measurements at high pressure, *Rev. Sci. Instrum.*, 1982, **53**, 644–650.
119 T. Nanba, High-pressure solid-state spectroscopy at UVSOR by Infrared Synchrotron Radiation, *Nuovo Cimento Soc. Ital. Fis., D*, 1998, **20**, 397–413.
120 R. Hemley, A. Goncharov, R. Lu, V. Struzhkin, M. Li and H. Mao, High-pressure synchrotron infrared spectroscopy at the National Synchrotron Light Source, *Nuovo Cimento Soc. Ital. Fis., D*, 1998, **20**, 539–551.
121 R. Beyer and M. Dressel, Piston pressure cell for low-temperature infrared investigations, *Rev. Sci. Instrum.*, 2015, **86**, 053904.
122 M. K. Tran, J. Levallois, A. Akrap, J. Teyssier, A. B. Kuzmenko, F. Lévy-Bertrand, R. Tediosi, M. Brandt, P. Lerch and D. van der Marel, Versatile setup for optical spectroscopy under high pressure and low temperature, *Rev. Sci. Instrum.*, 2015, **86**, 105102.
123 A. Voute, M. Deutsch, A. Kalinko, F. Alabarse, J. B. Brubach, F. Capitani, M. Chapuis, V. Ta Phuoc, R. Sopracase and P. Roy, New high-pressure/low-temperature set-up available at the AILES beamline, *Vib. Spectrosc.*, 2016, **86**, 17–23.
124 H. Okamura, Y. Ikemoto, T. Moriwaki and T. Nanba, Infrared spectroscopy techniques for studying the electronic structures of materials under high pressure, *Jpn. J. Appl. Phys.*, 2017, **56**, 05FA11.
125 A. F. Goncharov, L. Kong and H. K. Mao, High-pressure integrated synchrotron infrared spectroscopy system at the Shanghai Synchrotron Radiation Facility, *Rev. Sci. Instrum.*, 2019, **90**, 093905.
126 C. A. Almodovar, W. W. Su, C. L. Strand, R. Sur and R. K. Hanson, High-pressure, high-temperature optical cell for mid-infrared spectroscopy, *J. Quant. Spectrosc. Radiat. Transfer*, 2019, **231**, 69–78.
127 G. J. Piermarini, Alvin Van Valkenburg and the diamond anvil cell, *High Pressure Res.*, 1993, **11**, 279–284.
128 W. A. Bassett, Diamond anvil cell, 50th birthday, *High Pressure Res.*, 2009, **29**, 163–186.
129 J. H. Eggert, K. A. Goettel and I. F. Silvera, Ruby at high pressure. I. Optical line shifts to 156 GPa, *Phys. Rev. B*, 1989, **40**, 5724–5732.
130 M. K. Mishra, P. Ghalsasi, M. N. Deo, H. Bhatt, H. K. Poswal, S. Ghosh and S. Ganguly, *In situ* high pressure study of an elastic crystal by FTIR spectroscopy, *CrystEngComm*, 2017, **19**, 7083–7087.
131 S. Ganguly, R. Chinnasamy, S. Parikh, M. S. R. N. Kiran, U. Ramamurty, H. Bhatt, M. N. Deo, S. Ghosh and P. Ghalsasi, Understanding Structural Variations in Elastic Organic Crystals by *in Situ* High-Pressure Fourier Transform Infrared Spectroscopy and Nanoindentation Study, *Cryst. Growth Des.*, 2019, **19**, 2114–2122.
132 M. Matsunami, H. Okamura, A. Ochiai and T. Nanba, Pressure Tuning of an Ionic Insulator into a Heavy Electron Metal: An Infrared Study of YbS, *Phys. Rev. Lett.*, 2009, **103**, 237202.
133 K. A. Smith, S. P. Ramkumar, N. C. Harms, A. J. Clune, S.-W. Cheong, Z. Liu, E. A. Nowadnick and J. L. Musfeldt, Pressure-induced phase transition and phonon softening in h –$Lu_{0.6}Sc_{0.4}FeO_3$, *Phys. Rev. B*, 2021, **104**, 094109.
134 R. S. Chellappa, M. Somayazulu, V. V. Struzhkin, T. Autrey and R. J. Hemley, Pressure-induced complexation of $NH_3BH_3NH_3BH_3$, *J. Chem. Phys.*, 2009, **131**, 224515.
135 Y. Lin, W. L. Mao, V. Drozd, J. Chen and L. L. Daemen, Raman spectroscopy study of ammonia borane at high pressure, *J. Chem. Phys.*, 2008, **129**, 234509.
136 Y. Lin, E. Welchman, T. Thonhauser and W. L. Mao, The structure and unconventional dihydrogen bonding of a pressure-stabilized hydrogen-rich $(NH_3BH_3)\cdot(H_2)_x$ (x = 1.5) compound, *J. Mater. Chem. A*, 2017, **5**, 7111–7117.
137 S. Wang, W. L. Mao and T. Autrey, Bonding in boranes and their interaction with molecular hydrogen at extreme conditions, *J. Chem. Phys.*, 2009, **131**, 144508.
138 S. Najiba and J. Chen, High-pressure study of lithium amidoborane using Raman spectroscopy and insight into dihydrogen bonding absence, *Proc. Natl. Acad. Sci. U. S. A.*, 2012, **109**, 19140–19144.
139 R. S. Chellappa, D. Chandra, S. A. Gramsch, R. J. Hemley, J.-F. Lin and Y. Song, Pressure-Induced Phase Transformations in LiAlH4, *J. Phys. Chem. B*, 2006, **110**, 11088–11097.
140 R. S. Chellappa, D. Chandra, M. Somayazulu, S. A. Gramsch and R. J. Hemley, Pressure-Induced Phase Transitions in $LiNH_2$, *J. Phys. Chem. B*, 2007, **111**, 10785–10789.
141 L. George, V. Drozd, H. Couvy, J. Chen and S. K. Saxena, An extended high pressure temperature phase diagram of $NaBH_4$, *J. Chem. Phys.*, 2009, **131**, 074505.

142 A. Marizy, G. Geneste, G. Garbarino and P. Loubeyre, High pressure polymorphism of $LiBH_4$ and of $NaBH_4$, *RSC Adv.*, 2021, **11**, 25274–25283.
143 J. H. Park and T. S. Sudarshan, *Chemical Vapor Deposition*, ASM International, 2001.
144 J. E. Mahan, *Physical Vapor Deposition of Thin Films*, Wiley-VCH, 2000.
145 G. Cao, *Nanostructures & Nanomaterials: Synthesis, Properties & Applications*, Imperial College Press, London, 2004.
146 E. H. Yang, D. Datta, J. Ding and G. Hader, *Synthesis, Modelling and Characterization of 2D Materials and their Heterostructures*, Elsevier, Amsterdam, 2020.
147 F. Zaera, Infrared and molecular beam studies of chemical reactions on solid surfaces, *Int. Rev. Phys. Chem.*, 2002, **21**, 433–471.
148 H. Soonmin, Analysis of Thin Films by Infrared Spectroscopy: Review, *Ind. J. Nat. Sci.*, 2020, **10**, 27593–27599.
149 Y. Du, L. Li, X. Wang and H. Qiu, A Newly Designed Infrared Reflection Absorption Spectroscopy System for *In Situ* Characterization from Ultrahigh Vacuum to Ambient Pressure, *Appl. Spectrosc.*, 2018, **72**, 122–128.
150 H. Chadwick and R. D. Beck, Quantum state resolved gas-surface reaction dynamics experiments: a tutorial review, *Chem. Soc. Rev.*, 2016, **45**, 3576–3594.
151 H. Tiznado, M. Bouman, B. C. Kang, I. Lee and F. Zaera, Mechanistic details of atomic layer deposition (ALD) processes for metal nitride Film growth, *J. Mol. Catal. A: Chem.*, 2008, **281**, 35–43.
152 B. C. Kan, J. H. Boo, I. Lee and F. Zaera, Thermal Chemistry of Tetrakis(ethylmethylamido)titanium on Si(100) Surfaces, *J. Phys. Chem. A*, 2009, **113**, 3946–3954.
153 L. Guo and F. Zaera, Spatial resolution in thin Film deposition on silicon surfaces by combining silylation and UV/ozonolysis, *Nanotechnology*, 2014, **25**, 504006.
154 H. Hoffmann, P. Griffiths and F. Zaera, A RAIRS study on the surface chemistry of ethyl iodide on Pt(111), *Surf. Sci.*, 1992, **262**, 141–150.
155 M. Motyka, G. Sek, J. Misiewicz, A. Bauer, M. Dallner, S. Höfling and A. Forchel, Fourier transformed Photoreflectanceand photoluminescence of mid infrared GaSb based type II quantum wells, *Appl. Phys. Express*, 2009, **2**, 126505.
156 C. Nan, W. Yue, L. Tao and X. Yang, Fourier transform infrared nano-spectroscopy: Mechanism and applications, *Appl. Spectrosc. Rev.*, 2021, **56**, 531–552.
157 P. Patoka, G. Ulrich, A. E. Nguyen, L. Bartels, P. A. Dowben, V. Turkowski, T. S. Rahman, P. Hermann, B. Kästner, A. Hoehl, G. Ulm and E. Rühl, Nanoscale plasmonic phenomena in CVD-grown MoS_2 monolayer revealed by ultra-broadband synchrotron radiation based nano-FTIR spectroscopy and near-field microscopy, *Opt. Express*, 2016, **24**, 1154–1164.
158 S. Dai, *et al.*, Tunable Phonon Polaritons in Atomically Thin van der Waals Crystals of Boron Nitride, *Science*, 2014, **343**, 1125–1129.
159 J. Yang, M. Mayyas, J. Tang, M. B. Ghasemian, H. Yang, K. Watanabe, T. Taniguchi, Q. Ou, L. H. Li, Q. Bao and K. Kalantar-Zadeh, Boundary-Induced Auxiliary Features in Scattering-Type Near-Field Fourier Transform Infrared Spectroscopy, *ACS Nano*, 2020, **14**, 1123–1132.
160 R. Szostak, J. C. Silva, S.-H. Turren-Cruz, M. M. Soares, R. O. Freitas, A. Hagfeldt, H. C. N. Tolentino and A. F. Nogueira, Nanoscale mapping of chemical composition in organic–inorganic hybrid perovskite Films, *Sci. Adv.*, 2019, **5**, eaaw6619.
161 C.-F. Wang, T. G. Habteyes, T. S. Luk, J. F. Klem, I. Brener, H.-T. Chen and O. Mitrofanov, Observation of Intersubband Polaritons in a Single Nanoantenna Using Nano-FTIR Spectroscopy, *Nano Lett.*, 2019, **19**, 4620–4626.
162 G. Paul, C. Bisio, I. Braschi, M. Cossi, G. Gatti, E. Gianotti and L. Marchese, Combined solid-state NMR, FT-IR and computational studies on layered and porous materials, *Chem. Soc. Rev.*, 2018, **47**, 5684–5739.
163 R. M. Delgado, Structure and Stability of Gas Adsorption Complexes in Periodic Porous Solids as Studied by VTIR Spectroscopy: An Overview, *Appl. Sci.*, 2020, **10**, 8589.
164 N. Kornienko, Operando spectroscopy of nanoscopic metal/covalent organic framework electrocatalysts, *Nanoscale*, 2021, **13**, 1507–1514.
165 K. I. Hadjiivanov, D. A. Panayotov, M. Y. Mihaylov, E. Z. Ivanova, K. K. Chakarova, S. M. Andonova and N. L. Drenchev, Power of Infrared and Raman Spectroscopies to Characterize Metal-Organic Frameworks and Investigate Their Interaction with Guest Molecules, *Chem. Rev.*, 2021, **121**, 1286–1424.
166 B. Pal, A. Yasin, R. Kaur, M. Tebyetekerwa, F. Zabihi, S. Yang, C.-C. Yang, Z. Sofer and R. Jose, Understanding electrochemical capacitors with in-situ techniques, *Renewable Sustainable Energy Rev.*, 2021, **149**, 111418.
167 Z. Li, G. Zhu, G. Lu, S. Qiu and X. Yao, Ammonia Borane Confined by a MetalOrganic Framework for Chemical Hydrogen Storage: Enhancing Kinetics and Eliminating Ammonia, *J. Am. Chem. Soc.*, 2010, **132**, 1490–1491.
168 T. Hiraoka and S. Shigeto, Interactions of water confined in a metal-organic framework as studied by a combined approach of Raman, FTIR, and IR electroabsorption spectroscopies and multivariate curve resolution analysis, *Phys. Chem. Chem. Phys.*, 2020, **22**, 17798–17806.
169 A. F. Möslein, M. Gutiérrez, B. Cohen and J.-C. Tan, Near-Field Infrared Nanospectroscopy Reveals Guest Confinement in Metal-Organic Framework Single Crystals, *Nano Lett.*, 2020, **20**, 7446–7454.
170 V. Martinez, B. Karadeniz, N. Biliškov, I. Lončarić, S. Muratović, D. Žilić, S. M. Avdoshenko, M. Roslova, A. A. Popov and K. Užarević, Tunable Fulleretic Sodalite MOFs: Highly Efficient and Controllable Entrapment of C_{60} Fullerene *via* Mechanochemistry, *Chem. Mater.*, 2020, **32**, 10628–10640.
171 D. Ngo, H. Liu, Z. Chen, H. Kaya, T. Zimudzi, S. Gin, T. Mahadevan, J. Du and S. Kim, Hydrogen bonding interactions of H_2O and SiOH on a boroaluminosilicate glass corroded in aqueous solution, *npj Mater. Degrad.*, 2020, **4**, 1.

172 M. Delgado, Structure and stability of gas adsorption complexes in periodic porous solids as studied by VTIR spectroscopy: An overview, *Appl. Sci.*, 2020, **10**, 8589.
173 A. Ahmed, Zeolite-encapsulated transition metal chelates: Synthesis and characterization, *Rev. Inorg. Chem.*, 2014, **34**, 153–175.
174 B. Sreenivasulu, I. Sreedhar, P. Suresh and K. Raghavan, Development Trends in Porous Adsorbents for Carbon Capture, *Environ. Sci. Technol.*, 2015, **49**, 12641–12661.
175 J. Liu, W. Qian, Y. F. He and R. M. Wang, Mechanisms on formation of hierarchically porous carbon and its adsorption behaviors, *Water Sci. Technol.*, 2016, **74**, 266–275.
176 E. Qezelsefloo, S. Khalili, M. Jahanshahi and M. Peyravi, Adsorptive removal of CO_2 on Nitrogen-doped porous carbon derived from polyaniline: Effect of chemical activation, *Mater. Chem. Phys.*, 2020, **239**, 122304.
177 Y. Chen, X. Zhang, W. Chen, H. Yang and H. Chen, The structure evolution of biochar from biomass pyrolysis and its correlation with gas pollutant adsorption performance, *Bioresour. Technol.*, 2017, **246**, 101–109.
178 J. K. Lim, T. Liu, J. Jeong, H. Shin, H. J. Jang, S. P. Cho and J. S. Park, *In situ* syntheses of silver nanoparticles inside silver citrate nanorods *via* catalytic nanoconfinement effect, *Colloids Surf., A*, 2020, **605**, 125343.
179 Y. Ozaki, K. B. Beć, Y. Morisawa, S. Yamamoto, I. Tanabe, C. W. Huck and T. S. Hofer, Advances, challenges and perspectives of quantum chemical approaches in molecular spectroscopy of the condensed phase, *Chem. Soc. Rev.*, 2021, **50**, 10917–10954.
180 Z. Iqbal and F. J. Owens, *Vibrational spectroscopy of phase transitions*, U.S. Department of Energy, 1984.
181 P. M. A. Sherwood, *Vibrational Spectroscopy of Solids*, Cambridge University Press, 2011.
182 E. Bellur Atici and B. Karliğa, Quantitative determination of two polymorphic forms of imatinib mesylate in a drug substance and tablet formulation by X-ray powder diffraction, differential scanning calorimetry and attenuated total reflectance Fourier transform infrared spectroscopy, *J. Pharm. Biomed. Anal.*, 2015, **114**, 330–340.
183 D. Le Pevelen and G. Tranter, in *Encyclopedia of Spectroscopy and Spectrometry (Third Edition)*, ed. J. C. Lindon, G. E. Tranter and D. W. Koppenaal, Academic Press, Oxford, 3rd edn, 2017, pp. 750–761.
184 O. Y. Noda, *Isao Two-Dimensional Correlation Spectroscopy - Applications in Vibrational and Optical Spectroscopy*, John Willey & Sons, Hoboken, USA, 2004.
185 S. Šašić, Y. Katsumoto, H. Sato and Y. Ozaki, Applications of Moving Window Two-Dimensional Correlation Spectroscopy to Analysis of Phase Transitions and Spectra Classification, *Anal. Chem.*, 2003, **75**, 4010–4018.
186 B. Zimmermann and G. Baranović, Determination of Phase Transition Temperatures by the Analysis of Baseline Variations in Transmittance Infrared Spectroscopy, *Appl. Spectrosc.*, 2009, **63**, 1152–1161.
187 B. Zimmermann and G. Baranović, Thermal analysis of paracetamol polymorphs by FTIR spectroscopies, *J. Pharm. Biomed. Anal.*, 2011, **54**, 295–302.
188 B. Zimmermann and D. Vrsaljko, IR spectroscopy based thermal analysis of polymers, *Polym. Test.*, 2010, **29**, 849–856.
189 T. Mihelj, D. Vojta and V. Tomašić, The diversity in thermal behavior of novel catanionic cholates: The dominant effect of quaternary ammonium centers, *Thermochim. Acta*, 2014, **584**, 17–30.
190 D. Vojta, M. Vrankić, M. Bertmer and G. Schaumann, Dehydration of -oxalic acid dihydrate: Structural, spectroscopic and thermal study with implications on the disruption of water molecular bridges in soil organic matter, *Thermochim. Acta*, 2016, **643**, 73–82.
191 D. Vojta, A. Višnjevac, Z. Leka, M. Kosović and M. Vazdar, Temperatureinduced release of crystal water in the Co, Mo and Pt complexes of *N*,*N*-diacetatedithiocarbamate. FTIR spectroscopy and quantum chemical study, *J. Mol. Struct.*, 2016, **1103**, 245–253.
192 V. Tomašić, N. Biliškov, T. Mihelj and Z. Štefanić, Thermal behaviour and structural properties of surfactant-Picrate compounds: The effect of the ammonium headgroup number, *Thermochim. Acta*, 2013, **569**, 25–35.
193 T. Mihelj, V. Tomašić and N. Biliškov, 18-crown-6-sodium cholate complex: Thermochemistry, structure, and stability, *Langmuir*, 2014, **30**, 6274–6285.
194 N. Biliškov, *In Situ* Monitoring of a Quasi Solid-State Diffusion-Driven Cocrystallization in the Diphenylamine-Benzophenone System, *Cryst. Growth Des.*, 2021, **21**, 1434–1442.
195 I. Milanović, N. Biliškov, K. Užarević, S. Lukin, M. Etter and I. Halasz, Mechanochemical Synthesis and Thermal Dehydrogenation of Novel Calcium-Containing Bimetallic Amidoboranes. ACS Sust, *Chem. Eng.*, 2021, **9**, 2089–2099.
196 M. H. Köhler, M. Schardt, M. S. Rauscher and A. W. Koch, Gas Measurement Using Static Fourier Transform Infrared Spectrometers, *Sensors*, 2017, **17**, 2612.
197 K. Coenen, F. Gallucci, B. Mezari, E. Hensen and M. van Sint Annaland, An *in situ* IR study on the adsorption of CO_2 and H_2O on hydrotalcites, *J. CO2 Util.*, 2018, **24**, 228–239.
198 E.-M. Köck, M. Kogler, T. Bielz, B. Klötzer and S. Penner, *In Situ* FT-IR Spectroscopic Study of CO_2 and CO Adsorption on Y_2O_3, ZrO_2, and Yttria-Stabilized ZrO_2, *J. Phys. Chem. C*, 2013, **117**, 17666–17673.
199 S. E. Collins, M. A. Baltanás and A. L. Bonivardi, Infrared Spectroscopic Study of the Carbon Dioxide Adsorption on the Surface of Ga_2O_3 Polymorphs, *J. Phys. Chem. B*, 2006, **110**, 5498–5507.
200 M. Breunig, M. Dorner and J. Senker, Ultramicroporous polyimides with hierarchical morphology for carbon dioxide separation, *J. Mater. Chem. A*, 2021, **9**, 12797–12806.
201 E. Cueto-Díaz, A. Castro-Muniz, F. Suárez-García, S. Gálvez-Martínez, M. Torquemada-Vico, M. Valles-González and E. Mateo-Martí, Aptes-based silica nanoparticles as a potential modifier for the selective sequestration of CO_2 gas molecules, *Nanotechnology*, 2021, **11**, 2893.
202 J. Hua, Z. Duan, C. Gao, X. Xie, Z. Qiao, T. Feng and X. Ma, A 3,5-Connected 3D Nickel-Mixed Ligands Coordination Polymer with Selective Adsorption of Carbon Dioxide, *Russ. J. Coord. Chem.*, 2021, **47**, 646–652.

203 J. Hua, C. Yang, X. Zhang, N. Chen, B. Hu, Y. Bian and X. Ma, A three dimensional cobalt-mixed ligands framework with selective adsorption of carbon dioxide, *Inorg. Nano-Met. Chem.*, 2021, 1–6.
204 M. Lourenço, M. Fontana, P. Jagdale, C. Pirri and S. Bocchini, Improved CO_2 adsorption properties through amine functionalization of multi-walled carbon nanotubes, *Chem. Eng. J.*, 2021, **414**, 128763.
205 J. Pazdera, E. Berger, J. Lercher and A. Jentys, Conversion of CO_2 to methanol over bifunctional basic-metallic catalysts, *Catal. Commun.*, 2021, **159**, 106347.
206 K. Sugamata, S. Kobayashi, T. Iihama and M. Minoura, Gas Adsorption in R2-MOF-5 Difunctionalized with Alkyl Groups, *Eur. J. Inorg. Chem.*, 2021, 3185–3190.
207 Y. Zheng, X. Wang, C. Liu, B. Yu, W. Li, H. Wang, T. Sun and J. Jiang, Triptycenesupported bimetallic salen porous organic polymers for high efficiency CO_2 fixation to cyclic carbonates, *Inorg. Chem. Front.*, 2021, **8**, 2880–2888.
208 A. Kiani, R. Sakurovs, M. Grigore, A. Keshavarz and S. White, The Use of Infrared Spectroscopy to Determine Methane Emission Rates from Coals at Atmospheric Pressures, *Energy Fuels*, 2019, **33**, 238–247.
209 S. Creci, X. Wang, P.-A. Carlsson, A. Martinelli and M. Skoglundh, Methoxy ad-species in MFI zeotypes during methane exposure and methanol desorption followed by *in situ* IR spectroscopy, *Catal. Today*, 2021, **369**, 123–128.
210 K. Wang, F. Du and G. Wang, The influence of methane and CO_2 adsorption on the functional groups of coals: Insights from a Fourier transform infrared investigation, *J. Nat. Gas Sci. Eng.*, 2017, **45**, 358–367.
211 T. Kundu, B. B. Shah, L. Bolinois and D. Zhao, Functionalization-Induced Breathing Control in Metal-Organic Frameworks for Methane Storage with High Deliverable Capacity, *Chem. Mater.*, 2019, **31**, 2842–2847.
212 P. Mauron, M. Gaboardi, A. Remhof, A. Bliersbach, D. Sheptyakov, M. Aramini, G. Vlahopoulou, F. Giglio, D. Pontiroli, M. Riccó and A. Züttel, Hydrogen Sorption in $Li_{12}C_{60}$, *J. Phys. Chem. C*, 2013, **117**, 22598–22602.
213 S. T. Stripp, *In Situ* Infrared Spectroscopy for the Analysis of Gas-processing Metalloenzymes, *ACS Catal.*, 2021, **11**, 7845–7862.
214 Y. Liao, P. Picot, M. Lainé, J.-B. Brubach, P. Roy, A. Thill and S. Le Caër, Tuning the properties of confined water in standard and hybrid nanotubes: An infrared spectroscopic study, *Nano Res.*, 2018, **11**, 4759–4773.
215 R. Biswas and B. Bagchi, Anomalous water dynamics at surfaces and interfaces: synergistic effects of confinement and surface interactions, *J. Phys.: Condens. Matter*, 2018, **30**, 013001.
216 U. Manna, S. Halder and G. Das, Ice-like CyclicWater Hexamer Trapped within a Halide Encapsulated Hexameric Neutral Receptor Core: First Crystallographic Evidence of a Water Cluster Confined within a Receptor-Anion Capsular Assembly, *Cryst. Growth Des.*, 2018, **18**, 1818–1825.
217 M. T. Köhler, J. R. Bordin, C. F. de Matos and M. C. Barbosa, Water in nanotubes: The surface effect, *Chem. Eng. Sci.*, 2019, **203**, 54–67.
218 Y.-L. Zhang, Y.-Q. Liu, D.-D. Han, J.-N. Ma, D. Wang, X.-B. Li and H.-B. Sun, Quantum-Confined-Superfluidics-Enabled Moisture Actuation Based on Unilaterally Structured Graphene Oxide Papers, *Adv. Mater.*, 2019, **31**, 1901585.
219 L. Chen, X. He, H. Liu, L. Qian and S. H. Kim, Water Adsorption on Hydrophilic and Hydrophobic Surfaces of Silicon, *J. Phys. Chem. C*, 2018, **122**, 11385–11391.
220 M. Uhlig and R. Garcia, *In Situ* Atomic-Scale Imaging of Interfacial Water under 3D Nanoscale Confinement, *Nano Lett.*, 2021, **21**, 5593–5598.
221 F. Moučka, S. Zamfir, D. Bratko and A. Luzar, Molecular polarizability in open ensemble simulations of aqueous nanoconfinements under electric field, *J. Chem. Phys.*, 2019, **150**, 164702.
222 A. Knight, N. Kalugin, E. Coker and A. Ilgen, Water properties under nano-scale con finement, *Sci. Rep.*, 2019, **9**, 8246.
223 M. Ghasemi, S. Ramsheh and S. Sharma, Quantitative Assessment of Thermodynamic Theory in Elucidating the Behavior of Water under Hydrophobic Confinement, *J. Phys. Chem. B*, 2018, **122**, 12087–12096.
224 C. Sammon, C. Mura, J. Yarwood, N. Everall, R. Swart and D. Hodge, FTIR-ATR studies of the structure and dynamics of water molecules in polymeric matrixes. A comparison of PET and PVC, *J. Phys. Chem. B*, 1998, **102**, 3402–3411.
225 L. Zhang, J.-S. Hu, X.-H. Huang, J. Song and S.-Y. Lu, Particle-in-box nanostructured materials created *via* spatially confined pyrolysis as high performance bifunctional catalysts for electrochemical overall water splitting, *Nano Energy*, 2018, **48**, 489–499.
226 M. Rueda, L. M. Sanz-Moral, J. J. Segovia and A. Martín, Improvement of the kinetics of hydrogen release from ammonia borane confined in silica aerogel, *Microporous Mesoporous Mater.*, 2017, **237**, 189–200.
227 M. Hassanpour, H. Jafari, S. Sharifi, J. Rezaie, Z. Lighvan, G. Mahdavinia, G. Gohari and A. Akbari, Salicylic acid-loaded chitosan nanoparticles (SA/CTS NPs) for breast cancer targeting: Synthesis, characterization and controlled release kinetics, *J. Mol. Struct.*, 2021, **1245**, 131040.
228 M. Maleki, Z. Hadian, K. Abdi, P. Koohy-Kamaly and F. Bahmanyar, Study of the Physicochemical Properties and Antimicrobial Activities of Nanoparticles Containing-Cyclodextrin and Geranial, *J. Nanostr.*, 2021, **11**, 189–201.
229 C. Nkanga and R. Krause, Encapsulation of Isoniazid-conjugated Phthalocyanine-In-Cyclodextrin-In-Liposomes Using Heating Method, *Sci. Rep.*, 2019, **9**, 11485.
230 C. Nyamekye, J. Bobbitt, Q. Zhu and E. Smith, The evolution of total internal reflection Raman spectroscopy for the chemical characterization of thin films and interfaces, *Anal. Bioanal. Chem.*, 2020, 6009–6022.
231 M. Guerrero-Pérez and G. Patience, Experimental methods in chemical engineering: Fourier transform infrared spectroscopy|FTIR, *Can. J. Chem. Eng.*, 2020, **98**, 25–33.
232 J. Kubota, Z. Ma and F. Zaera, *In Situ* Characterization of Adsorbates in SolidLiquid Interfaces by Reflection Absorption Infrared Spectroscopy, *Langmuir*, 2003, **19**, 3371–3376.

233 A. Bewick and S. Pons, *Advances in Infrared and Raman Spectroscopy*, Chapter Infrared Spectroscopy of the Electrode-Electrolyte Solution Interface, Wiley, Heyden, New York, 1985, vol. 12, pp. 1–63.
234 F. M. Hoffmann, Infrared reflection-absorption spectroscopy of adsorbed molecules, *Surf. Sci. Rep.*, 1983, **3**, 107–192.
235 Y. Chabal, Surface infrared spectroscopy, *Surf. Sci. Rep.*, 1988, **8**, 211–357.
236 Y. Chabal, M. Hines, D. Feijóo, M. Hines and D. Feijóo, Characterization of silicon surfaces and interfaces by optical vibrational spectroscopy, *J. Vac. Sci. Technol., A*, 1995, **13**, 1719–1727.
237 R. G. Greenler, Infrared Study of Adsorbed Molecules on Metal Surfaces by Reflection Techniques, *J. Chem. Phys.*, 1966, **44**, 310–315.
238 S. Attia and S. Schauermann, Coverage-Dependent Adsorption Geometry of Acetophenone on Pt(111), *J. Phys. Chem. C*, 2020, **124**, 557–566.
239 D. Blaumeiser, C. Schuschke, L. Fromm, N. Taccardi, S. Schötz, R. Eschenbacher, H. Bühlmeyer, T. Xu, T. Bauer, P. Wasserscheid, A. Görling and J. Libuda, CO Permeability and Wetting Behavior of Ionic Liquids on Pt(111): An IRAS and PMIRAS Study from Ultrahigh Vacuum to Ambient Pressure, *J. Phys. Chem. C*, 2021, **125**, 15301–15315.
240 M. Hofman, E. Scoullos, J. Robbins, L. Ezeonu, D. Potapenko, X. Yang, S. Podkolzin and B. Koel, Acetic Acid Adsorption and Reactions on Ni(110), *Langmuir*, 2020, **36**, 8705–8715.
241 T. Wähler, R. Schuster and J. Libuda, Self-Metalation of Anchored Porphyrins on Atomically Defined Cobalt Oxide Surfaces: *In situ* Studies by Surface Vibrational Spectroscopy, *Chem. – Eur. J.*, 2020, **26**, 12445–12453.
242 X. Weng, Y. Cui, S. Shaikhutdinov and H.-J. Freund, CO_2 Adsorption on CaO(001): Temperature-Programmed Desorption and Infrared Study, *J. Phys. Chem. C*, 2019, **123**, 1880–1887.
243 F. Widdascheck, M. Kothe, S. Thussing, P. Jakob and G. Witte, Evolution of TiOPc Films on Au(111): From Seed Layer to Crystalline Multilayers, *J. Phys. Chem. C*, 2020, **124**, 14664–14671.
244 H. L. Pickering and H. C. Eckstrom, Heterogeneous Reaction Studies by Infrared Absorption, *J. Phys. Chem.*, 1959, **63**, 512–518.
245 P. Hollins and J. Pritchard, Infrared studies of chemisorbed layers on single crystals, *Prog. Surf. Sci.*, 1985, **19**, 275–349.
246 B. J. Barner, M. J. Green, E. I. Saez and R. M. Corn, Polarization modulation Fourier transform infrared re ectance measurements of thin films and monolayers at metal surfaces utilizing real-time sampling electronics, *Anal. Chem.*, 1991, **63**, 55–60.
247 W. G. Golden, D. D. Saperstein, M. W. Severson and J. Overend, Infrared reflection absorption spectroscopy of surface species: a comparison of Fourier transform and dispersion methods, *J. Phys. Chem.*, 1984, **88**, 574–580.
248 V. K. Agrawal and M. Trenary, An infrared study of NO adsorption at defect sites on Pt(111), *Surf. Sci.*, 1991, **259**, 116–128.
249 P. Hollins, The influence of surface defects on the infrared spectra of adsorbed species, *Surf. Sci. Rep.*, 1992, **16**, 51–94.
250 R. Mukerji, A. Bolina and W. Brown, A RAIRS and TPD investigation of the adsorption of CO on Pt211, *Surf. Sci.*, 2003, **527**, 198–208.
251 L. Vattuone, L. Savio and M. Rocca, Bridging the structure gap: Chemistry of nanostructured surfaces at well-defined defects, *Surf. Sci. Rep.*, 2008, **63**, 101–168.
252 A. Gutiérrez-González and R. Beck, Quantum state and surface-site-resolved studies of methane chemisorption by vibrational spectroscopies, *Phys. Chem. Chem. Phys.*, 2020, **22**, 17448–17459.
253 A. J. Walsh, R. van Lent, S. V. Auras, M. A. Gleeson, O. T. Berg and L. B. F. Juurlink, Step-type and step-density influences on CO adsorption probed by reflection absorption infrared spectroscopy using a curved Pt(111) surface, *J. Vac. Sci. Technol., A*, 2017, **35**, 03E102.
254 R. K. Brandt, R. S. Sorbello and R. G. Greenler, Site-specific, coupled-harmonicoscillator model of carbon monoxide adsorbed on extended, single-crystal surfaces and on small crystals of platinum, *Surf. Sci.*, 1992, **271**, 605–615.
255 H. Chadwick, H. Guo, A. Gutiérrez-González, J. P. Menzel, B. Jackson and R. D. Beck, Methane dissociation on the steps and terraces of Pt(211) resolved by quantum state and impact site, *J. Chem. Phys.*, 2018, **148**, 014701.
256 H. Chadwick, A. Gutiérrez-González, D. Migliorini, R. D. Beck and G.-J. Kroes, Incident Angle Dependence of CHD3 Dissociation on the Stepped Pt(211) Surface, *J. Phys. Chem. C*, 2018, **122**, 19652–19660.
257 H. Chadwick, A. Gutiérrez-González, R. D. Beck and G.-J. Kroes, Transferability of the SRP32-vdW specific reaction parameter functional to CHD_3 dissociation on Pt(110)-(2 × 1), *J. Chem. Phys.*, 2019, **150**, 124702.
258 H. Chadwick, A. Gutiérrez-González, R. D. Beck and G.-J. Kroes, CHD_3 Dissociation on the Kinked Pt(210) Surface: A Comparison of Experiment and Theory, *J. Phys. Chem. C*, 2019, **123**, 14530–14539.
259 L. Chen, H. Ueta, R. Bisson and R. D. Beck, Vibrationally bond-selected chemisorption of methane isotopologues on Pt(111) studied by reflection absorption infrared spectroscopy, *Faraday Discuss.*, 2012, **157**, 285–295.
260 A. Gutiérrez-González, M. Torio, H. Busnengo and R. Beck, Site Selective Detection of Methane Dissociation on Stepped Pt Surfaces, *Top. Catal.*, 2019, **62**, 859–873.
261 X. Yu, P. Schwarz, A. Nefedov, B. Meyer, Y. Wang and C. Wöll, Structural Evolution of Water on ZnO($10\bar{1}0$): From Isolated Monomers via Anisotropic H-Bonded 2D and 3D Structures to Isotropic Multilayers, *Angew. Chem., Int. Ed.*, 2019, **58**, 17751–17757.
262 M. Behrens, F. Studt, I. Kasatkin, S. Kühl, M. Hävecker, F. Abild-Pedersen, S. Zander, F. Girgsdies, P. Kurr, B.-L. Kniep, M. Tovar, R. W. Fischer, J. K. Nrskov and R. Schlögl,

The Active Site of Methanol Synthesis over $Cu/ZnO/Al_2O_3$ Industrial Catalysts, *Science*, 2012, **336**, 893–897.
263 S. Kuld, M. Thorhauge, H. Falsig, C. F. Elkjær, S. Helveg, I. Chorkendorff and J. Sehested, Quantifying the promotion of Cu catalysts by ZnO for methanol synthesis, *Science*, 2016, **352**, 969–974.
264 S. Kattel, P. J. Ramírez, J. G. Chen, J. A. Rodriguez and P. Liu, Active sites for CO_2 hydrogenation to methanol on Cu/ZnO catalysts, *Science*, 2017, **355**, 1296–1299.
265 F. Studt, M. Behrens, E. L. Kunkes, N. Thomas, S. Zander, A. Tarasov, J. Schumann, E. Frei, J. B. Varley, F. Abild-Pedersen, J. K. Nrskov and R. Schlögl, The Mechanism of CO and CO_2 Hydrogenation to Methanol over Cu-Based Catalysts, *ChemCatChem*, 2015, **7**, 1105–1111.
266 T. Lunkenbein, J. Schumann, M. Behrens, R. Schlögl and M. G. Willinger, Formation of a ZnO Overlayer in Industrial $Cu/ZnO/Al_2O_3$ Catalysts Induced by Strong Metal-Support Interactions, *Angew. Chem., Int. Ed.*, 2015, **54**, 4544–4548.
267 G. Grasa, B. González, M. Alonso and J. Abanades, Comparison of CaO-Based Synthetic CO_2 Sorbents under Realistic Calcination Conditions, *Energy Fuels*, 2007, **21**, 3560–3562.
268 S. Choi, J. H. Drese and C. W. Jones, Christopher Adsorbent Materials for Carbon Dioxide Capture from Large Anthropogenic Point Sources, *ChemSusChem*, 2009, **2**, 796–854.
269 H.-J. Freund and M. Roberts, Surface chemistry of carbon dioxide, *Surf. Sci. Rep.*, 1996, **25**, 225–273.
270 W. Taifan, J.-F. Boily and J. Baltrusaitis, Surface chemistry of carbon dioxide revisited, *Surf. Sci. Rep.*, 2016, **71**, 595–671.
271 U. Burghaus, Surface science perspective of carbon dioxide chemistry—Adsorption kinetics and dynamics of CO_2 on selected model surfaces, *Catal. Today*, 2009, **148**, 212–220.
272 F. Zaera, H. Hoffmann and P. Griffiths, Determination of molecular chemisorption geometries using reflection-absorption infrared spectroscopy: alkyl halides on Pt(111), *J. Electron Spectrosc. Relat. Phenom.*, 1990, **54–55**, 705–715.
273 K. Hinrichs, in *Surface and Thin Film Analysis: A Compendium of Principles, In strumentation, and Applications*, ed. G. Friedbacher and H. Bubert, Chapter Reflection Absorption IR Spectroscopy (RAIRS), 2nd edn, 2011, pp. 367–375.
274 N. Sheppard, in *Encyclopedia of Spectroscopy and Spectrometry*, ed. J. C. Lindon, G. E. Tranter and D. W. Koppenaal, Academic Press, Oxford, 3rd edn, 2017, pp. 455–462.
275 R. B. David, A. B. Yaacov and B. Eren, Effect of Surface Orientation on Methanol Adsorption and Thermally Induced Structural Transformations on Copper Surfaces, *J. Phys. Chem. C*, 2021, **125**, 6099–6107.
276 M. T. L. Casford, A. Ge, P. J. N. Kett, S. Ye and P. B. Davies, The Structure of Lipid Bilayers Adsorbed on Activated Carboxy-Terminated Monolayers Investigated by Sum Frequency Generation Spectroscopy, *J. Phys. Chem. B*, 2014, **118**, 3335–3345.
277 E. Mateo-Martí, C. Briones, E. Román, E. Briand, C. M. Pradier and J. A. Martín-Gago, Self-Assembled Monolayers of Peptide Nucleic Acids on Gold Surfaces: A Spectroscopic Study, *Langmuir*, 2005, **21**, 9510–9517.
278 E. Ingman, A. Shepherd and W. Brown, Using surface science techniques to investigate the interaction of acetonitrile with dust grain analogue surfaces behaviour of acetonitrile and water on a graphitic surface, *Johnson Matthey Technol. Rev.*, 2021, **65**, 600–614.
279 R. Iwamoto and H. Murase, Infrared spectroscopic study of the interactions of nylon-6 with water, *J. Polym. Sci., Part B: Polym. Phys.*, 2003, **41**, 1722–1729.
280 P. Concepción, in *Infrared Spectroscopy - Principles, Advances, and Applications*, ed. M. El-Azazy, IntechOpen, 2018.
281 D. Bianchi, A contribution to the experimental microkinetic approach of gas/solid heterogeneous catalysis: Measurement of the individual heats of adsorption of coadsorbed species by using the AEIR method, *Catalysts*, 2018, **8**, 265.
282 J. Kim, H.-E. Kim and H. Lee, Single-Atom Catalysts of Precious Metals for Electrochemical Reactions, *ChemSusChem*, 2018, **11**, 104–113.
283 L. Luo, R. Hernandez, X.-D. Zhou and H. Yan, Heterogeneous catalysis at metal-oxide interfaces using *in situ* and operando spectroscopy: From nanoparticles to single-atom sites, *Appl. Catal., A*, 2021, **624**, 118330.
284 K. Mudiyanselage and D. J. Stacchiola, *In situ Characterization of Heterogeneous Catalysts*, John Wiley Sons, Ltd, 2013, ch. 8, pp. 209–239.
285 M. A. Newton and M. Fernáandez-García, *In situ Characterization of Heterogeneous Catalysts*, John Wiley Sons, Ltd, 2013, ch. 14, pp. 369–409.
286 E. Stavitski, *In situ Characterization of Heterogeneous Catalysts*, John Wiley Sons, Ltd, 2013, ch. 9, pp. 241–265.
287 S. Pollitt, V. Truttmann, T. Haunold, C. Garcia, W. Olszewski, J. Llorca, N. Barrabés and G. Rupprechter, The Dynamic Structure of $Au_{38}(SR)_{24}$ Nanoclusters Supported on CeO_2 upon Pretreatment and CO Oxidation, *ACS Catal.*, 2020, **10**, 6144–6148.
288 L. Lukashuk, N. Yigit, R. Rameshan, E. Kolar, D. Teschner, M. Hävecker, A. Knop- Gericke, R. Schlögl, K. Föttinger and G. Rupprechter, Operando Insights into CO Oxidation on Cobalt Oxide Catalysts by NAP-XPS, FTIR, and XRD, *ACS Catal.*, 2018, **8**, 8630–8641.
289 A. Wolfbeisser, O. Sophiphun, J. Bernardi, J. Wittayakun, K. Föttinger and G. Rupprechter, Methane dry reforming over ceria-zirconia supported Ni catalysts, *Catal. Today*, 2016, **277**, 234–245.
290 A. Haghofer, D. Ferri, K. Föttinger and G. Rupprechter, Who Is Doing the Job? Unraveling the Role of Ga_2O_3 in Methanol Steam Reforming on Pd_2Ga/Ga_2O_3, *ACS Catal.*, 2012, **2**, 2305–2315.
291 F. Zaera, *In situ* and operando spectroscopies for the characterization of catalysts and of mechanisms of catalytic reactions, *J. Catal.*, 2021, **404**, 900–910.

292 S. Chansai, R. Burch, C. Hardacre, J. Breen and F. Meunier, The use of short timeon-stream *in situ* spectroscopic transient kinetic isotope techniques to investigate the mechanism of hydrocarbon selective catalytic reduction (HC-SCR) of NO_x at low temperatures, *J. Catal.*, 2011, **281**, 98–105.

293 J. Saavedra, H. A. Doan, C. J. Pursell, L. C. Grabow and B. D. Chandler, The critical role of water at the gold-titania interface in catalytic CO oxidation, *Science*, 2014, **345**, 1599–1602.

294 M. J. Kale and P. Christopher, Utilizing Quantitative *in Situ* FTIR Spectroscopy To Identify Well-Coordinated Pt Atoms as the Active Site for CO Oxidation on Al_2O_3-Supported Pt Catalysts, *ACS Catal.*, 2016, **6**, 5599–5609.

295 F. Zaera, Gold-Titania Catalysts for Low-Temperature Oxidation andWater Splitting, *Top. Catal.*, 2018, **61**, 336.

296 A. Abdel-Mageed, S. Chen, C. Fauth, T. Häring and J. Bansmann, Fundamental Aspects of Ceria Supported Au Catalysts Probed by *In Situ*/Operando Spectroscopy and TAP Reactor Studies, *ChemPhysChem*, 2021, **22**, 1302–1315.

297 W. Fan and M. Tahir, Current Trends and Approaches to Boost the Performance of Metal Organic Frameworks for Carbon Dioxide Methanation through Photo/Thermal Hydrogenation: A Review, *Ind. Eng. Chem. Res.*, 2021, **60**, 13149–13179.

298 Y. Liu, Z. Wu, H. Kuhlenbeck and H.-J. Freund, Surface Action Spectroscopy: A Review and a Perspective on a New Technique to Study Vibrations at Surfaces, *Chem. Rec.*, 2021, **21**, 1270–1283.

299 L. Chen, Y. Wang, X. Wang, Q. Wang, B. Li, S. Li, S. Zhang and W. Li, Brønsted acid enhanced hexagonal cerium phosphate for the selective catalytic reduction of NO with NH_3: *In situ* DRIFTS and DFT investigation, *J. Hazard. Mater.*, 2022, **424**, 127334.

300 B. Henry and A. Samokhvalov, Hygroscopic metal-organic framework MIL-160(Al): Insitu time-dependent ATR-FTIR and gravimetric study of mechanism and kinetics of water vapor sorption, *Spectrochim. Acta, Part A*, 2022, **267**, 120550.

301 L. Jothinathan, Q. Cai, S. Ong and J. Hu, Fe-Mn doped powdered activated carbon pellet as ozone catalyst for cost-effective phenolic wastewater treatment: Mechanism studies and phenol by-products elimination, *J. Hazard. Mater.*, 2022, **424**, 127483.

302 X. Li, H. Li, Y. Huang, J. Cao, T. Huang, R. Li, Q. Zhang, S.-C. Lee and W. Ho, Exploring the photocatalytic conversion mechanism of gaseous formaldehyde degradation on TiO2-x-OV surface, *J. Hazard. Mater.*, 2022, **424**, 127217.

303 S. Rajabi, A. Nasiri and M. Hashemi, Enhanced activation of persulfate by $CuCoFe_2O_4$@MC/AC as a novel nanomagnetic heterogeneous catalyst with ultrasonic for metronidazole degradation, *Chemosphere*, 2022, **286**, 131872.

304 C. Schröder, P. Haugg, A.-K. Baumann, M. Schmidt, J. Smyczek and S. Schauermann, Competing Reaction Pathways in Heterogeneously Catalyzed Hydrogenation of Allyl Cyanide: The Chemical Nature of Surface Species, *Chem. – Eur. J.*, 2021, **27**, 17240–17254.

305 N. Sivasankar and H. Frei, Direct Observation of Kinetically Competent Surface Intermediates upon Ethylene Hydroformylation over Rh/Al_2O_3 under Reaction Conditions by Time-Resolved Fourier Transform Infrared Spectroscopy, *J. Phys. Chem. C*, 2011, **115**, 7545–7553.

306 T. J. Johnson, A. Simon, J. M. Weil and G. W. Harris, Applications of Time-Resolved Step-Scan and Rapid-Scan FT-IR Spectroscopy: Dynamics from Ten Seconds to Ten Nanoseconds, *Appl. Spectrosc.*, 1993, **47**, 1376–1381.

307 J. Lai, Z. Ma, L. Mink, L. J. Mueller and F. Zaera, Influence of Peripheral Groups on the Physical and Chemical Behavior of Cinchona Alkaloids, *J. Phys. Chem. B*, 2009, **113**, 11696–11701.

308 J. Kubota and F. Zaera, Adsorption geometry of modifiers as key in imparting chirality to platinum catalysts, *J. Am. Chem. Soc.*, 2001, **123**, 11115.

309 M. Cavers, J. Davidson, I. Harkness, L. Rees and G. McDougall, Spectroscopic Identification of the Active Site for CO Oxidation on Rh/Al_2O_3 by Concentration Modulation *in situ* DRIFTS, *J. Catal.*, 1999, **188**, 426–430.

310 M. M. Schubert, T. P. Häring, G. Bräth, H. A. Gasteiger and R. J. Behm, New DRIFTS Cell Design for the Simultaneous Acquisition of IR Spectra and Kinetic Data Using On-Line Product Analysis, *Appl. Spectrosc.*, 2001, **55**, 1537–1543.

311 F. Meunier, A. Goguet, S. Shekhtman, D. Rooney and H. Daly, A modified commercial DRIFTS cell for kinetically relevant operando studies of heterogeneous catalyticreactions, *Appl. Catal., A*, 2008, **340**, 196–202.

312 J. M. Coronado, S. Kataoka, I. Tejedor-Tejedor and M. A. Anderson, Dynamic phenomena during the photocatalytic oxidation of ethanol and acetone over nanocrystalline TiO_2: simultaneous FTIR analysis of gas and surface species, *J. Catal.*, 2003, **219**, 219–230.

313 F. Zaera, Surface chemistry at the liquid/solid interface, *Surf. Sci.*, 2011, **605**, 1141–1145.

314 F. Meemken, P. Müller, K. Hungerbühler and A. Baiker, Simultaneous probing of bulk liquid phase and catalytic gas-liquid-solid interface under working conditions using attenuated total reflection infrared spectroscopy, *Rev. Sci. Instrum.*, 2014, **85**, 084101.

315 F. Zaera, Probing Liquid/Solid Interfaces at the Molecular Level, *Chem. Rev.*, 2012, **112**, 2920–2986.

316 B. L. Mojet, S. D. Ebbesen and L. Lefferts, Light at the interface: the potential of attenuated total reflection infrared spectroscopy for understanding heterogeneous catalysis in water, *Chem. Soc. Rev.*, 2010, **39**, 4643–4655.

317 F. Zaera, Infrared absorption spectroscopy characterization of liquid-solid interfaces: The case of chiral modification of catalysts, *Surf. Sci.*, 2018, **669**, 16–24.

318 O. Zandi and T. Hamann, Determination of photoelectrochemical water oxidation intermediates on haematite electrode surfaces using operando infrared spectroscopy, *Nat. Chem.*, 2016, **8**, 778–783.

319 Y. Zhang, H. Zhang, A. Liu, C. Chen, W. Song and J. Zhao, Rate-limiting O–O bond formation pathways for water oxidation on hematite photoanode, *J. Am. Chem. Soc.*, 2018, **140**, 3264–3269.

320 C. Chen, M. Song, L. Lu, L. Yue, T. Huang and A. Yu, Application of *In Situ* Raman and Fourier Transform Infrared Spectroelectrochemical Methods on the Electrode-Electrolyte Interface for LithiumOxygen Batteries, *Batteries & Supercaps*, 2021, **4**, 850–859.

321 L. Zhang, T. Qian, X. Zhu, Z. Hu, M. Wang, L. Zhang, T. Jiang, J.-H. Tian and C. Yan, *In situ* optical spectroscopy characterization for optimal design of lithiumsulfur batteries, *Chem. Soc. Rev.*, 2019, **48**, 5432–5453.

322 A. Cowan and L. Hardwick, Advanced Spectroelectrochemical Techniques to Study Electrode Interfaces Within Lithium-Ion and Lithium-Oxygen Batteries, *Annu. Rev. Anal. Chem.*, 2019, **12**, 323–346.

323 S. Hosseinpour and M. Johnson, Vibrational spectroscopy in studies of atmospheric corrosion, *Materials*, 2017, **10**, 413.

324 Z. Qian, S. Wang, X. Ye, Z. Liu and Z. Wu, Corrosion resistance and wetting properties of silica-based superhydrophobic coatings on AZ31B Mg alloy surfaces, *Appl. Surf. Sci.*, 2018, **453**, 1–10.

325 W. Zhao and C. M. Johnson, Nano infrared microscopy: Obtaining chemical information on the nanoscale in corrosion studies, *J. Electrochem. Soc.*, 2019, **166**, C3456–C3460.

326 G. Frankel and N. Sridhar, Understanding localized corrosion, *Mater. Today*, 2008, **11**, 38–44.

327 S. Hosseinpour, J. Hedberg, S. Baldelli, C. Leygraf and M. Johnson, Initial oxidation of alkanethiol-covered copper studied by vibrational sum frequency spectroscopy, *J. Phys. Chem. C*, 2011, **115**, 23871–23879.

328 R. Hillenbrand and F. Keilmann, Material-specific mapping of metal/semiconductor/dielectric nanosystems at 10 nm resolution by backscattering near-field optical microscopy, *Appl. Phys. Lett.*, 2002, **80**, 25–27.

329 S. Morsch, S. Emad, L. Farren, M. Goodall, S. Lyon and S. Gibbon, The unexpected role of carbonate impurities in polyphosphate corrosion inhibition, *Sci. Rep.*, 2018, **8**, 17450.

330 A. Wain and M. O'connell, Advances in surface-enhanced vibrational spectroscopy at electrochemical interfaces, *Adv. Phys.*, 2017, **2**, 188–209.

331 M. Matsui, S. Deguchi, H. Kuwata and N. Imanishi, In-operando FTIR Spectroscopy for Composite Electrodes of Lithium-ion Batteries, *Electrochemistry*, 2015, **83**, 874–878.

332 N. Saqib, G. M. Ohlhausen and J. M. Porter, In operando infrared spectroscopy of lithium polysulfides using a novel spectro-electrochemical cell, *J. Power Sources*, 2017, **364**, 266–271.

333 N. Saqib, C. J. Silva, C. M. Maupin and J. M. Porter, A Novel Optical Diagnostic for *In Situ* Measurements of Lithium Polysulfides in Battery Electrolytes, *Appl. Spectrosc.*, 2017, **71**, 1593–1599.

334 R. F. Aroca, D. J. Ross and C. Domingo, Surface-Enhanced Infrared Spectroscopy, *Appl. Spectrosc.*, 2004, **58**, 324A–338A.

335 M. Osawa, Dynamic Processes in Electrochemical Reactions Studied by Surface-Enhanced Infrared Absorption Spectroscopy (SEIRAS), *Bull. Chem. Soc. Jpn.*, 1997, **70**, 2861–2880.

336 R. Hillenbrand, T. Taubner and F. Keilmann, Phonon-enhanced light-matter interaction at the nanometre scale, *Nature*, 2002, **418**, 159–162.

337 Q. Xu, A. Berná, I. V. Pobelov, A. Rodes, J. M. Feliu, T. Wandlowski and A. Kuzume, ATR-SEIRAS study of CO adsorption and oxidation on Rh modified Au(111-25 nm) Film electrodes in 0.1 M H_2SO_4, *Electrochim. Acta*, 2015, **176**, 1202–1213.

338 F. W. Richey and Y. A. Elabd, *In Situ* Molecular Level Measurements of Ion Dynamics in an Electrochemical Capacitor, *J. Phys. Chem. Lett.*, 2012, **3**, 3297–3301.

339 F. W. Richey, B. Dyatkin, Y. Gogotsi and Y. A. Elabd, Ion Dynamics in Porous Carbon Electrodes in Supercapacitors Using *in Situ* Infrared Spectroelectrochemistry, *J. Am. Chem. Soc.*, 2013, **135**, 12818–12826.

340 Y. Elabd, M. Baschetti and T. Barbari, Time-Resolved Fourier Transform Infrared/Attenuated Total Reflection Spectroscopy for the Measurement of Molecular Diffusion in Polymers, *J. Polym. Sci., Part B: Polym. Phys.*, 2003, **41**, 2794–2807.

341 C. Merlet, B. Rotenberg, P. Madden, P.-L. Taberna, P. Simon, Y. Gogotsi and M. Salanne, On the molecular origin of supercapacitance in nanoporous carbon electrodes, *Nat. Mater.*, 2012, **11**, 306.

342 F. W. Richey, C. Tran, V. Kalra and Y. A. Elabd, Ionic Liquid Dynamics in Nanoporous Carbon Nanofibers in Supercapacitors Measured with in Operando Infrared Spectroelectrochemistry, *J. Phys. Chem. C*, 2014, **118**, 21846–21855.

343 Y. Liu, M. Ghaffari, R. Zhao, J.-H. Lin, M. Lin and Q. M. Zhang, Enhanced Electromechanical Response of Ionic Polymer Actuators by Improving Mechanical Coupling between Ions and Polymer Matrix, *Macromolecules*, 2012, **45**, 5128–5133.

344 J.-F. Ding, R. Xu, C. Yan, B.-Q. Li, H. Yuan and J.-Q. Huang, A review on the failure and regulation of solid electrolyte interphase in lithium batteries, *J. Energy Chem.*, 2021, **59**, 306–319.

345 Y. Gao, Z. Yan, J. Gray, X. He, D. Wang, T. Chen, Q. Huang, Y. Li, H. Wang, S. Kim, T. Mallouk and D. Wang, Polymer-inorganic solid-electrolyte interphase for stable lithium metal batteries under lean electrolyte conditions, *Nat. Mater.*, 2019, **18**, 384–389.

346 X. Zhang, P. Dong and M.-K. Song, MetalOrganic Frameworks for High-Energy Lithium Batteries with Enhanced Safety: Recent Progress and Future Perspectives, *Batteries & Supercaps*, 2019, **2**, 591–626.

347 W.-J. Kwak, J. Park, T. T. Nguyen, H. Kim, H. R. Byon, M. Jang and Y.-K. Sun, A dendrite- and oxygen-proof protective layer for lithium metal in lithium-oxygen batteries, *J. Mater. Chem. A*, 2019, **7**, 3857–3862.

348 G. V. Zhuang, K. Xu, T. R. Jow and P. N. Ross, Study of SEI Layer Formed on Graphite Anodes in PC/LiBOB Electrolyte Using IR Spectroscopy, *Electrochem. Solid-State Lett.*, 2004, **7**, A224.

349 G. V. Zhuang, H. Yang, B. Blizanac and P. N. Ross, A Study of Electrochemical Reduction of Ethylene and Propylene Carbonate Electrolytes on Graphite Using ATR-FTIR Spectroscopy, *Electrochem. Solid-State Lett.*, 2005, **8**, A441.

350 C. Meng, P. Das, X. Shi, Q. Fu, K. Müllen and Z.-S. Wu, *In situ* and operando characterizations of 2D materials in electrochemical energy storage devices, *Small Sci.*, 2021, **1**, 2000076.

351 K. S. Adarsh, N. Chandrasekaran and V. Chakrapani, *In situ* spectroscopic techniques as critical evaluation tools for electrochemical carbon dioxide reduction: A mini review, *Front. Chem.*, 2020, **8**, 137.

352 S. Bunea and A. Urakawa, *Carbon Dioxide Electrochemistry: Homogeneous and Heterogeneous Catalysis*, The Royal Society of Chemistry, 2021, ch. 9, pp. 347–407.

353 T. Yajima, H. Uchida and M. Watanabe, *In situ* ATR-FTIR spectroscopic study of electro-oxidation of methanol and adsorbed CO at PtRu alloy, *J. Phys. Chem. B*, 2004, **108**, 2654–2659.

354 N. Heidary, K. Ly and N. Kornienko, Probing CO_2 conversion chemistry on nanostructured surfaces with *operando* vibrational spectroscopy, *Nano Lett.*, 2019, **19**, 4817–4826.

355 F. Neubrech, C. Huck, K. Weber, A. Pucci and H. Giessen, Surface-enhanced infrared spectroscopy using resonant nanoantennas, *Chem. Rev.*, 2017, **117**, 5110–5145.

356 M. Papasizza and A. Cuesta, *In situ* monitoring using ATR-SEIRAS of the electrocatalytic reduction of CO_2 on Au in an ionic liquid/water mixture, *ACS Catal.*, 2018, **8**, 6345–6352.

357 D. Gao, H. Zhou, F. Cai, D. Wang, Y. Hu, B. Jiang, W.-B. Cai, X. Chen, R. Si, F. Yang, S. Miao, J. Wang, G. Wang and X. Bao, Switchable CO_2 electroreduction *via* engineering active phases of Pd nanoparticles, *Nano Res.*, 2017, **10**, 2181–2191.

358 W. Deng, L. Zhang, L. Li, S. Chen, C. Hu, Z.-J. Zhao, T. Wang and J. Gong, Crucial role of surface hydroxyls on the activity and stability in electrochemical CO_2 reduction, *J. Am. Chem. Soc.*, 2019, **141**, 2911–2915.

359 S. Zhu, B. Jiang, W.-B. Cai and M. Shao, Direct observation on reaction intermediates and the role of bicarbonate anions in CO_2 electrochemical reduction reaction on Cu surfaces, *J. Am. Chem. Soc.*, 2017, **139**, 15664–15667.

360 A. Rodes, E. Pastor and T. Iwasita, Structural effects on CO_2 reduction at Pt singlecrystal electrodes: Part 1. The Pt(110) surface, *J. Electroanal. Chem.*, 1994, **369**, 183–191.

361 A. Rodes, E. Pastor and T. Iwasita, Structural efects on CO_2 reduction at Pt singlecrystal electrodes: Part 2. Pt(111) and vicinal surfaces in the [011] zone, *J. Electroanal. Chem.*, 1994, **373**, 167–175.

362 A. Rodes, E. Pastor and T. Iwasita, Structural effects on CO_2 reduction at Pt singlecrystal electrodes: Part 3. Pt(100) and related surfaces, *J. Electroanal. Chem.*, 1994, **377**, 215–225.

363 K. Jiang, H. Wang, W.-B. Cai and H. Wang, Li electrochemical tuning of metal oxide for highly selective CO_2 reduction, *ACS Nano*, 2017, **11**, 6451–6458.

364 H. Kitano and M. Gemmei-Ide, Structure of water in the vicinity of amphoteric polymers as revealed by vibrational spectroscopy, *J. Biomater. Sci., Polym. Ed.*, 2010, **21**, 1877–1893.

365 A. Remizov, V. Povov and V. Lavrent'ev, *Polym. Sci. U.S.S.R.*, 1982, **24**, 1853.

366 J. Bravo-Suárez and P. Srinivasan, Design characteristics of *in situ* and operando ultraviolet-visible and vibrational spectroscopic reaction cells for heterogeneous catalysis, *Catal. Rev. Sci. Eng.*, 2017, **59**, 295–445.

367 Y. Wang, Y. Zhu, Z. Zhou, J. Yang, Y. Pan and F. Qi, Pyrolysis study on solid fuels: from conventional analytical methods to synchrotron vacuum ultraviolet photoionization mass spectrometry, *Energy Fuels*, 2016, **30**, 1534–1543.

368 K. Pielichowska and K. Nowicka, Analysis of nanomaterials and nanocomposites by thermoanalytical methods, *Thermochim. Acta*, 2019, **675**, 140–163.

369 A. Benhammada and D. Trache, Thermal decomposition of energetic materials using TGFTIR and TG-MS: a state-of-the-art review, *Appl. Spectrosc. Rev.*, 2020, **55**, 724–777.

370 X. Zheng, W. Xu and S. Xie, Study on ultraviolet aging mechanism of carbon nanotubes/SBS composite-modified Asphalt in two-dimensional infrared correlation spectroscopy, *Materials*, 2021, **14**, 5672.

371 N. M. Ainali, D. N. Bikiaris and D. A. Lambropoulou, Aging effects on low- and highdensity polyethylene, polypropylene and polystyrene under UV irradiation: An insight into decomposition mechanism by Py-GC/MS for microplastic analysis, *J. Anal. Appl. Pyrolysis*, 2021, **158**, 105207.

372 A. S. Mahdi, Z. Abdul-Malek, A. Naderipour, S. Ishak and M. N. K. Bin Hussein, *Investigation of SF_6 Decomposition Under Partial Discharge Induced by Protrusion Defect. 2021 IEEE International Conference on the Properties and Applications of Dielectric Materials (ICPADM)*, 2021, pp. 139–142.

373 W. Li, W. Zheng, L. Ren, H. Li, X. Zhao, C. Wang and J. Li, A comparative study on the insulation ageing of 10 kV XLPE cable via accelerated electrical test and accelerated water tree test, *J. Electic. Eng. Technol.*, 2021, 475–484.

374 E.-S. Jang, E. Song, M. Zain Siddiqui, S. Lim, G. Shin, D. Kim and Y.-M. Kim, The effect of seawater aging on the pyrolysis of fishing nets, *J. Anal. Appl. Pyrolysis*, 2021, **156**, 105160.

375 H. Peng, Y. Han, T. Liu, W. C. Tjiu and C. He, Morphology and thermal degradation behavior of highly exfoliated CoAl-layered double hydroxide/polycaprolactone nanocomposites prepared by simple solution intercalation, *Thermochim. Acta*, 2010, **502**, 1–7.

376 M.-C. Popescu and C. Vasile, Melting behavior of polytetra hydrofuran/cholesteryl palmitate blends investigated by two-dimensional infrared correlation spectroscopy, *Soft Mater.*, 2010, **8**, 386–406.

377 H. Tang, S. Sun, J. Wu, P. Wu and X. Wan, Conformational changes in novel thermotropic liquid crystalline polymer without conventional mesogens: A Raman spectroscopic investigation, *Polymer*, 2010, **51**, 5482–5489.

378 K. Zheng, R. Liu and Y. Huang, A two-dimensional IR correlation spectroscopic study of the conformational

changes in syndiotactic polypropylene during crystallization, *Polym. J.*, 2010, **42**, 81–85.
379 Y.-H. Cheng, W.-P. Chen, Z. Shen, X.-H. Fan, M.-F. Zhu and Q.-F. Zhou, Influences of hydrogen bonding and peripheral chain length on mesophase structures of mesogen-jacketed liquid crystalline polymers with amide side-chain linkages, *Macromolecules*, 2011, **44**, 1429–1437.
380 T. Pazderka and V. Kopecký, Two-dimensional correlation analysis of Raman optical activity – Basic rules and data treatment, *Vib. Spectrosc.*, 2012, **60**, 193–199.
381 F. Chai, Y. Chen, Z. You, Z. Xia, S. Ge, Y. Sun and B. Huang, Two Keggin-type heteropolytungstates with transition metal as a central atom: Crystal structure and magnetic study with 2D-IR correlation spectroscopy, *J. Solid State Chem.*, 2013, **202**, 161–167.
382 G.-W. Wang, Mechanochemical organic synthesis, *Chem. Soc. Rev.*, 2013, **42**, 7668–7700.
383 L. Wang, S. Di, W. Wang, H. Chen, X. Yang, T. Gong and S. Zhou, Tunable temperature memory effect of photo-cross-linked star PCL-PEG networks, *Macromolecules*, 2014, **47**, 1828–1836.
384 H. Hoshina, S. Ishii and C. Otani, Separation of overlapping vibrational peaks in terahertz spectra using two-dimensional correlation spectroscopy, *J. Mol. Struct.*, 2014, **1069**, 152–156.
385 L. Hou, K. Ma, Z. An and P. Wu, Exploring the volume phase transition behavior of POEGA- and PNIPAM-based core–shell nanogels from infrared-spectral insights, *Macromolecules*, 2014, **47**, 1144–1154.
386 H. Seo, B. Chae, J. H. Im, Y. M. Jung and S. W. Lee, Imidization induced structural changes of 6FDA-ODA poly(amic acid) by two-dimensional (2D) infrared correlation spectroscopy, *J. Mol. Struct.*, 2014, **1069**, 196–199.
387 H. J. Kim, S. B. Kim, J. K. Kim, Y. M. Jung, D. Y. Ryu, K. A. Lavery and T. P. Russell, Phase behavior of a weakly interacting block copolymer by temperature-dependent FTIR spectroscopy, *Macromolecules*, 2006, **39**, 408–412.
388 M. Unger, S. Morita, H. Sato, Y. Ozaki and H. W. Siesler, Variable-temperature Fourier transform infrared spectroscopic investigations of poly(3-hydroxyalkanoates) and perturbation-correlation moving-window two-dimensional correlation analysis. Part II: Study of poly(ε-caprolactone) homopolymer and a poly(3-hydroxybutyrate)|poly(ε-caprolactone) blend, *Appl. Spectrosc.*, 2009, **63**, 1034–1040.
389 M. Unger, H. Sato, Y. Ozaki and H. W. Siesler, Crystallization behavior of poly(3-hydroxybutyrate) (PHB), poly-(ε-caprolactone) (PCL) and their blend (50:50 wt%) studied by 2D FT-IR correlation spectroscopy, *Macromol. Symp.*, 2011, **305**, 90–100.
390 L. Jia, C. Guo, L. Yang, J. Xiang, Y. Tang, C. Liu and H. Liu, Mechanism of PEO-PPO-PEO micellization in aqueous solutions studied by two-dimensional correlation FTIR spectroscopy, *J. Colloid Interface Sci.*, 2010, **345**, 332–337.
391 B. Baumgartner, S. Freitag and B. Lendl, 3D printing for low-cost and versatile attenuated total reflection infrared spectroscopy, *Anal. Chem.*, 2020, **92**, 4736–4741.
392 E. J. Carrasco-Correa, E. F. Simó-Alfonso, J. M. Herrero-Martínez and M. Miró, The emerging role of 3D printing in the fabrication of detection systems, *TrAC, Trends Anal. Chem.*, 2021, **136**, 116177.
393 P. Dumas, M. C. Martin and G. L. Carr, in *Synchrotron light sources and free-electron lasers: Accelerator physics, instrumentation and science applications*, ed. E. J. Jaeschke, S. Khan, J. R. Schneider and J. B. Hastings, Springer International Publishing, Cham, 2020, pp. 2059–2113.
394 H. Lu, G. M. Carroll, N. R. Neale and M. C. Beard, Infrared quantum dots: Progress, challenges, and opportunities, *ACS Nano*, 2019, **13**, 939–953.
395 T. Elgayyar, R. Atwi, A. Tuel and F. C. Meunier, Contributions and limitations of IR spectroscopy of CO adsorption to the characterization of bimetallic and nanoalloy catalysts, *Catal. Today*, 2021, **373**, 59–68.
396 Y. Hu, N. I. López-Lorente and B. Mizaikoff, Graphene-based surface enhanced vibrational spectroscopy: Recent developments, challenges, and applications, *ACS Photonics*, 2019, **6**, 2182–2197.
397 T. Hayashi, Water at interfaces: Its behavior and roles in interfacial phenomena, *Chem. Lett.*, 2021, **50**, 1173–1180.
398 S. N. Steinmann and Z. W. Seh, Understanding electrified interfaces, *Nat. Rev. Mater.*, 2021, **6**, 289–291.
399 C. Brahms, F. Belli and J. C. Travers, Infrared attosecond field transients and UV to IR few-femtosecond pulses generated by high-energy soliton self-compression, *Phys. Rev. Res.*, 2020, **2**, 043037.
400 M. Maiuri, M. Garavelli and G. Cerullo, Ultrafast spectroscopy: State of the art and open challenges, *J. Am. Chem. Soc.*, 2020, **142**, 3–15.
401 A. Pushkin, E. Migal, D. Suleimanova, E. Mareev and F. Potemkin, High-power solid-state near- and mid-IR ultrafast laser sources for strong-field science, *Photonics*, 2022, **9**, 90.
402 H. A. Bechtel, S. C. Johnson, O. Khatib, E. A. Muller and M. B. Raschke, Synchrotron infrared nano-spectroscopy and -imaging, *Surf. Sci. Rep.*, 2020, **75**, 100493.
403 G. Ellis and M. Martin, Opportunities and challenges for polymer science using synchrotron-based infrared spectroscopy, *Eur. Polym. J.*, 2016, **81**, 505–531.
404 A. Babal, B. Souza, A. Möslein, M. Gutiérrez, M. Frogley and J.-C. Tan, Broadband dielectric behavior of an MIL-100 metal-organic framework as a function of structural amorphization, *ACS Appl. Electon. Mater.*, 2021, **3**, 1191–1198.
405 F. Li, G.-F. Han and J.-B. Baek, Nanocatalytic materials for energy-related small-molecules conversions: Active site design, identification and structure-performance relationship discovery, *Acc. Chem. Res.*, 2021, **55**, 110–120.
406 G. L. Carr, Resolution limits for infrared microspectroscopy explored with synchrotron radiation, *Rev. Sci. Instrum.*, 2001, **72**, 1613–1619.
407 E. N. Lewis, P. J. Treado, R. C. Reeder, G. M. Story, A. E. Dowrey, C. Marcott and I. W. Levin, Fourier transform spectroscopic imaging using an infrared focal-plane array detector, *Anal. Chem.*, 1995, **67**, 3377–3381.

408 X. Tang and Q. Hao, *Towards dual-band shot-wave and mid-wave infrared focal plane array by using colloidal quantum dots. Seventh Symposium on Novel Photoelectronic Detection Technology and Applications*, 2021, pp. 168–174.
409 A. Dazzi, C. B. Prater, Q. Hu, D. B. Chase, J. F. Rabolt and C. Marcott, AFMIR: Combining atomic force microscopy and infrared spectroscopy for nanoscale chemical characterization, *Appl. Spectrosc.*, 2012, **66**, 1365–1384.
410 A. Dazzi and C. B. Prater, AFM-IR: Technology and applications in nanoscale infrared spectroscopy and chemical imaging, *Chem. Rev.*, 2017, **117**, 5146–5173.
411 A. L. Bondy, R. M. Kirpes, R. L. Merzel, K. A. Pratt, M. M. Banaszak Holl and A. P. Ault, Atomic force microscopy-infrared spectroscopy of individual atmospheric aerosol particles: Subdifraction limit vibrational spectroscopy and morphological analysis, *Anal. Chem.*, 2017, **89**, 8594–8598.
412 C. T. Graefe, D. Punihaole, C. M. Harris, M. J. Lynch, R. Leighton and R. R. Frontiera, Far-field super-resolution vibrational spectroscopy, *Anal. Chem.*, 2019, **91**, 8723–8731.
413 L. Xiao and Z. D. Schultz, Spectroscopic imaging at the nanoscale: Technologies and recent applications, *Anal. Chem.*, 2018, **90**, 440–458.
414 J. Mathurin, A. Deniset-Besseau, D. Bazin, E. Dartois, M. Wagner and A. Dazzi, Photothermal AFM-IR spectroscopy and imaging: Status, challenges, and trends, *J. Appl. Phys.*, 2022, **131**, 010901.
415 I. Milanović and N. Biliškov, Mechanochemical pretreatment of ammonia borane: A new procedure for sodium amidoborane synthesis, *Int. J. Hydrogen Energy*, 2020, **45**, 7938–7946.
416 L. Gonnet, C. B. Lennox, J.-L. Do, I. Malvestiti, S. G. Koenig, K. Nagapudi and T. Friščić, Metal-catalyzed organic reactions by resonant acoustic mixing, *Angew. Chem., Int. Ed.*, 2022, e202115030.
417 F. Gomollón-Bel, Ten chemical innovations that will change our world: IUPAC identifies emerging technologies in Chemistry with potential to make our planet more sustainable, *Chem. Int.*, 2019, **41**, 12–17.
418 P. J. Dunn, Pharmaceutical Green Chemistry process changes – How long does it take to obtain regulatory approval?, *Green Chem.*, 2013, **15**, 3099–3104.
419 T. Welton, Solvents and sustainable chemistry, *Proc. R. Soc. London, Ser. A*, 2015, **471**, 20150502.
420 X. Liu, Y. Li, L. Zeng, X. Li, N. Chen, S. Bai, H. He, Q. Wang and C. Zhang, A review on mechanochemistry: Approaching advanced energy materials with greener force, *Adv. Mater.*, 2022, 2108327.
421 T. Friščić, C. Mottillo and H. M. Titi, Mechanochemistry for synthesis, *Angew. Chem., Int. Ed.*, 2020, **59**, 1018–1029.
422 F. Effaty, X. Ottenwaelder and T. Friščić, Mechanochemistry in transition metalcatalyzed reactions, *Curr. Opin. Green Sustainable Chem.*, 2021, **32**, 100524.
423 B. G. Fiss, A. J. Richard, T. Friščić and A. Moores, Mechanochemistry for sustainable and efficient dehydrogenation/hydrogenation, *Can. J. Chem.*, 2021, **99**, 93–112.
424 C. Bolm and J. G. Hernández, Mechanochemistry of gaseous reactants, *Angew. Chem., Int. Ed.*, 2019, **58**, 3285–3299.
425 K. J. Ardila-Fierro and J. G. Hernández, Sustainability assessment of mechanochemistry by using the twelve principles of green chemistry, *ChemSusChem*, 2021, **14**, 2145–2162.
426 A. P. Amrute, J. De Bellis, M. Felderhoff and F. Schüth, Mechanochemical synthesis of catalytic materials, *Chem. – Eur. J.*, 2021, **27**, 6819–6847.
427 S. Hwang, S. Grätz and L. Borchardt, A guide to direct mechanocatalysis, *Chem. Commun.*, 2022, **58**, 1661–1671.
428 D. Tan and T. Friščić, Mechanochemistry for organic chemists: An update, *Eur. J. Org. Chem.*, 2018, 18–33.
429 D. Tan and F. García, Main group mechanochemistry: From curiosity to established protocols, *Chem. Soc. Rev.*, 2019, **48**, 2274–2292.
430 C. Espro and D. Rodríguez-Padrón, Re-thinking organic synthesis: Mechanochemistry as a greener approach, *Curr. Opin. Green Sustainable Chem.*, 2021, **30**, 100478.
431 T. Friščić, I. Halasz, P. Beldon, A. Belenguer, F. Adams, S. Kimber, V. Honkimäki and R. Dinnebier, Real-time and *in situ* monitoring of mechanochemical milling reactions, *Nat. Chem.*, 2013, **5**, 66–73.
432 M. Juribašić, K. Užarević, D. Gracin and M. Ćurić, Mechanochemical C–H bond activation: Rapid and regioselective double cyclopalladation monitored by *in situ* Raman spectroscopy, *Chem. Commun.*, 2014, **50**, 10287–10290.
433 D. Gracin, V. Strukil, T. Friščić, I. Halasz and K. Užarević, Laboratory real-time and *in situ* monitoring of mechanochemical milling reactions by Raman spectroscopy, *Angew. Chem., Int. Ed.*, 2014, **53**, 6193–6197.
434 K. Užarević, I. Halasz and T. Friščić, Real-time and *in situ* monitoring of mechanochemical reactions: A new playground for all chemists, *J. Phys. Chem. Lett.*, 2015, **6**, 4129–4140.
435 P. Julien, K. Užarević, A. Katsenis, S. Kimber, T. Wang, O. Farha, Y. Zhang, J. Casaban, L. Germann, M. Etter, R. Dinnebier, S. James, I. Halasz and T. Friščić, *In situ* monitoring and mechanism of the mechanochemical formation of a microporous MOF-74 framework, *J. Am. Chem. Soc.*, 2016, **138**, 2929–2932.
436 S. Lukin, T. Stolar, M. Tireli, M. Blanco, D. Babić, T. Friščić, K. Užarević and I. Halasz, Tandem In Situ Monitoring for Quantitative Assessment of Mechanochemical Reactions Involving Structurally Unknown Phases, *Chem. – Eur. J.*, 2017, **23**, 13941–13949.
437 K. Užarević, N. Ferdelji, T. Mrla, P. Julien, B. Halasz, T. Friščić and I. Halasz, Enthalpy *vs.* friction: Heat ow modelling of unexpected temperature profiles in mechanochemistry of metal–organic frameworks, *Chem. Sci.*, 2018, **9**, 2525–2532.
438 K. Ardila-Fierro, S. Lukin, M. Etter, K. Užarević, I. Halasz, C. Bolm and J. Hernández, Direct visualization of a mechanochemically induced molecular rearrangement, *Angew. Chem., Int. Ed.*, 2020, **59**, 13458–13462.

439 L. Germann, A. Katsenis, I. Huskić, P. Julien, K. Užarević, M. Etter, O. Farha, T. Friščić and R. Dinnebier, Real-time *in situ* monitoring of particle and structure evolution in the mechanochemical synthesis of UiO-66 metal-organic frameworks, *Cryst. Growth Des.*, 2020, **20**, 49–54.

440 N. Biliškov, A. Borgschulte, K. Užarević, I. Halasz, S. Lukin, S. Milošević, I. Milanović and J. Novaković, *In situ* and real-time monitoring of mechanochemical preparation of Li2Mg(NH2BH3)4 and Na2Mg(NH2BH3)4 and their thermal dehydrogenation, *Chem. – Eur. J.*, 2017, **23**, 16274–16282.

441 T. Rathmann, H. Petersen, S. Reichle, W. Schmidt, A. Amrute, M. Etter and C. Weidenthaler, *In situ* synchrotron X-ray diffraction studies monitoring mechanochemical reactions of hard materials: Challenges and limitations, *Rev. Sci. Instrum.*, 2021, **92**, 114102.

